BEHAVIOUR OF GEOPOLYMER CONCRETE EXPOSED TO ELEVATED TEMPERATURES

A Thesis

Submitted by

BENNY JOSEPH

for the award of the Degree of

DOCTOR OF PHILOSOPHY

(Faculty of Engineering)

SCHOOL OF ENGINEERING
COCHIN UNIVERSITY OF SCIENCE AND TECHNOLOGY
KOCHI-682022

AUGUST 2015

Certificate

*Certified that the thesis entitled "**BEHAVIOUR OF GEOPOLYMER CONCRETE EXPOSED TO ELEVATED TEMPERATURES**" submitted to Cochin University of Science and Technology, Kochi-22, for the award of Ph.D. Degree, is the record of bonafide research carried out by Sri. Benny Joseph under my supervision and guidance at School of Engineering, Cochin University of Science and Technology. This work did not form part of any dissertation submitted for the award of any degree, diploma, associateship or other similar title or recognition from this or any other institution.*

Dr. George Mathew
(Supervising Guide),
Associate Professor,
Division of Safety and Fire Engineering
School of Engineering,
Cochin University of Science and Technology

Kochi-22
19-08-2015

DECLARATION

I Benny Joseph hereby declare that the work presented in this thesis entitled **"BEHAVIOUR OF GEOPOLYMER CONCRETE EXPOSED TO ELEVATED TEMPERATURES"** being submitted to Cochin University of Science and Technology for the award of Doctor of Philosophy under the Faculty of Engineering, is the outcome of the original work done by me under the supervision of Dr. George Mathew, Associate Professor, Division of Safety and Fire Engineering, School of Engineering, Cochin University of Science and Technology, Kochi-22. This work did not form part of any dissertation submitted for the award of any degree, diploma, associateship or other similar title or recognition from this or any other institution.

Kochi-22 **BENNYJOSEPH**

19-08-15 Reg. No. 3994

ACKNOWLEDGEMENTS

This thesis is the result of five years of hard work in which many people have supported me. I am happy that I now have the opportunity to express my sincere gratitude to all of them.

I have great pleasure in expressing my deep sense of gratitude and indebtedness to **Dr. George Mathew**, Professor, Department of Safety and Fire Engineering, School of Engineering, CUSAT, under whose inspiring guidance and supervision this study was carried out. His integral view on research, keen enthusiasm, and timely help led to the successful completion of this work.

I am thankful to **Dr. G. Madu**, Principal, School of Engineering, and members of the faculty of the Department of Safety and Fire Engineering as well as Civil Engineering, School of Engineering, CUSAT, Kochi, for the support given to me during the period of the work.

I express my sincere thanks to my doctoral committee member **Dr. Job Thomas**, for his critical evaluation and creative suggestions.

I express my sincere gratitude to **Management** and **Principal**, of TKM College of Engineering, Kollam for giving me permission to do the doctoral work. I owe a debt of gratitude to all the **Faculty members** and **Technical staff** of Department of Civil Engineering, TKM College of Engineering, Kollam for the whole hearted help rendered during the investigation.

I would like to acknowledge the financial support provided by **Kerala State Council for Science Technology and Environment** (KSCSTE) that enabled me to purchase equipments and material for the project.

I would like to express my love and thanks to my **family** and **parents** for their understanding and support over the years.

Besides all, I thank the **almighty** power above, who granted me the wisdom, strength, and perseverance to finish this research work.

Benny Joseph

ABSTRACT

BEHAVIOUR OF GEOPOLYMER CONCRETE EXPOSED TO ELEVATED TEMPERATURES

The research in the area of geopolymer is gaining momentum during the past 20 years. Studies confirm that geopolymer concrete has good compressive strength, tensile strength, flexural strength, modulus of elasticity and durability. These properties are comparable with OPC concrete.

There are many occasions where concrete is exposed to elevated temperatures like fire exposure from thermal processor, exposure from furnaces, nuclear exposure, etc.. In such cases, understanding of the behaviour of concrete and structural members exposed to elevated temperatures is vital.

Even though many research reports are available about the behaviour of OPC concrete at elevated temperatures, there is limited information available about the behaviour of geopolymer concrete after exposure to elevated temperatures.

A preliminary study was carried out for the selection of a mix proportion. The important variable considered in the present study include alkali/fly ash ratio, percentage of total aggregate content, fine aggregate to total aggregate ratio, molarity of sodium hydroxide, sodium silicate to sodium hydroxide ratio, curing temperature and curing period. Influence of different variables on engineering properties of geopolymer concrete was investigated. The study on interface shear strength of reinforced and unreinforced geopolymer concrete as well as OPC concrete was also carried out.

Engineering properties of fly ash based geopolymer concrete after exposure to elevated temperatures (ambient to 800 °C) were studied and the corresponding results were compared with those of conventional concrete.

Scanning Electron Microscope analysis, Fourier Transform Infrared analysis, X-ray powder Diffractometer analysis and Thermogravimetric analysis of geopolymer mortar or

paste at ambient temperature and after exposure to elevated temperature were also carried out in the present research work.

Experimental study was conducted on geopolymer concrete beams after exposure to elevated temperatures (ambient to 800 °C). Load deflection characteristics, ductility and moment-curvature behaviour of the geopolymer concrete beams after exposure to elevated temperatures were investigated.

Based on the present study, major conclusions derived could be summarized as follows.

There is a definite proportion for various ingredients to achieve maximum strength properties. Geopolymer concrete with total aggregate content of 70% by volume, ratio of fine aggregate to total aggregate of 0.35, NaOH molarity 10, Na_2SiO_3/NaOH ratio of 2.5 and alkali to fly ash ratio of 0.55 gave maximum compressive strength in the present study.

An early strength development in geopolymer concrete could be achieved by the proper selection of curing temperature and the period of curing. With 24 hours of curing at 100 °C, 96.4% of the 28th day cube compressive strength could be achieved in 7 days in the present study. The interface shear strength of geopolymer concrete is lower to that of OPC concrete. Compared to OPC concrete, a reduction in the interface shear strength by 33% and 29% was observed for unreinforced and reinforced geopolymer specimens respectively.

The interface shear strength of geopolymer concrete is lower than ordinary Portland cement concrete.

The interface shear strength of geopolymer concrete can be approximately estimated as 50% of the value obtained based on the available equations for the calculation of interface shear strength of ordinary portland cement concrete (method used in Mattock and ACI).

Fly ash based geopolymer concrete undergoes a high rate of strength loss (compressive strength, tensile strength and modulus of elasticity) during its early heating period (up to 200 °C) compared to OPC concrete.

At a temperature exposure beyond 600 °C, the unreacted crystalline materials in geopolymer concrete get transformed into amorphous state and undergo polymerization.

As a result, there is no further strength loss (compressive strength, tensile strength and modulus of elasticity) in geopolymer concrete, whereas, OPC concrete continues to lose its strength properties at a faster rate beyond a temperature exposure of 600 °C.

At present no equation is available to predict the strength properties of geopolymer concrete after exposure to elevated temperatures. Based on the study carried out, new equations have been proposed to predict the residual strengths (cube compressive strength, split tensile strength and modulus of elasticity) of geopolymer concrete after exposure to elevated temperatures (upto 800 °C). These equations could be used for material modelling until better refined equations are available.

Compared to OPC concrete, geopolymer concrete shows better resistance against surface cracking when exposed to elevated temperatures. In the present study, while OPC concrete started developing cracks at 400 °C, geopolymer concrete did not show any visible cracks up to 600 °C and developed only minor cracks at an exposure temperature of 800 °C.

Geopolymer concrete beams develop crack at an early load stages if they are exposed to elevated temperatures.

Even though the material strength of the geopolymer concrete does not decrease beyond 600 °C, the flexural strength of corresponding beam reduces rapidly after 600 °C temperature exposure, primarily due to the rapid loss of the strength of steel.

With increase in temperature, the curvature at yield point of geopolymer concrete beam increases and thereby the ductility reduces. In the present study, compared to the ductility at ambient temperature, the ductility of geopolymer concrete beams reduces by 63.8% at 800 °C temperature exposure.

Appropriate equations have been proposed to predict the service load crack width of geopolymer concrete beam exposed to elevated temperatures. These equations could be used to limit the service load on geopolymer concrete beams exposed to elevated temperatures (up to 800 °C) for a predefined crack width (between 0.1mm and 0.3 mm) or vice versa.

The moment-curvature relationship of geopolymer concrete beams at ambient temperature is similar to that of RCC beams and this could be predicted using strain compatibility approach

Once exposed to an elevated temperature, the strain compatibility approach underestimates the curvature of geopolymer concrete beams between the first cracking and yielding point.

ABBREVIATIONS AND NOMENCLATURE

CO_2	-	Carbondioxide
C-S-H	-	Calcium Silicate Hydrates
FTIR	-	Fourier Transform Infrared Spectroscopy
GGBS	-	Ground Granulated Blast Furnace Slag
GP	-	Geopolymer
GPC	-	Geopolymer Concrete
KOH	-	Potassium Hydroxide
K_2SO_4	-	Potassium Silicate
OPC	-	Ordinary Portland Cement
RCC	-	Reinforced Cement Concrete
SEM	-	Scanning Electron microscope
TGA	-	Thermo Gravimetric Analysis
XRD	-	X-Ray Diffraction
SD	-	Standard deviation
NaOH	-	Sodium Hydroxide
Na_2SO_4	-	Sodium Silicate
Aggr.	-	Aggregate
Comp.	-	Compressive strength
C_{wa}	-	Crack width at ambient temperature in mm
C_{wt}	-	Crack width at temperature T ºC in mm
My	-	Yield moment
Mu	-	Ultimate Moment
f_{ckT}	-	Cube compressive strength of geopolymer concrete after exposure to a temperature of T °C
f_{ck}	-	Cube compressive strength of geopolymer concrete at ambient temperature
f_{tT}	-	Split tensile strength of geoplymer concrete after exposure

		to a temperature of T °C
f_t	-	Split tensile strength of geopolymer concrete at ambient temperature
E_{cG}	-	Modulus of elasticity of geopolymer concrete at ambient temperature
E_{cT}	-	Modulus of elasticity of geopolymer concrete at T °C
Pu_{exp}	-	Ultimate load- Experimental
Pu_{th}	-	Ultimate load- Theoretical
T	-	Exposure temperature in °C
Φy	-	Radius of curvature at yield point
Φu	-	Radius of curvature at ultimate stage

TABLE OF CONTENTS

LIST OF TABLES

LIST OF FIGURES

CHAPTER 1

INTRODUCTION

Concrete is one of the widely used manmade construction materials and its consumption is second only to water. Portland cement is the primary cementitious ingredient in concrete.

Production of cement is not only energy intensive, but also responsible for emission of carbon dioxide (CO_2) in large quantity.

It is estimated that, approximately $94.76x10^6$ Joules of energy is required for the production of each ton of cement [1]. Further, the production of one ton of cement releases approximately an equal quantity of CO_2 to the atmosphere [2, 3].

Cement production has increased over the years in developing countries [4]. Statistics shows that with nearly 381 million tons of cement production capacity, India was the second largest cement producer in the world [5] in the year 2013.

The world Earth Summits held in 1992 and 1997 expressed its concern about the unchecked and increased emission of green house gases to the atmosphere. [3].

The quantity of CO_2 produced due to cement manufacturing contributes to about 5% of the total release of CO_2 to the atmosphere [6]. If an alternate material other than OPC is used in concrete, the corresponding CO_2 release to the atmosphere can be reduced.

In India, one of the major sources of material for power generation is coal and it's by product- fly ash- is an environmental threat to the public, if not disposed off properly. Statistics shows that, during the year 2012 -2013, production of fly ash in India was 163.56 Million tons [7].

Only about 38 % of fly ash generated in India is utilized for construction purposes and the remaining quantity is disposed in ash ponds or lagoons. Deposition of the fly ash in storage places can have a negative influence on water and soil because of its

granulometric and mineral composition as well as morphology and filtration properties [8]. Therefore the safe disposal of fly ash is still a major concern.

There are various methods to reduce the consumption of cement in concrete, like the partial replacement of cement with cementitious materials. However, partial replacement of cement with supplementary materials in concrete reduces the release of CO_2 gas only to a limited extent, and a complete replacement is always preferable. Geopolymer concrete is one such material, wherein, a building material (geopolymer) is formed by the process of alkali activation of alumino-silicate materials. The most commonly available alumino-silicate material is fly ash.

So, the use of geopolymer concrete with fly ash as alumino-silicate material not only helps to reduce the release of CO_2 emission (by eliminating the production of cement), but also effectively disposes off fly ash, an industrial waste produced in large quantities.

The research in the area of geopolymer concrete has been gaining momentum since 1990. The study focuses on the influence of various ingredients, like alumino-silicate materials, alkalis etc. on the physical and chemical behaviour of geopolymer concrete.

There are many occasions where concrete is exposed to elevated temperatures like fire exposure, exposure from thermal processes, exposure from furnaces, nuclear exposure, etc.. In such cases, understanding of the behaviour of concrete and structural members exposed to elevated temperatures is vital.

Even though many research reports are available about the behaviour of OPC concrete at ambient temperatures [9, 10, 11], only limited information available is about the behaviour of geopolymer concrete after exposure to elevated temperatures.

The present research work focuses on the influence of different variables on the mechanical properties of geopolymer concrete, both at ambient temperature and after exposure to elevated temperatures, and the flexural behaviour of geopolymer concrete beams after exposure to elevated temperatures.

A brief description of each chapter of the thesis is as follows.

Chapter 1 is the introductory chapter and discusses the need of the present research work and the highlights of the study carried out. A brief out line of each chapter is also presented here.

Chapter 2 presents a review of the published literatures relevant to the area of the present study. The literature review has been grouped in to different areas such as the chemistry of geopolymer; material for making geopolymer; microstructural analysis of geopolymer; factors influencing properties of geopolymer; properties and durability of geopolymer paste, mortar and concrete; shear and flexural strength of geopolymer concrete beams; properties of geopolymer paste; mechanical properties of mortar and concrete after exposure to elevated temperatures (ambient to 800 °C) and flexural behaviour of R.C.C concrete beam after exposure to elevated temperatures. A critical discussion has been presented based on the review of literature carried out. Objectives and scope of the present study have been formulated based on the above discussion and the same is presented in this chapter.

Chapter 3 discusses the physical, chemical and morphological characteristics of various materials used in the study. Methods of casting specimens and testing methods for the determination of different properties of concrete, both at fresh and hardened stage, are presented. Reinforcement details, test set up and loading methods employed for the Push-off and beams specimens are described. The method of heating and cooling of specimens are also presented in this chapter.

Chapter 4 discusses the preliminary study carried out for the selection of a mixture proportion. The important variables considered in the present study include alkali/fly ash ratio, percentage of total aggregate content, fine aggregate to total aggregate ratio, molarity of sodium hydroxide, sodium silicate to sodium hydroxide ratio and curing temperature. The influence of different variables on the engineering properties of geopolymer concrete is presented in this chapter. The study on the interface shear strength of reinforced and unreinforced geopolymer concrete as well as OPC concrete are also presented in this chapter. The conclusion derived based on the above mentioned studies have been presented at the end of this chapter.

Chapter 5 discusses the engineering properties of fly ash based geopolymer concrete after exposure to elevated temperatures (ambient to 800 °C) and compares the corresponding results with those of conventional concrete. Residual compressive strength, split tensile strength, flexural strength and modulus of elasticity of geopolymer concrete after exposure to elevated temperatures has been presented in this chapter. New equations are proposed to predict the residual compressive strength, split tensile strength and modulus of elasticity of geopolymer concrete after exposure to elevated temperatures.

Details of Scanning Electron Microscope analysis for geopolymer mortar and Fourier Transform Infrared analysis, X-ray powder Diffractometer analysis and Thermogravimetric analysis of geopolymer paste at ambient temperature and after exposure to elevated temperature are also presented in this chapter. The cracking behaviour of geopolymer concrete after exposure to elevated temperatures has been studied and this has been compared with that of OPC concrete in this chapter. The conclusion derived based on the above study has been presented at the end of this chapter.

Chapter 6 illustrates the details of experimental study conducted on geopolymer concrete beams after exposure to elevated temperatures (ambient to 800 °C). Load deflection characteristics, ductility and moment-curvature behaviour of the geopolymer concrete beams after exposure to elevated temperatures are discussed in this chapter. The conclusions derived based on the above study are presented at the end of this chapter.

Chapter 7 contains the summary of the studies carried out in the present research work and the major conclusions derived. The scope for future work is also mentioned in this chapter.

****

CHAPTER 2

REVIEW OF LITERATURE

2.1 INTRODUCTION

This chapter contains details of the literature review carried out on the area relevant to the present research work. Review has been carried out on the development of geopolymer paste, mortar and concrete. The important parameters influencing the behaviour of geopolymer concrete such as the source materials, curing temperature, curing time, Si/Al ratio in the mix, alkali concentration and water/solid ratio have been reviewed and discussed here. A review on the behaviour of OPC concrete and geopolymer (GP) concrete after exposure to elevated temperatures are included. A brief review on the behavior of RCC beam under ambient temperature and after exposure to elevated temperatures has been presented. Based on the literature review carried out, the objectives and scope of the work have been defined in this chapter.

2.2 HISTORY OF THE DEVELOPMENT OF GEOPOLYMER

The method of making cementitious materials was known to human civilization even in the 8^{th} century B.C. According to Davidovits, the technique of making a sort of cement paste by dissolution of rocks and using this paste to agglomerate aggregates or/and sands was used during this period for making statues and large stone blocks [12]. According to Davidovits, the large stone blocks used to construct the pyramid of the Pharaoh at Cheops were cast in place with this technique [13]. However, this hypothesis has not been accepted fully by many Jana [14].

Ancient terra-cotta vases of the 7^{th} to 9^{th} century were made of earth and were made by a method of low temperature synthesis (up to 200 °C) on the mixture of clay soils and alkalis **[**15**].** Ancient Roman concrete (an analog of geopolymer concrete) structures like the Coliseo (2000 years old) are still functioning today and thereby could provide historical documentation of the extended durability of geopolymeric cements [16].

Prudon, cited by Torgal [17] carried out investigation on the formation of alkali activated cement (binder) in 1940. The investigator used blast furnace slag as alumino-silicate material and sodium hydroxide as alkali. Since then, alkali activation studies were carried out in different countries but it picked up momentum only in the 1990s. Roy [18] compiled the history of the development of alkali-activated cement and the same is reproduced in Table 2.1.

Table 2.1. History of some important events about alkali-activated binders [18]

Sl.No	Author	Year	Significance
1	Feret	1939	Slag used for cement
2	Purdon	1940	Alkali- slag combinations
3	Glukhovsky	1959	Theoretical basis and development of alkaline Cement
4	Glukhovsky	1965	First called "alkaline cement"
5	Davidovits	1979	"Geopolymer" term indroduced
6	Malinowsky	1979	Ancient aqueducts characterized.
7	Forss	1983	Clinger free cement (slag-alkali-superplsticizer)
8	Langton and Roy	1984	Ancient building materials Characterized
9	Davidovits	1985	Patent of "Pyrament" cement
10	Krivenko	1986	DSc thesis, R_2O- Al_2O_3-SiO_2- H_2O
11	Malolepsy and Petri	1986	Activation of synthetic melilite slags
12	Malek. et al.	1986	Slag cement-low level radioactive wastes forms
13	Davidovits	1987	Ancient and modern concretes compared
14	Deja and Malolepsy	1989	Resistance to chlorides shown
15	Kaushal et al.	1989	Adiabatic cured nuclear wastes forms from alkaline mixtures
16	Roy and Langton	1989	Ancient concretes analogs
17	Majundar et al.	1989	Monocalcium Aluminate – slag activation
18	Talling and Brandstetr	1989	Alkali-activated slag
19	Wu et al.	1990	Activation of slag cement
20	Roy et al.	1991	Rapid setting alkali-activated cements
21	Roy and Silsbee	1992	Alkali-activated cements: an overview
22	Palomo and Glasser	1992	CBC (Chemically bonded cement) with Metakaolin
23	Roy and Malek	1993	Slag cement
24	Glukhovsky	1994	Ancient, modern and future concretes
25	Krivenko	1994	Alkaline cements
26	Wang and Scrivener	1995	Slag and alkali-activated microstructure

Different terminologies have been used by investigators for the products developed using geopolymerization synthesis since 1940s like “soil silicate concrete", "soil cement”, “alkali-activated cement”, “inorganic cement” etc. [19, 20]. However, the most widely accepted terminology is the term “geopolymer”, coined by Davidovits in 1979 [21]. Davidovit selected the name “Geopolymer” because of the similarities with organic condensation of polymers as far as their hydro thermal synthesis conditions are concerned.

2.3 CHEMISTRY OF GEOPOLYMER

Geopolymer is formed by alkali activation of alumino-silicate materials under warm atmosphere. The exact reaction mechanism which explains the setting and hardening of alkali-activated binders is not yet quite understood, although it is thought to be dependent on the prime material as well as on the alkaline activator [17]. Different researchers have proposed slightly different reaction processes for the formation of geopolymer.

Davidovits [22] proposed two stages in the reaction mechanism for the formation of geopolymer, namely the chemical reaction of geopolymeric precursors (like alumino-silicate oxides with alkali silicate forming Monomers - Orthosialate ions) and the exothermal polycondensation of monomers.

According to Davidovits [23] depending on the content of silica and alumina in the source material, there are three types of amorphous to semi-crystalline three dimensional alumino-silicate structures (geopolymer) namely,

- The poly(sialate) type (Si-O-Al-O-)
- The poly(sialate-sil-oxo) type (Si-O-Al-O-Si-O-)
- The poly(sialate-disil-oxo) type (Si-O-Al-O-Si-O-Si-O-)

When the silica and alumina content in the source material is in the ratio of 1:1, the reaction with alkali forms orthosialate. This further reacts with alkali to form polysialate structure. This reaction mechanism is explained in equations 2.1 and 2.2.

$$(Si_2O_5.Al_2O_2)_n + 3nH_2O \xrightarrow{NaOH/KOH} n(OH)_3\text{-}Si\text{-}O\text{-}Al\text{-}(OH)_3^{(-)} \quad \text{-------} \quad (2.1)$$

$$n(OH)_3\text{-Si-O-Al-}(OH)_3 \xrightarrow{NaOH/KOH} (Na,K)\text{-Si-O-Al-O-})n + 3nH_2O \quad \text{---------- (2.2)}$$

(-)

O O

Orthosialate (Na,K)-Polysialate

When the silica and alumina content in the source material is in the ratio of 2:1, the reaction with alkali form orthosialate-siloxo. This further reacts with alkali to form polysialate-siloxo structure. This reaction mechanism is explained in equations 2.3 and 2.4.

$$(Si_2O_5,Al_2O_2)n + nSiO_2 + 4n\ H_2O \xrightarrow{NaOH/KOH} n(OH)_3\text{-Si-O-Al-}(OH)_3 \quad \text{---------- (2.3)}$$

(-)

$$n(OH)_3\text{-Si-O-Al-}(OH)_3 \xrightarrow{NaOH/KOH} (K\text{-Na})\text{-(Si-O-Al-O-Si-O-)}_n + 4n\ H_2O \quad \text{----------(2.4)}$$

O O O

Ortho(sialate-siloxoxo) (Na,K)-Polysialate-siloxo

When the silica and alumina content in the source material is in the ratio of 3:1, due to the action of alkali on alumino-silicate material, ortho-sialate and di-siloxonate are initially formed. They further undergo polycondensation and forms polysialate di-siloxo. This reaction mechanism is explained in equation 2.5

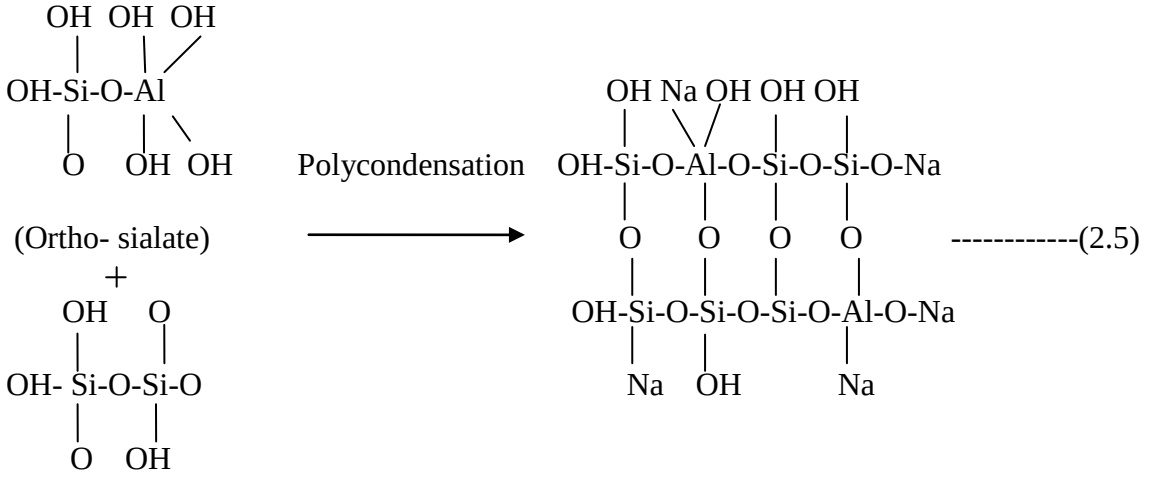

----------(2.5)

Xu et al. [24] proposed a three step reaction mechanism for the formation of geopolymer

- Dissolution of Si and Al atoms from the source material through the action of hydroxide ions and thus form precursor ions.
- Condensation of precursor ions into monomers.
- Polycondensation /polymerization of monomers into polymeric structures.
- Following reaction scheme has been proposed by them for the polycondensation process of geopolymerization from minerals:

Al-Si materials +MOH (aq)+ Na_2SiO_3 (aq) ----------(2.6)

↓

Al-Si materials +[$M_z(AlO_2)_x(SiO_2)_y$.nMOH.mH_2O] gel ----------(2.7)

↓

Al-Si materials +[$M_a(AlO_2)_a(SiO_2)_b$.nMOH.mH_2O] ----------(2.8)

(Geopolymers with amorphous structure)

Weng and Sagoe-Crentsil [25] presented the chemistry associated with the formation of geopolymer system having low Si/Al ratio, generally referred to as poly (sialate) geopolymer system. He also proposed three steps during the formation of geopolymer namely dissolution, hydrolysis and condensation.

He has represented the dissolution and hydrolysis process as follows.

$Al_2O_3 + 3H_2O + 2OH^- \longrightarrow 2Al(OH)_4^-$ ----------(2.9)

$SiO_2 + H_2O + OH^- \longrightarrow [SiO(OH)_3]^-$ ----------(2.10)

$SiO_2 + 2OH^- \longrightarrow [SiO_2(OH)_2]^{2-}$ ----------(2.11)

These reactions show that H_2O molecules and OH^- iron are consumed with continuous dissolution.

During the condensation reaction between $Al(OH)_4^-$ and $[\ SiO(OH)_3]^-$, the $[Al(OH)_4]^-$ and $[\ SiO(OH)_3]^-$ species are linked to each other by the attraction between one of the OH groups from $[\ SiO(OH)_3]^-$ and Al ion of $[Al(OH)_4]^-$, which results in an intermediate complex (Alumino-silicate hydrates). The two OH group in the intermediate complex then condense to form an alumino-silicate species by releasing H_2O molecules. The following equation explains this condensation reaction.

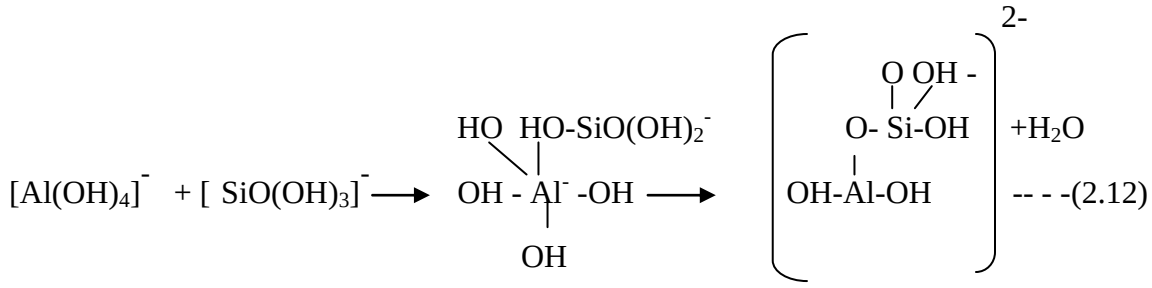

However the most widely accepted mechanism consists of three reaction stages namely dissolution, hydrolysis and polycondensation [24- 26].

The reaction mechanism for the formation of geopolymer and molecular structure are entirely different from the reaction mechanism during the hydration of portland cement and the molecular structure of the hydrated cement.

The chemical structure of the geopolymer is three dimensional and amorphous [27]. Fig. 2.1 shows the coordination mechanism of oxygen atom with silica iron as proposed by Davidovits. With the short setting and hardening time, geopolymers are formed with tightly packed polycrystalline structures [24].

On the other hand the main constituents in hydrated cement paste are calcium silicate hydrate, Calcium hydroxide and ettringite. About 60% of the hydrated cement is C-S-H [28]. Figure 2.2 shows the model of C-S-H in which the blue and white spheres are oxygen and hydrogen atoms of water molecules, respectively; the green and gray spheres are inter and intra-layer calcium ions, respectively; yellow and red sticks are silicon and oxygen atoms in silica tetrahedra.

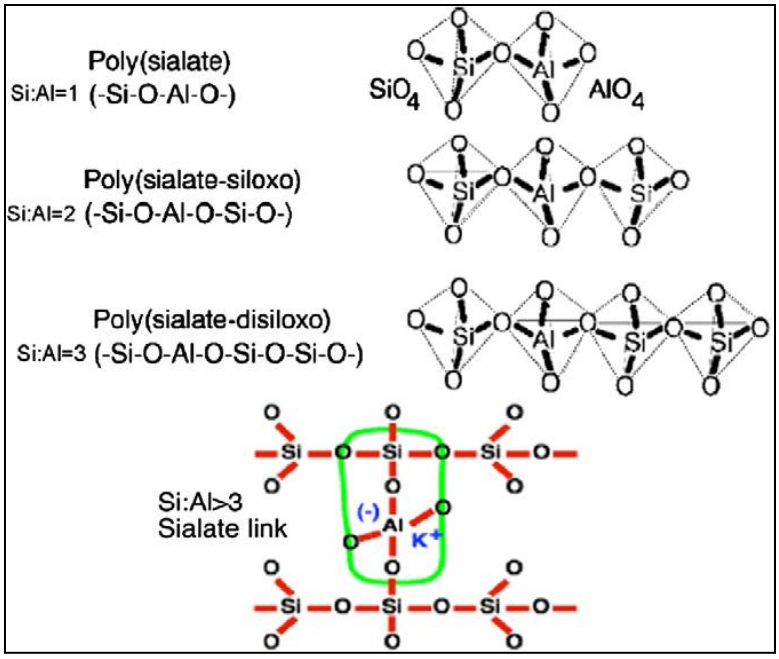

Fig. 2.1. Coordination mechanism of oxygen atom with Si^{4+} and Al^{4+} [27]

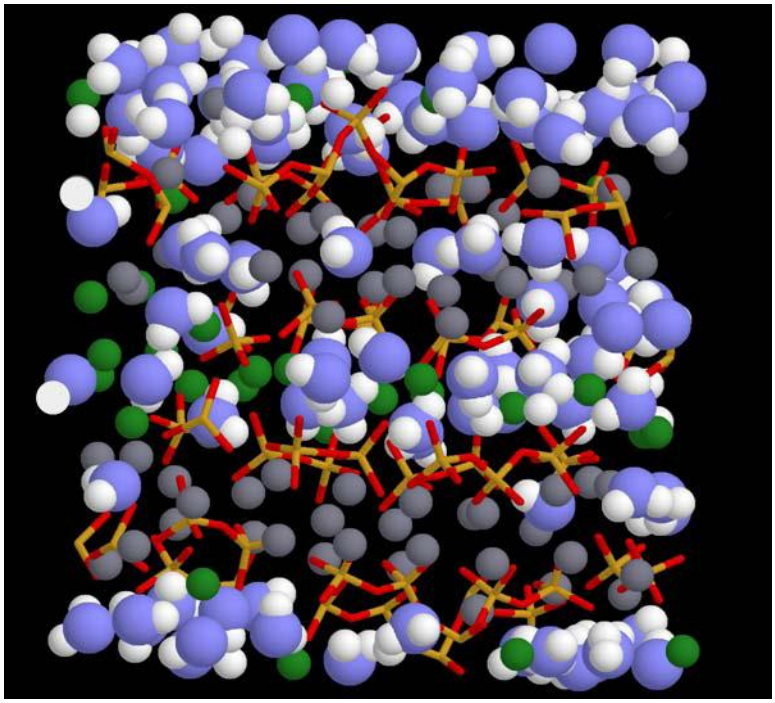

Fig. 2.2. Model of C-S-H molecule [29]

.

2.4 MATERIALS FOR MAKING GEOPOLYMER

Two types of materials are required to make a geopolymer. One is the source material containing alumina and silica and other is an alkali that activates the polymerization reaction.

The source materials (alumino-silicate) may be natural minerals, such as kaolinite, calcined kaolinite (metakaolin) and clays [23, 24, 30, 31]. Alternatively, industry waste products such as fly ash, slag, red mud, rice-husk ash and silica fume may be used as source material for the synthesis of geopolymers [32-39].

The source material should be amorphous and degree of polymerization mainly depends on the degree of amorphosity and fineness of alumin-osilicate materials.

Kaolinite is a clay mineral having the chemical composition $Al_2Si_2O_5(OH)_4$. Rocks that are rich in kaolinite are known as kaolin or china clay. Metakaolin is manufactured by the dehydration of kaolinite at temperature ranging between 550 °C to 900 °C. Other clay minerals containing oxides of alumina and silica are also used as source material for making geopolymer [40].

Fly ash is an industrial waste produced in Thermal power stations where coal is used as the fuel. Slag is formed in blast furnace during the manufacturing process of iron from its ore. Red mud is an industrial waste produced in Aluminium manufacturing industry where Bauxite is used as the raw material. Rice Husk is produced by the controlled burning of raw rice husk. Silica fume is a byproduct of producing silicon metal or ferrosilicon alloys.

The alkali component used as an activator is a compound from the elements of the first group in the periodic table. The common activators are NaOH, Na_2SO_4, water glass, Na_2CO_3, K_2CO_3, KOH, K_2SO_4 or a little amount of cement clinker and complex alkali component [41].

For the preparation of the alkali solution a single alkali type or a mixture of different alkalis can be used. The most commonly used alkali for the manufacture of geopolymer is a mixture of the solutions of NaOH or KOH and Na_2SiO_3 [42, 43].

2.5 GEOPOLYMER PASTE

Xu and Van Deventer [40] conducted a study on the geopolymerisation of alumino silicate materials. They used 15 natural Al-Si minerals for their research. Those minerals were Almandine (ortho-di and ring silicate), Sillimanite, Andalusite, Kyanite, Pumpellyite (Garnet group), Spodumene, (chain silicate), Lepidolite (sheet silicate), Illite (mica group), Celsian (claygroup), Sodalite (FeldsparGroup), Hydroxyapophyllite, Stilbite, Heulandite (Sodalite group), Anorthite (Zeolite group). They used NaOH and KOH solutions as alkalis. The specimens were temperature cured at 35 °C for 72 hours.

They observed that, the extent of dissolution depended on the type of alumino-silicate material and the type of alkali used. They also found that the compressive strength of geopolymer pastes made using different composition, are influenced by the percentage of sodium and potassium hydroxides and Si to Al ratio. Stilbite, in the presence of potassium hydroxide showed maximum compressive strength of 18MPa. They concluded that, all natural alumino-silicate materials could be used for making geopolymer.

Duxson et al. [42] have carried out investigation on geopolymer made using metakaolin and alkaline liquid. For this purpose sodium silicate solution with the composition SiO_2/M_2O (M is N_a or K) 0.0, 0.5, 1.0, 1.5, 2.0 were prepared by dissolving amorphous silica in the alkali hydroxide solution. Samples of 25mm diameter and 50mm length were cured for 20 hours at 40 °C. They reported that there is a rapid increase in the compressive strength and Young's modulus of geopolymer with increase in Si/Al ratio up to1.9 whereas, the specimen with Si/Al ratio 2.15 exhibited a reduced strength and modulus of elasticity.

Based on SEM microstructure analysis, they suggested that, there is a change in the microstructure of GP paste for Si/ Al ratio between1.4 and 1.65. Specimen with Si/Al ratio $\leq$ 1.4 exhibited a microstructure comprising large interconnected pores loosely structured precipitate and unreacted materials. Geopolymer with Si/Al ratio $\geq$1.65 had a better homogenous binder containing smaller isolated pores a few microns in size. The improvement in microstructure homogeneity in the latter case was due to the presence of a large concentration of soluble silica in the activating solution. They suggested that, the change in pore size, distribution and change in the microstructure homogeneity explain

the reason for the change in the mechanical properties of a geopolymer paste. Finally they have concluded that, the Si/Al ratio influences the microstructure of GP paste and thereby the mechanical properties.

Duxson et al. [43] reported the effect of the type of cation used and the Si/Al ratio on the compressive strength and Young's modulus of metakaolin based geopolymer with mixed alkali type (sodium and potassium at different proportion) and Si/Al ratios. Sodium silicate solution with composition SiO_2/M_2O (M is N_a or K) 0.0, 0.5, 1.0, 1.5, 2.0 were prepared and NaOH, KOH and a mixture of both were used for making the geopolymer. In this study Si/Al ratio selected was 1.15, 1.4, 1.65, 1.9 and 2.15. The samples were cured for 20 h at 40 °C. They reported that, after 28 days, the compressive strength of mixed alkali specimens with Si/Al ratio $\geq$ 1.95 was increased by up to 30% compared to the specimen made with a single alkali. The specimen with Si/Al ratio $\leq$1.4, the mixed alkali specimen exhibited a reduced Young's modulus compared to Na and K specimen, whereas the specimen with Si/Al ratio $\geq$ 1.65 the mixed alkali specimen gave maximum Young's modulus. They concluded that, the type of cation used and its concentration influence the compressive strength and Young's modulus and that, the mixed cation yields a higher compressive strength and Young's modulus compared to that of the single cation.

Temuujin et al. [44] studied the effect of the mechanical activation (reduction of particle size) of fly ash on the properties of the geopolymer, cured at ambient temperature. Raw fly ash having the median size 14.4 μm and milled fly ash having the median size 6.8μm were used in the investigation. They used Na_2SO_3 solution and 14 molar NaOH solution for making GP specimens. Samples were cured for 20 h at room temperature. They obtained a 28^{th} day compressive strength of 16 MPa and 45 MPa for unmilled and mechanically activated fly ash based samples respectively. They concluded that, the contribution to the increased compressive strength of the geopolymer is due to the reduction of particle size and this change in the morphology (Phase change) of the fly ash used, causes higher dissolution rate of the fly ash particle.

Xu and Deventer [45] studied the effect of the structural and surface properties of source materials on geopolymerization. In their work, kaolinite, albite, and fly ash were chosen as alumino-silicate source materials. Alkaline potassium and silicate solutions

were used for the study. Samples were cured for 24 h at 40 °C. X-ray diffraction, X-ray fluorescence, X-ray photoelectron spectroscopy, ^{27}Al and ^{29}Si magic-angle spinning nuclear magnetic resonance (MAS NMR) spectroscopy, and scanning electron microscopy (SEM) were used to study the effect of source materials on geopolymerization. They observed that, the fly ash that has an amorphous structure and possesses the lowest binding energies in its structure showed the highest reactivity during geopolymerization and thereby more compressive strength. The content of K and Ca in the gel also influences the geopolymerization and the compressive strength. They observed a higher geopolymerization in mixtures of two or three source materials (both alumino- silicate and alkalis) compared to that of a single source material.

Diaz et al. [46] studied the behavior of geopolymer paste using two types of "class F" fly ash and three "class C" fly ash obtained from different sources. NaOH and Na_2SiO_3 solution were used as alkali. Samples were cured for 3 days at 60 °C. Chemical, X-ray diffraction (XRD) and particle size distribution (PSD) analyses were performed on the fly ash samples. Geopolymer paste was analyzed using XRD and Raman spectroscopy. In addition, setting time and compressive strength tests were performed on geopolymer concrete specimens. NaOH solution and Na_2SiO_3 solution with a 1:1 ratio was used for the study. It was reported that of the behaviour of fresh mixture and the mechanical properties of the hardened matrix were mainly influenced by three factors; the chemical, crystallographic and physical properties of the fly ash. They observed a positive influence of CaO content on the compressive strength. However high CaO content causes rapid setting (less than 3 minutes).

Pozzolanic material-based geopolymer has been proposed by Verdolotti et al. [47] as a solving methodology to the geohazards, due to pozzolanic collapsible soils widely present in South Italy. Pozzolanic material was activated by 10 molar NaOH or slurry of $NaAlO_2$ in 10 molar NaOH solutions for the geopolymer synthesis. The specimens were cured at 25 °C for a period varying from 7 days to one year. The effect of the two activation methods on the properties of the geopolymer was investigated by means of X-ray diffraction, scanning electron microscopy (SEM), FTIR spectroscopy, nuclear magnetic resonance (^{27}Al and ^{29}Si NMR) and uniaxial compression tests. They concluded that, the amorphous and crystalline phases were formed after the geopolymerisation. The

geopolymeric reactions occurred mainly at the surface of the pozzolana particulates. Furthermore, the compressive strength increases gradually upon the curing time and the maximum compressive strength of 42 MPa (for geopolymer made using slurry of $NaAlO_2$ in 10 molar NaOH solution) was observed after a curing period of 1 year.

Yunfen et al. [48] investigated the influence of concentration and modulus of sodium silicate (SiO_2/Na_2O) and curing mode on the phase composition, microstructure and strength development in the geopolymer prepared using Class F fly ash. Different curing modes were used for temperature curing: room temperature, 50 °C, 65 °C and 80 °C for 1, 2, 3, 6,7 and 28 days. They observed an increase in the compressive strength of the geopolymer paste with an increase in the modulus of sodium silicate solution (SiO_2/Na_2O) up to 1.4 beyond which it decreased. They suggested that, one day pre-curing at ambient temperature increases the compressive strength by about 50%.

Further, the FTIR spectra of alkali activated fly ash samples showed an increase in chain length and more alumino-silicate gel formation for the sample pre-cured for one day before temperature curing.

From the XRD of geopolymer, cured in different modes, they observed that, the geopolymers prepared using Class F fly ash and sodium silicate solutions were amorphous. However the crystalline compounds initially present in the fly ash like Quartz, mullite and hematite have not undergone dissolution process during the reaction.

Reaction kinetics and mechanism of geopolymers were studied by Rahier et al. [49]. For their study, dehydrated kaolinite at 700 °C (alumina-silicate) and silicate solution (SiO_2/R_2O = 1.4 where R is either Na or K and H_2O/R_2O = 10.0) were used. For the study of the influence of H_2O/R_2O ratio on the reaction rate, sodium silicate solution with SiO_2/R_2O ratio1.4 was used. To study the influence of SiO_2/R_2O on the reaction rate, sodium or potassium silicate solution were used with H_2O/R_2O =10. The Al/R ratio was always set to one. They observed that, the dissolved silicate concentration decreases from the beginning of the reaction. Further they noted that the setting time of the reaction mixture increases with increase in SiO_2/R_2O ratio and that the reaction is slower for metakaolin potassium silicate based system compared to sodium silicate based system. They observed that for a particular value of H_2O/R_2O ratio, the reaction rate is maximum in the case of the sodium silicate system.

Li and Liu [50] conducted study on the influence of slag on compressive strength of class F fly ash based geopolymer. NaOH and Na_2SiO_3 solutions were used as alkali. Curing was done at room temperature for 24 hours. From the study, they observed that the addition of slag significantly increases the compressive strength of geopolymer. The mechanism of slag as additive on the enhancement of the compressive strength of geopolymers was investigated using X-Ray diffractometre (XRD), Fourier Transform Infrared Spectroscopy (FTIR), X-Ray photoelectron spectroscopy (XPS) and Mercury intrusion porosimetry (MIP). From their XRD and FTIR results they observed that, the addition of slag could generate more amorphous product and accelerate the reaction rate of the raw material resulting in an increase in its compressive strength. From the XPS analysis they observed a binding energy and broadening of peak for Si 2*p*, Al 2*p* and O 1*s* element due to the Ca^{2+} provided by slag. From the result of MIP they suggested that, 4% slag addition improves the pore structure of the geopolymer and enhances its compressive strength.

Sing et al. [51] conducted a study on geopolymers by ^{29}Si and ^{27}Al MAS NMR, in an attempt to understand polymer structural details. They used Metakaolin, Sodium hydroxide solution and sodium silicate solution for the preparation of the geopolymer. The samples prepared were cured at room temperature for different duration. From the experimental result, they suggested that the geopolymer structure is a complex network consisting of chains, sheet-like and three dimensional networks made up of various Q unit (different bridging oxygen) types of connected SiO_4 and AlO_4 tetrahedra. They also suggested that geopolymerisation occurs in a distinct compositional region. At high alkalinity [>30% (mol/mol) overall Na_2O content], connectivity of silicate anions was reduced, which cause poor polymerization. At low alkalinity [(<10% (mol/mol) overall Na_2O content], unreacted metakaolin was observed.

Papakonstantinou and Balaguru [52] studied the flexural fatigue behaviour of a carbon geopolymer composite and compared its performance with composites made with other types of organic and inorganic matrices (made by other researchers).

They observed that, the performance of the carbon-geopolymer composite under fatigue loading is similar to that of other composite materials.

Giancaspro et al. [53] studied the fire performance of balsa sandwich panels made using inorganic geopolymer resin and high-strength fiber facings. A thin layer of a fire-resistant paste composed of geopolymer and hollow glass microspheres was applied to the facings to serve as a protective fire barrier and to improve the fire resistance of the sandwich panels. Using 17 sandwich panel specimens, the primary objective of this program was to establish the minimum amount of fireproofing necessary to satisfy the Federal Aviation Administration (FAA) requirements for heat and smoke release. The influence of this fireproofing insulation on the increase in mass of the panels was also evaluated. They concluded that a 1.8-mm-thick layer of fireproofing with geopolymer resin satisfies the FAA requirements for both heat release and smoke emission

Sindhunata et al. [54] studied the leaching, pore network alteration and gel crystallization of geopolymers. They used Class F fly ash as alumino-silicate material. Activating solutions were prepared by mixing potassium hydroxide or sodium hydroxide with water and commercial silicate solutions. The concentration of alkali and silicate in the activating solution was expressed in terms of the H_2O/M_2O and SiO_2/M_2O ratios, (M is Na or K). The H_2O/M_2O ratio was kept constant at 14.85, while the SiO_2/M_2O ratio varied (0.0, 0.2, and 0.79). Geopolymer specimens were cured at 50 °C for 24 h. The demoulded geopolymer specimens were immersed in various alkali and carbonate solutions (at room temperature) namely NaOH, KOH, Na_2CO_3, and K_2CO_3, as well as distilled water. They observed that in alkaline hydroxide or carbonate solutions with up to pH 14 have little effect in terms of leaching of Si and/or Al species, pore network alteration, or gel crystallization. More concentrated hydroxide solutions lead to a more significant extent of leaching, as well as the collapse of the geopolymer gel structure and the formation of detectable quantities of crystalline zeolites. Immersion in water does not show significant leaching of Si or Al species.

Bakharev [55] had conducted durability test on geopolymer paste made using class F fly ash and three type of activating solutions, namely sodium silicate, sodium hydroxide and a mixture of sodium hydroxide and potassium hydroxide. The mixtures were cured for 24 h at room temperature; after that, the mixtures were heated to 95 °C and cured at this temperature for 24 h. Three tests were used to determine the resistance of the geopolymer materials. The tests involved immersions for a period of 5 months into

5% solutions of sodium sulphate, 5% magnesium sulphate solution, and a solution of 5% sodium sulphate and 5% magnesium sulphate. He compared the test result with OPC specimen. The evolution of weight, compressive strength, products of degradation and microstructural changes were studied. It was concluded that when immersed in sodium sulphate solution, the specimen prepared with sodium silicate solution and mixture of sodium hydroxide and potassium hydroxide experienced a strength reduction of 18% and 65% respectively. However a strength increase of 4% was observed in the specimen made using sodium hydroxide. On the other hand, when immersed in the magnesium sulphate solution, 12% and 35% strength increase was observed in the specimens made using sodium hydroxide solution and mixture of sodium hydroxide and potassium hydroxide solutions, respectively and a strength decline of 24% was noticed in samples made using sodium silicate solution. When immersed in the solution of 5% sodium sulphate and 5% magnesium sulphate, he observed a strength gain of 12% and 10% respectively in specimens prepared using sodium hydroxide solution and mixture of sodium hydroxide and potassium hydroxide solution, while a strength loss of 4.5 % was noticed in specimen prepared using sodium silicate solution. The material prepared using sodium hydroxide had shown the best performance. In all solution, OPC specimen experienced strength loss. He observed a weight loss between 0.4% and 5.3 % in geopolymer specimen, while a weight loss between 3.2% and 5.3% in OPC specimens. Finally he concluded that geopolymer specimens prepared with sodium hydroxide were more stable in sulphate solutions than specimens prepared using sodium silicate or mixture of sodium and potassium hydroxide solutions, and OPC specimens.

2.6 GEOPOLYMER MORTAR

Ravindra et al. [56] reported results of an experimental study on the development of the compressive strength and microstructure of geopolymer paste and mortar. Specimens were prepared by thermal activation of Indian fly ash with sodium hydroxide and sodium silicate solutions Curing temperature adopted ranged from 45 °C to 120 °C and curing period from 48 hours to 28 days. They observed that, the alkali content, silica content, water to geopolymer solid ratio and sand to fly ash ratio of the geopolymer mix, and changing processing parameters such as curing time and curing temperature are the

influencing factors on compressive strength and formation of geopolymer microstructure. They observed the formation of new amorphous alumino-silicate phase such as hydroxysodalite and herschelite after the geopolymerisation, which influences the development of compressive strength.

Chindaprasirt et al. [57] reported the experimental study on high strength geopolymer using fine high calcium fly ash. The effect of fly ash with different particle size on the setting time of geopolymer paste, workability, strength development and drying shrinkage of geopolymer mortars made from classified fine high calcium fly ash were investigated. Sodium hydroxide (NaOH) and sodium silicate were used as alkali. Different curing regimes were employed for making the mortar specimen (35 °C to 90 °C for 1 day to 5 days). It was observed that, the geopolymer paste with finer fly ash set faster than that with a coarser particle and the particle size and shape has a dominant influence on the workability of the geopolymer mortars. The effect of delay time (before heat curing) on the strength development of geopolymer mortars is dependent on the fineness of the fly ash. The more the fineness, the lesser the delay time needed for optimum strength development.

Further, they observed that, the high calcium fly ash based geopolymer mortar continues to gain strength when kept in normal atmospheric condition after the initial heat curing period.

García-Lodeiro et al. [58] evaluated the performance of low-calcium fly ash-based geopolymer mortars in the context of an alkali-aggregate reaction. An 8 molar solution of NaOH was used as the activator to make the fly ash mortar. Three series of specimens were prepared. The first series contained 100% siliceous aggregate, the second 100% opal aggregate and the third a combined siliceous and opal aggregate mix in a proportion of 90:10 by weight. The mortar specimens were cured at 85 °C for 24 hours. OPC mortar specimens were also prepared for comparing the test result. They observed that fly ash-based geopolymer systems are less likely to generate expansion by alkali-silica reaction than the portland cement system. The authors suggested that, the expansive nature of the gel is due to the presence of calcium in the materials.

Test result of 16 alkali activated geopolymer mortar samples and a control ordinary Portland cement (OPC) mortar cured under room temperature were presented by

Yang and Song [59]. Both fly ash and ground granulated blast-furnace slag (GGBS) as the source material were activated independently by a combination of sodium silicate and sodium hydroxide powders. The specimens were cured at room temperature for a period from 1 day to 90 days. The main variables examined were the mixing ratio of sodium oxide (Na_2O) of the activators to source material by weight, and the fineness of the GGBS. The flow loss, compressive strength development, hydration products and microstructural characteristics of the geopolymer pastes sampled from geopolymer mortars were investigated to evaluate the effect of the type and fineness of source material on the compressive strength of the geopolymer mortar. They concluded that, the flow of different mortar decreases linearly with time and the rate of flow loss of the geopolymer mortar is higher than that of control OPC mortar. Further initial flow (at zero time) of the geopolymer mortar decreased with increase of alkali SiO_2/Na_2O and increase of fineness of source material.

Li et al. [60] conducted test on geopolymer composites (sand mortar reinforced with short polyvinyl alcohol fibers). They observed that there is a good bond between fiber and geopolymer mortar and that on the addition of fiber the ductility of the geopolymer mortar increased.

Experimental investigation was carried out by Thokchom et al. [61] to study the effect of alkali content in geopolymer mortar specimens after exposure to sulphuric acid. Geopolymer mortar specimens were made from Class F fly ash by activation with a mixture of sodium hydroxide and sodium silicate solution containing 5% to 8% Na_2O. Specimens were cured at 85 °C for 48 hours. Durability of specimens were assessed by immersing them in 10% sulphuric acid solution and periodically monitoring surface deterioration and depth of dealkalization, changes in weight and residual compressive strength over a period of 24 weeks. Microstructural changes in the specimens were studied with Scanning electron microscopy (SEM) and EDAX. They observed that, the alkali content in the activator solution significantly affects the durability of fly ash based geopolymer mortars exposed to sulphuric acid. Specimens made with higher alkali content performed better than those with lower alkali content.

Fernando et al. [62] reported the acid resistance and abrasion resistance of alkali activated Tungsten Mine Waste Mud mortar. Tungsten Mine Waste used in this study

was subjected to a thermal treatment at 950 °C for 2 hours. Tungsten Mine Waste and calcium hydroxide were mixed with a mass ratio of 5:1. Sodium hydroxide and sodium silicate solution were used with a mass ratio of 1:2.5 as activator. The fresh mortar was cast and allowed to set at room temperature for 24 hours before being removed from the moulds and kept at a room temperature of 20 °C until tested in compression. Acid resistance was tested by submerging samples in solutions of sulfuric acid, nitric acid, and hydrochloric acid. Abrasion resistance was assessed by the mass loss of cubic specimens when subjected to 1,000 rotations with the Los Angeles apparatus test machine. They observed that, the Tungsten Mine Waste mortar binders possessed higher acid and abrasion resistance than OPC based concrete mixtures.

2.7 GEOPOLYMER CONCRETE

Hardjito et al. [63] investigated the influence of the alkali activator solution, curing temperature, curing time, age of curing and water content on the compressive strength of geopolymer concrete. Shrinkage, creep and sulphate resistance in geopolymer concrete were also investigated. They used class F fly ash, Na_2SiO_3 and NaOH solution for making geopolymer. They used 8 molar and 14 molar NaOH solutions and considered the ratio of Na_2SiO_3/NaOH as 0.4 and 2.5. Specimens were cured at 30 °C to 90 °C for 3 hours to 100 hours. They observed that the molarity of NaOH, the ratio of Na_2SiO_3/NaOH, and curing temperature influences the compressive strength of GP concrete. Further, they observed a decrease in compressive strength when water content decreases. They also observed a low drying shrinkage, creep strain and high sulphate resistance for GP concrete at water content corresponding to maximum compressive strength.

Reddy et al. [64] conducted test on Geopolymer concrete prepared using low lime based fly ash and a mixture of sodium hydroxide and sodium silicate solution. They observed an increase in compressive strength and decreased workability with increased molarity of NaOH solution.

Fernández-Jiménez et al. [65] reported the result of experimental research on engineering properties of alkali-activated fly ash concrete (geopolymer concrete) and concrete made with Ordinary Portland Cement (OPC). Two different type of alkaline solution, namely 8 molar NaOH (first solution) and mixture of 85% of NaOH (8 molar)

solution and 15% of Na_2SiO_3 solution (second solution) were used for making geopolymer concrete. Coarse aggregate (6 to 12 mm), river sand, first solution / the fly ash ratio 0.4 and second solution/ fly ash ratio 0.5 were used in geopolymer. All GP concrete specimens were cured at temperature of 85 °C for 20 hours. They observed that, GP concrete with mixed alkali solution gives more strength than that with single alkali. They further observed that bond strength of GP concrete is better than that of OPC concrete.

Sarker [66] investigated bond strength of Fly ash based GP concrete and compared the test result with that of OPC concrete. He concluded that, bond strength of GP concrete is better than that of OPC concrete and further, he suggested that the existing analytical expressions for bond strength of OPC concrete can be conservatively used for predicting the bond strength of GP concrete.

Borges et al. [67] used the Andreasen particle packing method, commonly used for ceramic materials, to improve the geopolymer formulations studied on the development of microconcretes. Based on the study on mechanical strength, porosity and apparent density parameters, they concluded that the Andreasen method may be used to change the rheology and to develop GP concrete for different application.

Sofi et al. [19] conducted test on geopolymer concretes and compared the test result with Australian code recommendations for OPC concrete. The study included, determination of the modulus of elasticity, Poisson's ratio, compressive strength, and the splitting tensile strength and flexural strength of geopolymer concrete, formulated using three different sources of Class-F fly ash. Sodium carbonate (Na_2CO_3), sodium silicate (Na_2SiO_3), and sodium hydroxide (NaOH) were used as alkali solution. Specimens were steam cured for 24 hours. 14 mm single-size angular shaped Basalt crushed rock and granulated blast furnace slag were used as aggregates. They observed that, in most cases, the engineering properties of GP concrete compare favorably to those predicted by the relevant Australian Standards for OPC concrete mixtures.

Vora and Deve [68] evaluated the effect of various parameters affecting the compressive strength of geopolymer concrete. Class F fly ash and mixture of Na_2SiO_3 and NaOH solutions were used for making geopolymer. River sand and crushed aggregate were used for making concrete. Specimens were heat cured in an oven at

different temperatures and for different time periods. Parameters like ratio of alkaline liquid to fly ash, concentration of sodium hydroxide, ratio of sodium silicate to sodium hydroxide, curing time, curing temperature, dosage of superplastiziser, rest period and additional water content in the mix were considered in this study. It was reported that, the compressive strength increases with increase in the curing time, curing temperature, rest period, concentration of sodium hydroxide solution and decreases with increase in the ratio of water to geopolymer solids by mass and admixture dosage. The addition of naphthalene based superplastiziser improves the workability of fresh geopolymer concrete. It is further observed that the water content in the geopolymer concrete mix plays a significant role in achieving the desired compressive strength.

Wongapa et al. [35] used a mixture of fly ash and rice husk ash to produce geopolymer concrete. They used a fixed SiO_2/Al_2O_3 ratio in their study by keeping the ratio of fly ash to rice husk ash at 80:20 by weight. Sodium hydroxide solution and sodium silicate solution were used as alkali. Compressive strength, modulus of elasticity, and water permeability of the GP concrete were determined at specified intervals up to 90 days. They have reported that Si/Al ratio and p/Agg. ratio (p= alkali +fly ash) influence the compressive strength, modulus of elasticity, and water permeability of GP concrete. Higher Si/Al ratios and higher p/Agg. ratios result in lower compressive strength and higher water permeability. For the same compressive strength, the water permeability coefficient of GP concrete is much higher than that of conventional concrete. The differences in water permeability become smaller when the compressive strength is higher.

Ravikumar et al. [69] reported the influence of the concentration of the alkali and alkali to binder ratio on the compressive strength, pore structure features, and microstructure of geopolymer concretes containing source material as either Class F fly ash or ground granulated blast furnace slag (GGBFS). NaOH solution of 8 molar concentration was used as the activating agent. The coarse aggregate (9.5mm maximum size) to fine aggregate ratio by mass was approximately 1:1 for all concrete mixes. The specimens were heat cured at 70 °C for 48 hours. They have observed maximum compressive strength in geopolymer concrete when the source material used was 18% by volume of concrete in the case of fly ash and 25% in the case of GGBS. Higher porosity

was observed at higher alkali to binder ratio. More unreacted particles were observed in microstructure of geopolymer made using 4 molar NaOH than in geopolymer made using 8 molar NaOH.

Yang et al. [70] presented results of test conducted on geopolymer concrete (alkali activated concrete) made using Hwangtoh (alumino-silicate material) calcium hydroxide (alkali). Specimens were cured at room temperature. The main variables investigated were the water-binder ratio and fine aggregate–total aggregate ratio to ascertain the reliable mixing design of hwangtoh-based cementless concrete. They observed that, the mechanical properties of hwangtoh-based concrete are significantly influenced by the water binder ratio and to a less extent by fine aggregate–total aggregate ratio. Based on the measured mechanical properties and code provisions, they suggested that the hwangtoh-based alkali-activated concrete could be used as a structural concrete when the water-binder ratio is less than 40%.

Sumajouw and Rangan [71] presented research report on the experimental study of flexural behavior of fly ash based geopolymer concrete beam. In this study, the low-calcium (ASTM Class F) fly ash was used as the base material. A combination of sodium silicate solution and sodium hydroxide solution was used as the alkali solution. Beams of size 200 mm x300 mm x 3000 mm were designed to fail in a flexural mode. Four different tensile reinforcement ratios were used. The specimens were tested under monotonically increasing four point load until failure. They observed that the load deflection characteristics, crushing pattern and failure patterns of GP concrete beams are similar to those of conventional OPC concrete beams.

Dattatreya et al. [72] conducted a study on the flexural behaviour of reinforced GP concrete beam and the results were compared with that of the R.C.C. beam. They used fly ash and a mixture of sodium silicate and sodium hydroxide for making the geopolymer. They used beams of size 1500 mm x 100 mm x 150 mm. They found that the load carrying capacity of most of the GP concrete beams were marginally more than that of the corresponding conventional R.C.C concrete beams. The deflections at different stages including service load and peak load stage were higher for GP concrete beams. However, the ductility factor was comparable to that of R.C.C beams. They suggested that, the conventional RC theory could be used for reinforced GP concrete flexural beams

for the computation of moment capacity, deflection, and crack width within reasonable limits.

Jeyasehar et al. [73] reported details of flexural strength test conducted on four GP concrete beams and one OPC concrete beam. Fly ash and a mixture of NaOH and Na_2SiO_3 solutions were used for making geopolymer concrete beams. River sand as fine aggregate and crushed rock as coarse aggregate was used for making GP beams. The beams were cured at temperature of 60 °C for 24 hours. The size of the beams used for the study was 3200 mm x 150 mm x 250 mm. They compared the moment curvature behaviour of all the beams and compared them with the theoretically calculated moment curvature relationship of R.C.C. beams. They observed that, the moment curvature relationship of all the geopolymer concrete beams is close to the values calculatedfor RCC beams.

Sumajouw et al. [74] carried out an experimental study on the behavior and strength of reinforced geopolymer concrete column subjected to uniaxial bending. Fly ash, sodium silicate, sodium hydroxide, coarse aggregate (10 mm to 7 mm size) and river sand were used to cast the column specimen of size 175 mm x 175 mm x 1500 mm. 12 mm deformed bars were used to make two types of column with 1.42% and 2.95% of steel. They observed that, the load capacity of columns correlate well with the value calculated using a simplified stability analysis as well as agree well with the value calculated using the design provisions contained in the Australian Standard (AS3600) and American Concrete Institute Building Code (ACI 318–02).

Chang [75] reported the shear behavior and bond behavior of reinforced fly ash based geopolymer concrete. He used fly ash as the source material, sodium silicate and sodium hydroxide as alkali, 20 mm nominal size coarse aggregate and sand were used to make geopolymer concrete. He used 200 mm x 300 mm x 2000 mm size beam specimen for shear study and 200 mm x 300 mm x2500 mm size beam specimens, reinforced with 2 no. of 16 mm, 20 mm, and 24 mm diameter steel for bond study. He has reported that the modes of failure and crack patterns of GP concrete specimens are similar to portland cement concrete beams.

Maranan et al. [76] studied the bond characteristics between geopolymer concrete and FRP reinforcement. Geopolymer concrete was composed of alkali-activated fly ash,

ground granulated blast-furnace slag, gravel, and sand. The compressive strength of geopolymer concrete was 33MPa. The effects of parameters such as bar diameter (12.7 mm, 15.9 mm, 19.0 mm) and embedment length (5*db*, 10*db*, 15*db* where *db* is the bar diameter) were evaluated. They concluded that, the sand-coated Glass Fiber Reinforced Polymer (GFRP) bars embedded into geopolymer concrete offered sufficient bond between the bar and the geopolymer concrete. They further observed that, the specimens with a shorter embedment length (5*db*) failed due to bar pullout while the specimens with a longer embedment length failed due to concrete splitting. As the bar diameter increases, concrete splitting type of failure became more dominant in specimens with longer embedment length. For specimens that failed due to bar pull out, the increase in bar diameter causes the peak average bond stress to decrease. The increase of embedment length resulted in a lower average bond stress due to the different types of failure.

Dias and Thaumaturgo [77] conducted an experimental study to evaluate the fracture toughness critical stress intensity factor and critical crack mouth opening displacement of geopolymeric concretes reinforced by different volumetric fractions of basalt fibres (0%, 0.5% and 1% by volume). The results were compared with similar specimens made using basalt fibre and OPC concrete. They concluded that, the geopolymeric concretes have better fracture properties than conventional Portland cement concrete.

Kupwade-Patil and Allouche [78] reported the findings of an experimental investigation on the alkali silica reaction between reactive aggregates (quartz, sandstone, and siliceous limestone) and the geopolymer matrix. They observed substantially lower alkali silica reaction with reactive aggregates in fly ash-based geopolymer concretes compared to that in the case of ordinary portland cement-based concrete.

Lee and Deventer [79] reported the study conducted on the microstructure and the bonding strength of the interface between natural siliceous aggregates and fly ash (Class F) based geopolymers. Sodium silicate solution, NaOH and/or KOH, distilled/deionised water in the appropriate proportions, with and without inorganic salt (KCl and K_2CO_3) were used for the preparation of geopolymer. The geopolymeric products were cured at 40 °C for 24 hours. It was observed that, when the activating solution contained no or little soluble silicates, the compressive strengths of the geopolymeric binders, mortars

and concretes were significantly weaker than those activated with high dosages of soluble silicates. The presence of soluble silicates in the initial activating solution is also effective in improving the interfacial bonding strengths between rock aggregates and geopolymeric mortars. They observed no apparent interfacial transition zone near the aggregates when the systems are free from chloride contamination. On the other hand the presence of chloride decreased the interfacial bonding strength between the aggregates and the binders and this may be due to the gel crystallization occurring near the aggregate surfaces, resulting in debonding.

Song et al. [80] presented experimental data on the durability of fly ash based Geopolymer concretes exposed to 10% sulphuric acid solutions for up to 8 weeks. NaOH and Na_2SiO_3 solutions were used for the preparation of Class F type geopolymer concrete. Specimens were cured either at 23 °C or 70 °C for 24 hours. The compressive strength of 50 mm cubes at an age of 28 days ranged from 53 MPa to 62 MPa. After immersion in a 10% sulphuric acid, the samples were tested at 7, 28, and 56 days. Mass loss, compressive strength reduction, and the residual alkalinity were determined. From their study they concluded that geopolymer concrete is highly resistant to sulphuric acid in terms of a very low mass loss (less than 3%). Further, they observed that the geopolymer cubes are structurally intact and had substantial load capacity even though the entire sections were neutralized by sulphuric acid.

Bernal et al. [80] assessed the mechanical and durability performance of concretes produced using ground granulated blast furnace slag (GGBFS) as sole binder and compared the corresponding performance with reference concretes produced using portland cement (OPC). The alkaline activation of the GBFS was carried out using a commercial sodium silicate solution. Crushed gravel and river sand were used as coarse and fine aggregates. Compressive strength test, carbonation test, Rapid chloride penetration test. Total porosity and absorption test and capillary sorptivity test were conducted on specimens made with two types of binders. They observed that the alkali-activated slag concretes display lower water absorption, total porosity and capillarity at comparable binder content and these values decreases with increasing binder content. While they observed a higher resistance to chloride penetration for alkali activated concrete, these specimens showed higher susceptibility to carbonation.

The durability of reinforced specimen made from alkali-activated fly ash and ordinary portland cement was evaluated by Kupwade-Patil and Allouche [81]. Fly ash and a mixture of 14 molar NaOH and Na_2SiO_3 solutions were used for the preparation of the geopolymer. Electro chemical method, chloride diffusion and contents analysis, chemical and mechanical analysis and visual examination were employed for the experimental evaluation. The result of experimental investigation revealed that GP concrete specimens exhibit lower diffusion coefficient, chloride content and porosity compared with OPC concrete specimen. GP concrete specimen exhibited significantly higher resistance to chloride-induced corrosion compared with that of OPC specimens.

Geopolymers derived from various combinations of granulated blast-furnace slag, Class C fly ash, clay, sand, and basalt were tested by Goretta et al. [82] for resistance to solid-particle erosion. Based on the test result they observed that the specimen which contained both fly ash and slag performed better when tested for erosion of solid particles.

Gourley and Johnson [83] reported the properties of precast fly ash based geopolymer concrete products, such as sewer pipes, railway sleepers and wall panels produced on a commercial scale. For sewer pipes, conventional pipe-making processes were used to make geopolymer concrete pipes with diameters in the range of 375 mm to 1800 mm. They observed that pipes made of GP concrete pass the structural load capacity required by the Australian Standard.

Geopolymer concrete railway sleepers, were manufactured using conventional pre-stressing processes with a compressive strength in the range of 60 to 80 MPa. These products passed all Australian Standard static and cyclic load tests and there was no slippage of steel up to ultimate load.

2.8 TEMPERATURE CURING AND CURING PERIOD

Hardjito et al. [63] carried out test on fly ash based geopolymer concrete in order to find out various parameters that influence the compressive strength of the geopolymer concrete. They used mixture of Na_2SiO_3 and NaOH solution (8 molar or 14 molar) as alkali. They observed that, curing temperature corresponding to maximum compressive strength was 90 °C. Further they noticed that, the difference in 7^{th} day compressive strength between 100 hours and 24 hours temperature curing period was 25% with

respect to compressive strength at 100 hours temperature curing period (60 °C curing temperature). The compressive strength of geopolymer concrete beyond 48hours curing period was insignificant.

Thakur and Ghosh [56] investigated the influence of various parameters on the compressive strength of fly ash based geopolymer mortar. They used mixture of Na_2SiO_3 and NaOH solution. They observed that, for all specimens, curing temperature corresponding to maximum compressive strength was 120 °C. Further they noticed that, the difference in 7^{th} day compressive strength between 80 hours and 24 hours temperature curing period was 23% with respect to compressive strength at 80 hours temperature curing period (85 °C curing temperature). The compressive strength of geopolymer mortar beyond 48hours curing period was insignificant.

Chindaprasirt et al. [57] investigated the influence of various parameters on the compressive strength of geopolymer mortar. They used high calcium fly ash and mixture of Na_2SiO_3 and NaOH solution respectively as alumino-silicate and alkali. They observed that, for all the specimens, the curing temperature corresponding to maximum compressive strength was 75 °C. Further they noticed that, difference in 7^{th} day compressive strength between 72 hours and 24 hours temperature curing was 37% with respect to compressive strength at 72 hours temperature curing period (75 °C curing temperature). They noticed that, the compressive strength of geopolymer mortar beyond 72 hours curing period was decreased.

2.9 BEHAVIOUR AT ELEVATED TEMPERATURES

2.9.1 Method of Testing

The performance of concrete at elevated temperatures can be studied and determined under, three test methods. These are named as stressed, unstressed and unstressed residual strength tests [84].

In the stressed tests, a preload (20% to 40% of the compressive strength at 28 °C) is applied to the specimen prior to heating and is sustained during the heating period. Heat is applied at a constant rate until a target temperature is reached, and is maintained for a time until a thermal steady state is achieved. Load or strain is then increased at a prescribed rate until the specimen fails.

In the unstressed test, the specimen is heated without preload at a constant rate to the target temperature, which is maintained until a thermal steady state is achieved. Load or strain is then applied at a prescribed rate until failure occurs.

In the unstressed residual strength test, the specimen is heated without preload at a prescribed rate to the target temperature, which is maintained until a thermal steady state is reached within the specimen. The specimen is then allowed to cool to room temperature. Load or strain is applied at room temperature until the specimen fails. Three types of test explained are schematically shown in Fig. 2.3.

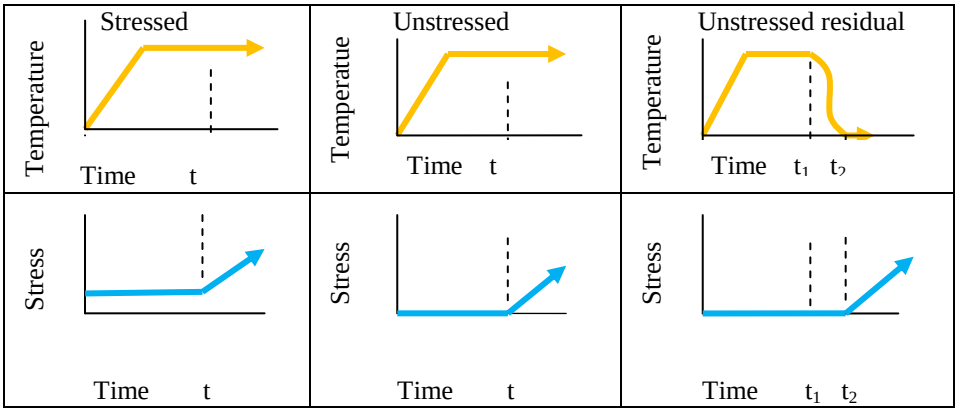

Fig. 2.3. Temperature and load histories for temperature test [84]

Stressed tests are used for structural component and need heavy and costly test set up. However this test method is more realistic than the other two methods, because in actual condition load exist on the structural component. Unstressed and unstressed residual tests are mainly employed for materials and the equipment needed are less costly than that required for stressed test.

Two types of heating methods are generally adopted for study under elevated temperatures. One is constant rate of heating and the other is to heat as per a standard temperature rise – time curve corresponding to a fire. The constant rate of heating is generally used for studying the properties of materials after exposure to high temperature. The rate of heating is adopted on the basis of the purpose of the test. Fig.2.4 shows the temperature-time graph for low rate of heating.

The second type of heating is generally adopted to simulate an actual fire exposure to structural members. Standard temperature rise – time graphs are available to

simulate fire and different codes proposes slightly different curves. Figure 5 shows some of the standard curves [86-88].

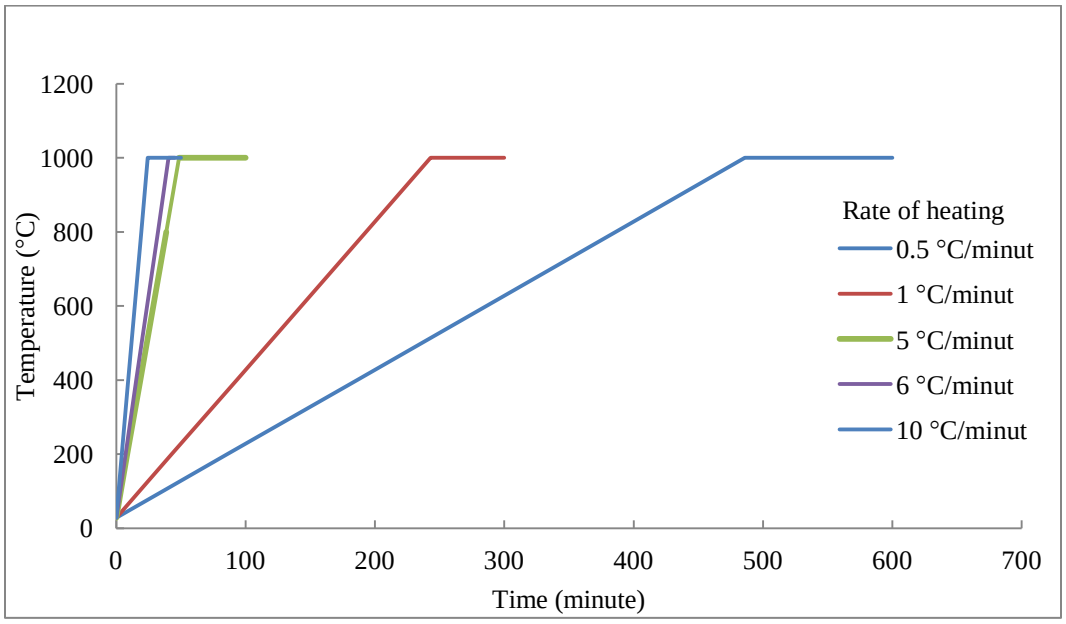

Fig. 2.4. Variation of temperature with time [85]

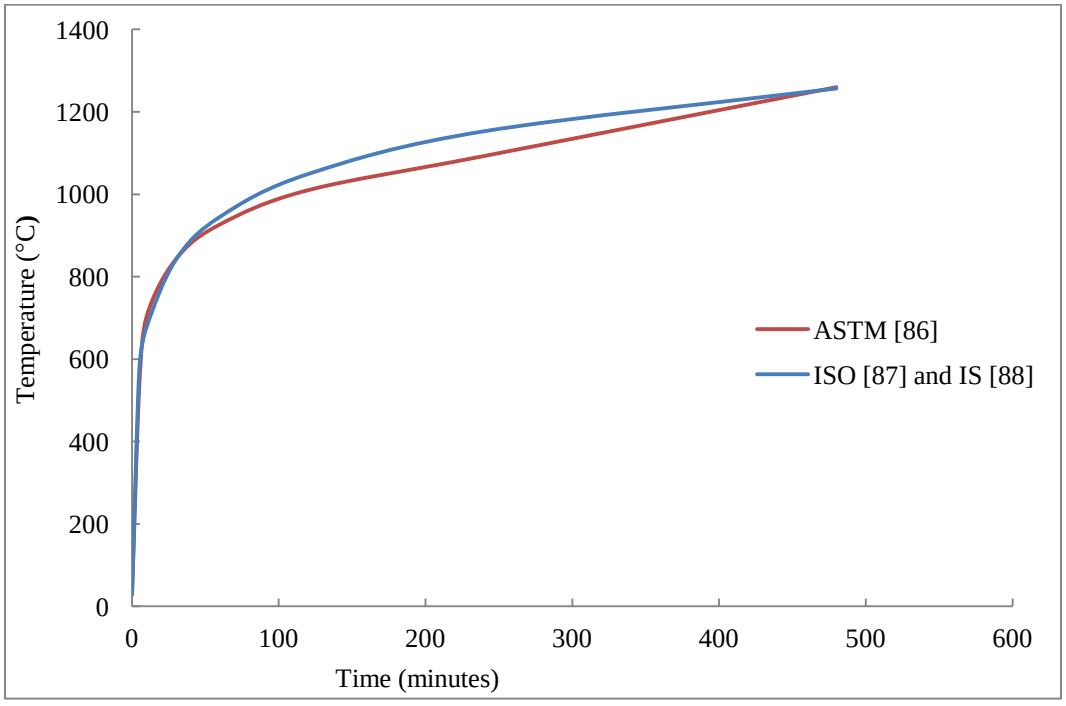

Fig. 2.5. Temperature rise- time curve

2.9.2 OPC Concrete

William et al. [89] carried out a review of literature on damage mechanism of concrete at high temperature. They pointed out that, there were four types of major damage mechanisms responsible for the deterioration of properties of concrete under high temperatures: phase transformations taking place in cement paste; phase transformations taking place in aggregate; thermal incompatibility between the cement paste and aggregate; and spalling of concrete. The first three damage mechanisms result in reduced strength and stiffness of concrete, while the last one leads to reduced cross section of structural members and loss of structural integrity.

Phan [90] carried out a review of literature on the behaviour of OPC concrete exposed to elevated temperatures and reported that, for unstressed test, the strength-temperature relationships are characterized by three stages: initial strength loss(ambient to 200 °C), stabilizing and regaining stages (100 °C to 450 °C), permanent strength loss stage (beginning around 450 °C).

Line et al. [91] presented results of scanning electron microscopy (SEM) and stereo microscopy investigations of fire-damaged concrete. Samples were either taken from concrete that was subjected to heating and cooling at controlled temperatures in the laboratory or removed from concrete and masonry units exposed to fires in the field. This study has focused on microstructures of cement pastes/aggregates, micro voids/cracks, and separation of the cement paste from aggregates in heated concrete samples. They observed that, for the temperature exposure of up to 250 °C, the compressive strength of OPC concrete is influenced by morphological changes in hydrates. They observed cracking around aggregate particle boundaries and intra-paste between 300 °C and 500 °C. They reported that, the hydration products decompose quickly at 500 °C and resulted in serious cracks within the cement paste and around aggregate particles.

An experimental investigation on the effects of temperatures up to 800 ºC on the strength characteristics, pore structure, and calculated permeability coefficients of concrete at the ‘Mochovce nuclear power plant’ (Slovakia) was reported by Janotka and Bagel [92]. They concluded that, no significant changes could be formed in modulus of elasticity, strength, average pore radius, or calculated permeability coefficients for tested

specimens exposed to temperatures up to 400 ºC. However between 400 °C and 800 ºC they observed the development of large pore structures and suggested that this could be the reason for a significant concrete strength decrease (between 400 °C and 800 ºC). The collapse of the concrete's structural integrity was observed beyond 800 ºC temperature exposure.

Ahemed et al. [93] studied the influence of temperature (100 °C to 700 °C) on the residual compressive strength of concrete made using lime stone aggregate. They observed that, at100 °C there was 17% increase in the residual compressive strength due to accelerated hydration of the cement. The strength of the concrete after exposure to 150°C was reduced due to the loss of moisture and incompatibility in thermal expansion between the cement paste and the aggregate. 21% strength loss was noticed at 200 °C and they evaluated that this reduction in strength is due to the loss of physically bound water in the hydrated cement gel. They suggested that loss of strength between 400 °C and 500 °C is due to the dehydration of calcium hydroxide and evaporation of combined water.

Abram, cited by Phan [90] reported that, the strength loss in OPC concrete made using different types of aggregate after exposure to temperature up to 480 °C is the same and that the residual strength in OPC concrete beyond 480° C is influenced by the type of aggregate used.

From the study, on the effect of temperature on the thermal properties of fiber reinforced HSC, Kodur and Sultan [94] established that the type of aggregate, weakening of aggregate- paste bond and strength of concrete have significant influence on the thermal properties of HSC, while the presence of steel fiber reinforcement has very little influence on the thermal properties of HSC.

Youssef and moftah [95] studied the general stress strain relationship for concrete at elevated temperature and proposed various models to predict the compressive strength and modulus of elasticity of concrete at elevated temperatures.

Lie cited by Youssef and Moftah [95] proposed the following prediction equation for strength of concrete in three temperature zones.

$f_{cT} = f_{ck}\,(1\text{-}0.001\,T)$, $T \leq 500$ °C ..... (2.7)

$f_{cT} = f_{ck}\,(1.375\text{-}0.001175\,T)$, 500 °C $\leq T \leq 700$ °C ..... (2.8)

$f_{cT} = 0$, $T \geq 700$ °C ..... ……(2.9)

The Euro code cited by Youssef and Moftah [95] also predicts the strength of concrete with temperature in three temperature zones, and the same is given as equations 2.10 to 2.12.

$f_{cT} = f_{ck}$, $T \leq 100$ °C ..... (2.10)

$f_{cT} = f_{ck}\,(1.067 - 0.00067\ T)$, $100\ °C \leq T \leq 400\ °C$ ..... (2.11)

$f_{cT} = f_{ck}\,(1.44 - 0.0016\ T) \geq 0$, $T > 400$ °C..... (2.12)

The Lie and Lin cited by Youssef and Moftah [95] proposes a single equation to predict the strength of concrete with temperature and is presented in equation 2.13.

$f_{cT} = f_{ck}\,(2.011 - 2.353(T-20)/1000) \leq f_{ck}$ ..... (2.13)

Li and Purkiss [96] proposed the following third order equation to predict the strength variation in concrete with temperature.

$f_{cT} = f_{ck}\,[0.00165(T/100)3 - 0.03(T/100)2 + 0.025(T/100) + 1.002]$ ..... (2.14)

Hertz cited by Youssef and Moftah [95] proposed the following model that recognizes the influence of the type of aggregates on the strength variation of concrete with temperature.

$f_{cT} = f_{ck}\,[1/\{1+(T/T1)+(T/T2)^2+(T/T8)^8+(T/T64)^{64}\}]$ ..... ……..(2.15)

In the above equation, values for T1, T2, T8 and T64 are different for siliceous, light weight and other types of aggregates.

Li and Guo cited by Xiao and Konig [97] proposed the following model for the prediction of strength variation with temperature.

$f_{cT} = f_{ck}/\,[1+2.4(T-200)6\times10^{-17}]$ ..... (2.16)

Researchers have proposed models for predicting the tensile strength of concrete after exposure to high temperatures. An accurate prediction of the tensile strength of concrete will help in mitigating cracking problems, improve shear strength prediction and minimise the failure of concrete in tension due to inadequate methods of tensile strength prediction.

Li and Guo cited by Xiao and Konig [97] suggested a simplified equation as given by equation (2.17) for the prediction of tensile strength of concrete (f_{TT}) with temperature exposure up to 1000°C.

$f_{TT} = (1-0.01T)f_T$, $T=(20\text{-}1000\ °C)$ ..... (2.17)

Xie and Qian cited by Youssef and Moftah [95] proposed the following second-order fitting formula (equation 2.18) and a simplified two-part formula (equation 2.19 to 2.20) to estimate the tensile strength
of concrete.

$f_{TT} = [2.08(T/100)^2 – 2.666(T/10) +104.79] f_T$, ... (2.18)

Where T is between 20 °C -1000 °C

$f_{TT} = [0.58(1.0 – T/300) + 0.42] f_T$..... (2.19)

Where T is between 20 °C -300 °C

$f_{TT} = [0.42 (1.6- T/300) +0.42] f_T$..... (2.20)

Where T is between 300 °C -1000 °C

Francis cited by Sukumar et al. [98], reported the following equation showing the relation between split tensile strength and cylinder compressive strength (f_{cy}) of concrete.

$f_T = 0.206 (f_{cy}) 0.79$ ..... (2.21)

Prediction models are available for elastic modulus of concrete after exposed to elevated temperatures. Xiao and Konig cited by Lu [97] suggested the following tri-linear model expression between E_T and T.

$E_T = (1-0.0015T)E_C$..... (2.22)

Where T is between 20 °C -300 °C

$E_T = (0.87-0.0084T)E_C$ ..... (2.23)

Where T is between 200 °C to 700 °C

$E_T = 0.28 E_C$, T >700 °C ..... (2.24)

Li and Guo cited by Youssef and Moftah [95] and Xiao and Konig [97] suggested a bi-linear equation between E_T and T, which is represented as equations 2.25 and 2,26.

$E_T = E_C$ ..... (2.25)

Where T is between 20 °C to 60 °C

$E_T = (0.83-0.0011T) E_C$ .....(2.26)

Where T is between 60 °C -1000 °C

Khennane and Baker cited by Youssef and Moftah [95] proposed the following model for unloaded concrete.

$E_T = (-0.001282 T + 1.025641) E_C$, $20 \leq T \leq 800$ °C ..... (2.27)

Chan et al. [99] investigated the behaviour of high-performance silica fume concrete with different moisture content, after exposure to standard fire temperature (ISO). They used concrete cube and slab for testing. They observed that, spalling of concrete depend on both the strength and moisture content of concrete. For concrete strengths less than 60 MPa, they observed no spalling even with the concrete fully saturated. However when the concrete strength exceeded 60 MPa, they observed, greater spalling probability for concrete with higher moisture content.

2.9.3 Geopolymer Paste and Mortar

A study has been conducted on geopolymer mortar after exposure to elevated temperature by Pan et al. [100] Specimens of strengths 5 to 60 MPa were prepared using two different types of fly ashes. They observed that, strength gain or loss of geopolymer mortars after exposure to elevated temperatures depends on strength of the GP mortar at ambient temperature. Specimen having compressive strength greater than 16 MPa, showed strength loss after 800 °C temperature exposure, while specimen having compressive strength less than 16 MPa showed a strength gain. They suggested that the strength gain is attributed to cindering of unreacted material and further polymerization. The strength loss is due to the thermal incompatibility between paste and aggregate. Further they observed that the geopolymer mortars with lower initial strength had greater ductility and mortar with high initial strength exhibit low ductility after exposure to elevated temperature.

Kong et al. [101] had done experimental investigation on geopolymer paste after being exposed to the elevated temperature of 800 °C. Two types of alumino-silicate materials-metakaolin and fly ash were used for preparing the specimen. There was significant change of color in fly ash and metakaolin specimens at the temperature exposure of 800 °C. Micro-cracks in the order of 0.1 mm to 0.2 mm were developed on the surface of metakaolin based specimen, whereas there was no surface crack on fly ash based geopolymer specimen. At the temperature exposure of 800 °C, compressive strength of metakaolin based geopolymer paste specimen decreased slightly where as the compressive strength of fly ash based geopolymer increased slightly.

From the thermogravimetric analysis (TGA) they concluded that the exposure of geopolymer to high temperatures leads to changes in chemical structure of geopolymer

and the dehydration of free and chemically-bound water. As the external temperature increases, moisture within the specimen rapidly migrates towards the surface of the specimen and escapes. This in turn causes surface-cracking and internal damage in the overall structure of the geopolymer.

Kong and Sanjayan [102] presented a study on geopolymer paste and geopolymer concrete made with fly ash after exposure to elevated temperatures (up to 800 °C). For preparing the specimens, Na_2SiO_3 and KOH solutions were used as alkali. They observed that, the fly ash to alkali ratio was the most influencing factor for strength and fire resistance of the geopolymer paste. Further, at 800 °C they observed an increase in strength in the geopolymer paste specimen but a strength loss in geopolymer concrete. They suggested that the decline in strength of geopolymer concrete was caused by differential thermal expansion between paste and aggregate.

Pan and Sanjayan [103] reported stress strain relationship of geopolymer paste tested while the specimens were kept at elevated temperatures, with the aim of studying the fire resistance of geopolymer. Fly ash and mixture of sodium hydroxide and sodium silicate were used for making the geopolymer paste. Tests were performed at temperatures from 23 to 680 °C as well as after cooling. For the temperature range from 200 °C to 290 °C, they observed an increase in strength of geopolymer and slight contraction in the specimen size. On the other hand, for temperature range between 380 °C and 520 °C, while the strength continued to increase, the specimen expanded. They observed a brittle type of failure for geopolymer concrete after exposure to elevated temperatures.

Dombrowiski et al. [104] investigated the influence of calcium content on the structure and thermal properties of fly ash based geopolymers. They observed that, 8% substitution of CaOH in place of fly ash, in fly ash based geopolymer, showed better performance at room temperature as well as at high temperature. Finally they concluded that calcium act as a reaction germ which quickens the reaction to a more structure forming product, and thus results in more strength.

Pernica et al. [105] studied the effects of the loading rate and of the testing temperature on the mechanical properties, particularly on the stiffness and on the ultimate tensile strength, of a geopolymer reinforced with glass or carbon fibres. The displacement

rate was varied from 0.002 mm/s to 2 mm/s and the testing temperature was increased from the room temperature to 300 °C. They observed that, the ultimate strength and flexure stiffness of all reinforced specimens decreased with the increase of the temperature. Further, the ultimate strength and flexural stiffness of all specimens increased when the loading rate was increased from 0.002 mm/s to 2 mm/s.

Studies were conducted by Kong and Sanjayan [106] on fly ash based geopolymer paste, mortar and concrete after exposure to elevated temperatures. They examined the influence of specimen size, aggregate size, aggregate type and super plasticizer type on compressive strength of geopolymer paste, mortar and concrete. It was found that specimen size and aggregate size are the main influencing factors on properties of geopolymer concrete after exposure to elevated temperatures. Strength degradation was observed due to the addition of superplasticizer and depends on the dosage and type of superplasticizer. They observed a residual strength of 26%, 0% and 41.5% in geopolymer paste, mortar and concrete respectively after exposure to 800 °C.

Based on the experimental investigation Dimas et al. [107] suggested that the water that remains in the sodium silicate gel after the formation of geopolymer is associated primarily with physically bound water on sianol groups (Si-OH) and secondarily with surface hydroxyl groups. The first type of incorporated water in gels gets totally removed when heated to 150 °C, whereas the latter ones get completely removed at temperatures as high as 500 °C.

Provis et al. [108] established the correlation between mechanical and dilatometric properties of alumino-silicate geopolymer. Geopolymer samples were prepared by mixing fly ash with sodium silicate (with different modular ratio). Different activator/ash ratios were selected for making the geopolymer samples. They showed that, the geopolymers which display the best strength performance showed a small expansion in the temperature range 700–800 °C. Further, they suggested that, the expansion was due to the swelling of a high-silica phase present as pockets within the geopolymeric gel structure.

Alarcon-Ruiz et al. [109] reported studies on a cement paste fired to various temperature regimes up to 800 °C in steps of 100 °C for a constant period of 24 hours. This work was carried out using thermal analysis technique to study the effect of

temperature in the mineralogical composition of cement hydration products. They concluded that, the TGA curve can be divided into three major parts, representing two different kinds of reaction. The first part represents the loss of water up to 200 $^{\circ}$C, mainly due to the dehydration of the C-S-H. The second part represent major weight loss, observed at 450–500 °C, corresponds to the dehydroxylation of portlandite, another hydration product. The third part represent loss of weight appears at 750 °C and corresponds to the decarbonation of calcium carbonate coming from the clinker and the filler.

TGA analysis on geopolymer paste done by Kong [101,102] showed that, the rate of change of mass loss is maximum around 100 °C and beyond the temperature of about 250 °C, it is more or less constant. And most of the free water within the geopolymer paste escapes at a temperature below 200 °C.

2.9.4 RCC Beams

Rahul and Mundhada [110] reported the result of experimental investigation on R.C.C beam after exposure to elevated temperatures. It was observed that up to 550 °C, the weight loss for RCC beams was negligible and, the flexural strength reduced by 1/3rd at 550 °C. No cracking, spalling or scaling was observed up to 550 °C. At 750 °C, there was a further drop in weight, flexural strength, and cracks appeared, but there was hardly any spalling or scaling. At 950 °C, the weight loss exceeds 10%, flexural strength comes down by 2/3rd, and major cracking, spalling and scaling was observed.

LI et al. [111] studied the mechanical performances of RCC beam after they were heated up to different temperature levels in a loading state, followed by cooling in the air or by water jet. They used 2600 mm x 150 mm x 250 mm size beams for the study. They observed that, ultimate strength of RCC beam, which is exposed previously to a fire and then cooled, deceases linearly with an increase in heating temperature, and the air cooling results in a greater reduction in the ultimate strength of the RCC beam. It is also reported that, deformation of RCC beam increases with increase in temperature. Further they noticed that, deflection of the RCC beam cooled in the air is smaller than that cooled by water jet.

Six R.C.C beams with different concrete cover 10 mm to 30 mm were tested by Shi et al. [112] to investigate the influence of the concrete cover on the properties of

reinforced concrete flexural members exposed to fire. The size of the beams was 300 mm x 100 mm x 180 mm. The specimens were heated on their bottom and two lateral surfaces. From these test results, they observed that the bottom concrete cover has significant influence on the specimen ultimate loading capacity, but the extent of this influence will decrease with an increase in the thickness of the concrete cover.

They suggested that, the continuous widening of the concrete cracks at the tensile zone, the effect of the bottom concrete cover thickness will decrease gradually. This is particularly so when the bottom concrete cover thickness is greater. Therefore, for important flexural members or those with larger spans and sustaining greater vertical load, it is not practical to strengthen their fire resistance only through increasing the concrete cover thickness.

Kodur and Phan [113] had done literature review on the material, structural and fire characteristics that influences the performance of High strength concrete (HSC) under fire conditions. They observed that, there is a concern on the occurrence of spalling and lower fire endurance of HSC as compared to normal strength concrete (NSC). They observed that, the main parameters that influence fire performance of HSC at material level are: concrete strength, silica fume, concrete moisture content, concrete density, fiber reinforcement, and type of aggregate. At the structural level, tie spacing, confinement, tie configuration, load levels and size of the members play an important role in determining the fire endurance. Further, they observed that, the addition of polypropylene fiber reduces the spalling of HSC concrete after exposure to elevated temperature and bent tie reinforcement enhances the fire endurance of HSC column.

2.10 FLEXURAL BEHAVIOUR OF R.C.C BEAM

The moment-cuvature relationship for an under reinforced beam, in which the tension steel yield can be idealized to the trilinear relationship as in literature presented by Park and Paulay [114]. The first stage is to cracking, second stage is to yield of tension steel and the third to the limit of useful strain in the concrete.

Further, with sufficient accuracy the moment-curvature curve can be idealized to bilinear relationship. Once cracks have developed, as would be the case in most of the beam under service loading, the m-φ relationship is nearly linear from zero loads to the

onset of yield. Therefore the bilinear curve is an accurate approximation for initially cracked beams.

In limit and seismic design, the ductility is usually expressed as the ratio of the ultimate deformation (curvature) to the deformation at first yield. Ductility of a structure is one of the most important factors affecting its seismic performance. It has been clearly observed that well designed and detailed reinforced structures behave better during earthquake and the gap between the actual and design lateral force is narrowed down by providing ductility in the structure. The method of calculation of curvature at different loading stages is explained by Srikanth et al. in the literature [115].

Youcef and Chemrouk [116] presented a method for calculating the ductility of reinforced concrete rectangular beams considering nonlinear beaviour of both concrete and steel. Based on the calculations they observed that the ductility of reinforced concrete beam increases with the reduction in the quantity of tension steel; reduction in yield strength of tension steel; and increases as the ratio of compression to tension steel increases.

A dimensional analysis criterion was proposed by Bosco et al. [117] to compute the minimum amount of reinforcement for high strength concrete members in flexure. For this purpose they used fracture mechanics and defined a brittleness number which could be used for accessing actual brittleness or ductility. They suggested that, the dimensionless brittleness number is able to describe the size effect on the failure process.

The analytical moment curvature relation obtained using various models were compared with experimental results by Srikanth et al. [115]. For this purpose six R.C.C. beams were tested. From their experimental result, they conclude that the curvature in a beam is influenced by the percentage of tension steel and compressive strength of concrete.

Kalkan [118] compared the actual load deflection of concrete beam with load deflection estimates proposed by Brason (1965) and Bischoff (2005). He observed that the estimated load deflection, agrees closely with the experimental load defection behaviour of reinforced concrete beam. Further, he observed that the actual response of reinforced concrete beams with shrinkage cracks is significantly weaker than the estimated response.

Crack width is one of the serviceability criteria to be considered in R.C.C beam design. There are different model for predicting the crack width, while designing a R.C.C beams. The BIS code of practice [119] gives the equation for calculating crack width.

Design surface crack width = $(3a_{cr} * \varepsilon_m)/(1+2(a_{cr} - c_{min})/ (h-x))$ …… (2.28)

Where, a_{cr} = distance from the point considered to the surface of the nearest longitudinal bar,

ε_m = average strain at the level where the cracking is being considered, c_{min} = minimum cover to the tension steel, h = overall depth of section, x = depth of neutral axis.

The BS code [120] also suggests a similar equation for the calculation of crack width.

Eurcode[121] present the following equation for calculating crack width, which accounts for the effect of imposed deformation and tension stiffening.

$w_k = s_{r,max} (\varepsilon_{sm} - \varepsilon_{cm})$ …… (2.29)

where

$s_{r,max}$ is the maximum crack spacing

ε_{sm} is the mean strain in the reinforcement under the relevant combination of loads.

ε_{cm} is the mean strain in the concrete between cracks

$\varepsilon_{sm} - \varepsilon_{cm}$ may be calculated from the expression:

$\varepsilon_{sm} - \varepsilon_{cm} = [\sigma_s - (k_t f_{ct,ef} (1+ \alpha_e \rho_{p,ef}))/ \rho_{p,ef}]/ E_s] \geq 0.6 \sigma_s$ ……(2.30)

where, σs is the stress in the tension reinforcement assuming a cracked section. α_e is the ratio E_s/E_{cm} , $\rho_{p,eff} = (A_s + \xi_1^2 A_p.)/A_{c,eff}$ ……..……(2.31)

A_p. is the area of pre or post-tensioned tendons within $A_{c,eff}$. $A_{c,eff}$ is the effective area of concrete in tension surrounding the reinforcement or prestressing tendons of depth, hc,ef , where hc,ef is the lesser of 2,5(h-d), (h-x)/3 or h/2 . Where, h is the overall depth, d is the effective depth, x is the depth of the neutral axis.

ξ_1 is the adjusted ratio of bond strength taking into account the different diameters of reinforcing steel.

k_t is a factor dependent on the duration of the load

k_t = 0.6 for short term loading

k_t = 0.4 for long term loading

Chi and Kirstein [122], studied the mechanism by which cracks are formed in beams. On the basis of the test result on 16 beams they suggested that, after some initial cracks have occurred the tensile force in the concrete is resisted by an "effective area" of concrete immediately surrounding the steel, which is less than the total area of the concrete in the tensile zone of the beam. Further cracking of the concrete is attributed to the direct tension developed through bond and due to the strain in the steel.

Allam et al. [123] conducted a literature review for comparing crack width reinforcement ratio, bar surface, and reinforcement arrangement. Their work mainly focused on the effect of concrete cover, steel stress, reinforcement ratio, bar surface and reinforcement arrangement. On the basis of the study, they have drawn the following conclusions. Values of crack width predicted based on codes (Euro code 2, Egyptian code ECP 203, ACI 318, BS 8110) show a large scatter among the different code equations and those obtained by other researchers. With the increase of reinforcement ratio, the concrete contribution in tension decreases, the mean steel strain increases, consequently the crack width increases. Bar arrangement (larger number, smaller diameter), better bond between concrete and steel occurs resulting in a reduction in the crack spacing. The effect of bar surface deformation on the calculation of crack width not only affects the crack spacing, but also affects the mean strain. Most equations proposed by the building codes overestimate the effect of the concrete cover on the calculated values of crack width when compared with the experimental results.

Frosch [124] developed the following simple, theoretically-derived equation to predict crack widths

$w_{max} = (\ 2f_s /E_s)*d^1\ \beta$ …… (2.32)

where, d^1 is the controlling cover distance and is taken as the greater of

$\sqrt{(d_c^2 + d_s^2)}$ and $\sqrt{(d_c^2 + (s/2)^2}$, $\beta = (h-x)/(d-x)$, where h, x,s ,dc and d_s respectively are over all depth, depth of neutral axis, spacing of reinforcement ,cover to bottom reinforcement and side cover.

On the basis of statistical analysis of experimental data from several researchers

Gergely and Lutz [125] suggested that, the major variables which influence the crack width are the effective area of concrete, the number of bars, the side or bottom cover, and the steel stress. He proposed the following equation.

$W_{cr} = (11x\ 10^{-6})\ (d_c\ A_e/n)^{1/3}\ (D - x)/(d-x) * f_{st}$ ……... (2.33)

Where D,d,x,n and d_c respectively are over all depth, effective depth, depth of neutral axis, number of tension bar and effective cover to bottom reinforcement.

A_e is the effective area of concrete surrounding the main tension reinforcement

f_{st} is the stress in steel

2.11 INTERFACE SHEAR

The connective distress found in precast construction is centered around the shear interfaces (Place where shear stress causes sliding type of failure along a well defined plane) associated with corbels, bearing shoes, ledger beam bearing, coupled shear wall, wall to foundation, deep beams etc.. Study of shear- slippage at the interface of reinforced and unreinforced, monolithic and precast construction is very important where interface shear is critical.

Studies were made in the past to understand the interface shear strength in ordinary portland cement (OPC) concrete. Birkeland and Birkeland [126] proposed a shear friction concept to evaluate the interface shear strength of concrete block. Their hypothesis suggests that the external shear load tends to produce slippage along the interface plane and it is resisted by the shear friction and not by bond. They further proposed that, the reinforcement across the interface is stressed in tension and that the dowel action is insignificant. Accordingly, the ultimate shear capacity across the interface of a monolithic concrete with reinforcement across the shear plane could be calculated as $A_s \times f_y \times \tan ø$, where A_s and f_y are the total cross sectional area of the reinforcement across the shear plane and yield strength of reinforcement respectively. The angle of internal friction, ø varies with the nature of interface and is to be determined by tests. They suggested a value of 1.7 for 'tan ø'.

Mast [127], based on the experimental study on monolithic concrete and concrete having crack at the interface, suggested the value for 'tan ø' between 1.4 and 1.7. He proposed a lower bound value of 1.4 for design purposes.

Hofbeck et al. [128] reported a study on the shear strength of reinforced concrete with and without a crack existing along the shear plane of push off specimens and concluded that shear transfer stress depends on initial crack condition, product of reinforcement ratio and yield strength of shear reinforcement. It is suggested that, the

dowel action of reinforcing bars crossing the shear plane is insignificant in initially uncracked concrete, but is substantial in concrete with a pre-existing crack along the shear plane.

The shear-friction design proposed by ACI 318 [129] suggested the value for the coefficient of friction (μ or tanø) for monolithically placed concrete as 1.4λ, where the value of λ for normal weight concrete is one. The value of λ depends on the type of concrete; namely normal weight (λ =1), sand lightweight (λ = 0.85) and lightweight (λ = 0.75).

On the basis of experimental investigations using push-off specimen, Mattock et al**.** [130] proposed an alternate equation for predicting the ultimate interface shear capacity**,** given by $V_u = 0.8 (A_s f_y) + (A_c\ 400\ psi)$. …….. (2.34)

Mattock [131] and Lawrence and Andrew [132] have conducted experimental research and proposed modification to the ACI equation to predict the interface shear strength of high strength concrete. They proposed three equations at different conditions at the interface.

2.12 CONCLUDING REMARK

Even though the method of alkali activation, or geopolymerization (as coined by Davidovits) for making cementitious materials was initiated way back in 1930's, it took wide acceptance among researchers from 1990 onwards. Combination of different source materials (alumino-silicate) and alkali is possible for geopolymerization (alkali activation).

Depending on the content of silica and alumina in the source materials, three different types of amorphous to semicrystalline three dimensional alumino-silicate structures (geopolymers) could be formed.

Study has been carried out on the behaviour of geopolymer paste, mortar and concrete in the past by many investigators. Studies have identified the role of different alumino-silicate materials on the strength, durability and other properties of geopolymer paste, mortar and concrete. Class F fly ash (as alumino-silicate material) and a combination of NaOH and Na_2SiO_3 (as alkali materials) are the widely used material for making geopolymer concrete. However, review of literature reveals that, the role of aggregate content on the properties of geopolymer concrete has not been clearly brought

out. The amorphous state of the alumino-silicate material, Si/Al ratio, particle size distribution, quantity and type of alkali, water content, etc. are also important variables deciding the mechanical properties of geopolymer concrete.

There are many occasions where concrete members are exposed to elevated temperatures. Behaviour of concrete exposed to elevated temperatures is different from those when they are at ambient temperature. Many studies have been reported on the behaviour of concrete exposed to elevated temperatures.

While considering geopolymer concrete as an alternate material for cement concrete, information on the behaviour of geopolymer concrete at elevated temperatures is also vital, particularly when they are exposed to such conditions. However a systematic study addressing the behaviour of geopolymer concrete exposed to elevated temperatures is lacking at present.

Further, structural members exposed to elevated temperatures behave differently compared with the behaviour of materials at elevated temperatures. Hence it is also important to know the structural behaviour of members made of geopolymer concrete after exposure to elevated temperatures. However, for the best of the author's knowledge, such study has not been reported.

2.14 OBJECTIVES

Based on the literature review carried out and the gap area identified, it has been decided to have the following objectives for the present study.

- To study the influence of aggregate content on the mechanical properties of geopolymer concrete.
- To study about the different parameters that influences the mechanical properties of geopolymer concrete.
- To study the behaviour of geopolymer concrete after exposure to elevated temperatures.
- To study the flexural behaviour of reinforced geopolymer concrete after exposure to elevated temperatures.

2.15 SCOPE

Having defined the objectives, the scope of the present study has been limited to the following.

- To consider class F fly ash as source material and NaOH and Na_2SiO_3 as the alkali materials for the complete study.
- To prepare geopolymer specimen by considering different variables and to compare their relative mechanical properties for arriving at a suitable mixture proportion for geopolymer concrete. The variables to be considered for the present study include
    - Aggregate content
    - Curing temperature
    - Curing period
    - Molarity of NaOH
    - Na_2SiO_3/NaOH ratio
- To study the influence of the aggregate content on the interface shear behaviour of geopolymer concrete.
- To study the residual strength and cracking behaviour of geopolymer concrete after exposure to elevated temperatures (from ambient to 800 °C) and cooled to ambient temperature under different conditions (air cooling and water cooling).
- To study the microstructural behaviour of geopolymer paste and mortar after exposure to elevated temperatures.
- To study the deflection, moment-curvature and cracking behaviour of geopolymer concrete beams after exposure to elevated temperatures.

****

CHAPTER 3

MATERIALS AND METHODS

3.1 INTRODUCTION

Details of different materials used, method of casting and curing of specimens and details of different tests conducted related to the present study are presented in this chapter.

3.2 MATERIALS

3.2.1 Fly Ash

Fly ash was obtained from the thermal power plant at Tuticorin, Tamilnadu, India. The chemical composition of fly ash as provided by the supplier is presented in the Table 3.1.

Table 3.1. Chemical composition of fly ash

Sl.No	Parameter	Content(% mass)
1	SiO_2	59.70
2	Al_2O_3	28.36
3	Fe_2O_3 +Fe_2O_4	4.57
4	CaO	2.10
5	Na_2O	0.04
6	MgO	0.83
7	Mn_2O_3	0.04
8	TiO_2	1.82
9	SiO_3	0.40
10	Loss of ignition	1.06

From this table it could be observed that, the fly ash has low calcium content and satisfies the criteria of class F fly ash as per ASTM standard (Class F fly ash has SiO_2 + Al_2O_3 + Fe_2O_3 content of 70% or more and has less than 5% CaO).

X-ray Diffraction (XRD) analysis and particle size distribution curve of fly ash is depicted in Fig 3.1and 3.2 respectively.

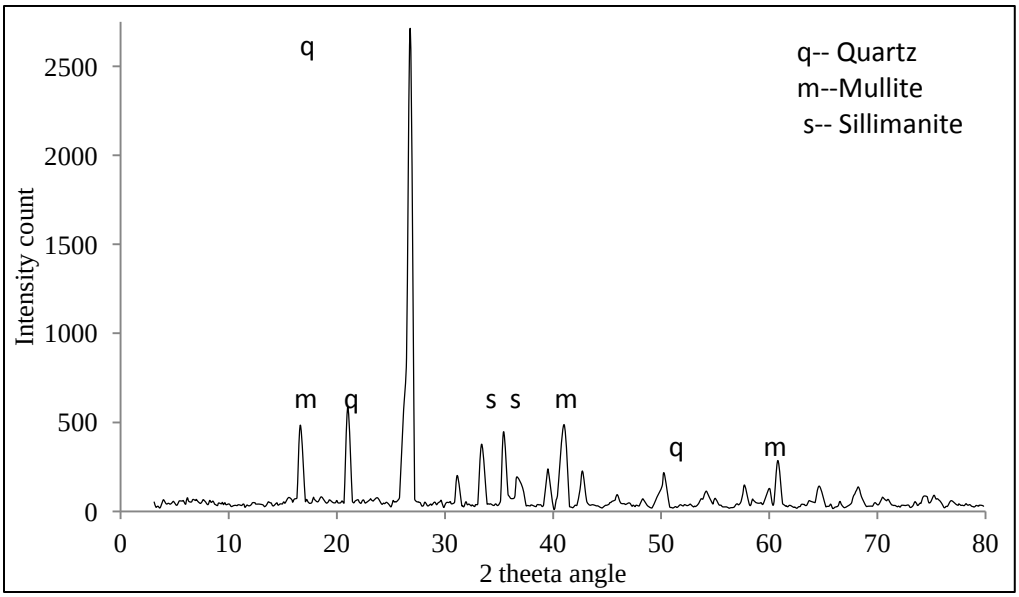

Fig. 3.1. XRD spectrum of fly ash

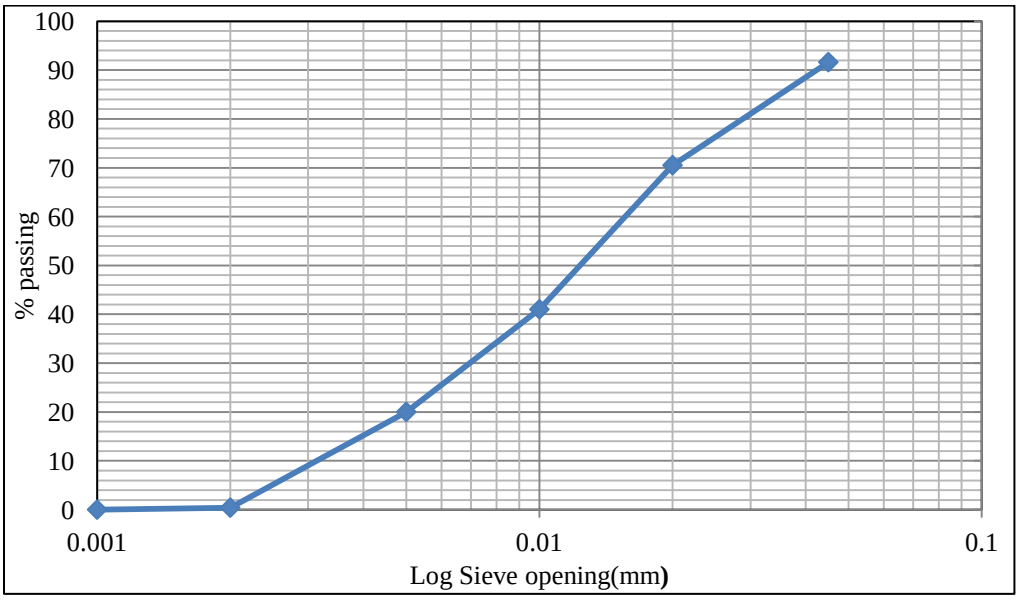

Fig. 3.2. Particle size distribution curve of fly ash

From Fig 3.1, it could be observed that the fly ash used was amorphous with a very small percentage of crystalline materials (quartz, mullite Sillimanite). Further, Fig. 3.2 shows that the mass median diameter of the fly ash used was 14 micron.

3.2.2 Alkali

The alkalis used for making geopolymer for the present study were NaOH and Na_2SiO_3.

NaOH pellets of 98% purity were purchased from the local market. The Na_2SiO_3 solution purchased from the local market had 34.64% SiO, 16.27% Na_2O, and 49.09% water.

3.2.3 Cement

For making OPC concrete, 53 grade cement conforming to BIS [133] has been used and its physical properties are given in the Table 3.2.

Table 3.2. Properties of cement

Sl.No.	Parameter	Value
1	Specific gravity	3.14
2	Fineness (90 μm sieve)	5.0%
3	Standard consistency	27.5%
4	Initial setting time	55 minutes
5	Final setting time	247 minutes

3.2.4 Fine Aggregate

Natural river sand was used as fine aggregate. The material was tested for its physical properties as per Indian Standard Code of Practices [134, 135]. Fig. 3.3 depicts the plot of particle size distribution for fine aggregates and the data corresponding to this plot are presented in Table A.1 of Appendix A. The fine aggregate used had a fineness modulus of 2.66; specific gravity 2.62 and water absorption 0.88%.

3.2.5 Coarse Aggregate

Locally available crushed granite of 20 mm nominal size has been used as coarse aggregate for the present work. The coarse aggregate used had a fineness modulus 7.3, specific gravity 2.66 and water absorption 0.19%. The details of the sieve analysis of coarse aggregates are presented in Table A2 of Appendix A.

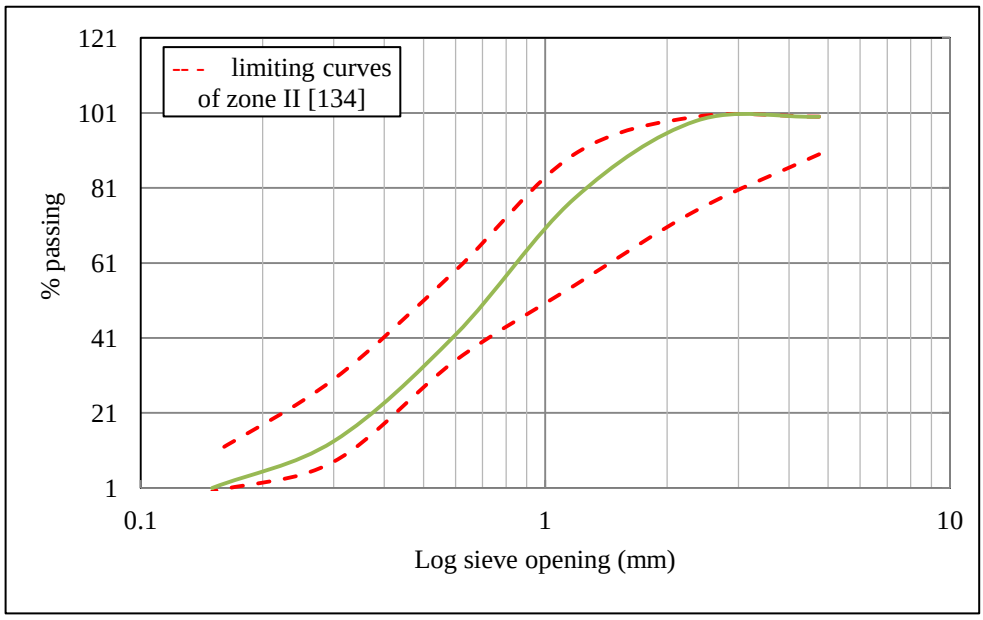

Fig. 3.3. Particle size distribution curve of fine aggregate

3.2.6 Superplasticizer

Naphthalene based water reducing admixture (commercial name-CERAPLAST 300) has been used to improve the workability of the mixture. Solid content and specific gravity of superplasticizer used was 40% and 1.24 respectively.

3.3 PREPARATION OF TEST SPECIMENS

3.3.1 Preparation of Alkali Solutions

The NaOH solution was first prepared at the required molarity. The details about the method of making NaOH with the required molarity has been presented in Appendix A.

The alkali solution for geopolymer (GP) concrete was made by mixing NaOH and Na_2SiO_3 solutions. The reaction between NaOH and Na_2SiO_3 is exothermic. Different investigators propose different methods of mixing of alkali solutions. While some investigators premix the alkali solutions 24 hours before mixing with the other constituents for making GP concrete [48,50, 63,], others [57, 136] recommend adding the alkali solutions separately during the dry mixing itself. For the present study, the alkali solution was first prepared by thoroughly mixing the NaOH and Na_2SiO_3 solutions 24 hours prior to its use.

3.3.2 Mixing, Casting and Curing of Geopolymer Concrete Specimens

Coarse and fine aggregates in saturated surface dry condition were well mixed with fly ash in a pan mixture. Naphthalene based water reducing admixture (commercial name-CERAPLAST 300) was used to improve the workability of the mixture. An admixture dosage of 2% by mass of fly ash, arrived at based on trial mixes, has been found suitable in the present study. The alkali solution (mixture of NaOH and Na_2SiO_3) and the admixture were separately added to the dry mix, and the whole mixture was mixed together for 5 minutes to make GP concrete.

All geopolymer concrete specimens were cast using standard steel moulds. The GP concrete was compacted with the help of a table vibrator. The top of the moulds were covered with steel plates immediately after casting to avoid loss of water from the specimens. The specimens thus prepared were kept at room temperature for 60 min, before they were temperature cured. The specimens (with moulds and cover plates) were then subjected to temperature curing in an electric oven. Typical temperature curing set up of a beam specimen is shown in Fig. 3.4. Specimens were taken out of the oven at the end of the curing period, demoulded and kept at room temperature under laboratory conditions until they were tested.

Standard specimens like cubes of size 150 mm, cylinders of size 150 mm diameter and 300 mm long, beam of size 500 mm x100 mm x100 mm , push off specimen of size 500 mm x 200 mm x 100 mm and reinforced beam of size 1100 mm x 150 mm x 100 mm were cast for testing.

Fig. 3.4. Photograph of electric oven for temperature curing of geopolymer concrete beam

3.3.3 Mixing and Casting OPC Concrete Specimens

OPC concrete was prepared in a pan mixer in a standard manner and the concrete was filled in the moulds in 3 layers and compacted with the help of a table vibrator. The OPC concrete specimens were kept in the mould for 24 hours under laboratory conditions and then they were demoulded and immersed in water for curing.

Standard specimen like cubes of size 150 mm, cylinder of size 150 mm diameter and 300 mm long and beams of size 500 mm x100mm x100 mm were cast for testing.

3.3.4 Heating and Cooling of Specimens

An electrically operated furnace was used to heat the specimens to elevated temperatures. The furnace has a capacity of heating up to 1200 °C. A photograph of the furnace is shown in Fig. 3.5.

Fig. 3.5. Photograph of electric furnace

Specimens were heated to set temperatures at a constant rate of 5.5 °C/minute. The rate of heating was decided based on the capacity of electric furnace and is in line with the generally considered heating rate for material study (0.5 °C/minute to 10 °C/minute). After reaching the target temperature, the specimens were kept at the set temperature for 60 minutes to ensure uniform heating within the specimen.

Two cooling methods were adopted for bringing down the temperature of the specimens to ambient temperature, namely air cooling and water cooling.

For the air cooling method, immediately after the soaking period (60 minutes) the specimens were taken out of the furnace and left for natural cooling. On the other hand, for water cooling method, after taking out the specimens from the furnace, water was sprayed on the specimen. This was to replicate the thermal shock imparted on the concrete members due to the application of water after they were exposed to fire. Typical photograph of air cooling and water cooling methods are presented in Fig. 3.6 and Fig. 3.7 respectively.

Fig. 3.6. Photograph of heated specimen on bench for air cooling

Fig. 3.7. Photograph of water spray cooling of specimen

3.3.5 Preparation of Specimens for SEM Analysis

Mortar specimens of size 10 mm diameter and 10 mm thickness, were prepared for SEM analysis. GP or OPC mortar of the same composition as that used for making GP or OPC concrete was used for preparing the specimens. Plain aluminium tubes were used as moulds for making these specimens. Figure 3.8 depicts the photograph of the specimens.

Fig.3.8. Photograph of specimens used for SEM analysis

After temperature curing and demoulding, the specimens were exposed to target temperatures (200 °C, 400 °C, 600 °C and 800 °C) using a muffle furnace.

3.3.6 Preparation of Specimens for XRD, FTIR and TGA Analysis

Geopolymer paste having the same proportion as that present in GP concrete was prepared, placed in mortar cubes (70.7 mm size) and were temperature cured. The specimens were then exposed to the target temperature in a muffle furnace. Then the prepared specimen was ground to powder for XRD and FTIR analysis.

For TGA, the powder of GP paste was taken before the specimens were subjected to elevated temperatures.

3.3.7 Method of Testing of Specimens

Testing for various physical properties like slump, compacting factor, compressive strength, tensile strength, young's modulus, etc. of specimen has been carried out as per relevant Indian standards specifications [137, 138].

3.4 CONCLUSION

A brief description about the materials used, method of preparation of geopolymer as well as OPC specimens are discussed in this chapter.

****

CHAPTER 4

ENGINEERING PROPERTIES OF GEOPOLYMER CONCRETE AT AMBIENT TEMPERATURE

4.1 INTRODUCTION

This chapter deals with the preliminary study conducted for evaluating the influence of various parameters on the engineering properties of fly ash based geopolymer concrete. The effect of different parameters like alkali content, fly ash content, quantity of aggregate, sodium silicate content, molarity of sodium hydroxide, curing temperature and curing time on the compressive strength of geopolymer concrete has been discussed. Effect of the ratio of water to geopolymer solid on workability has also been studied.

This chapter also presents an experimental investigation conducted to study the influence of aggregate content on the interface shear strength of geopolymer concrete. Push–off specimens, both reinforced and unreinforced were used to study the interface shear strength.

4.2 MIXTURE PROPORTION

Since there are many parameters that influence the physical properties of GP concrete, it is proposed to consider the parameters one by one as variable while keeping others constant. Accordingly, it has been proposed to prepare 3 groups of specimens namely M1, M2 and M3.

The first group of specimens, M1 group, has been planned to study the influence of the aggregate content on the various properties of geopolymer concrete.

The alkali-fly ash ratio considered by different investigators ranges from 0.25 to 0.75 and the ratio of Na_2SiO_3 to NaOH ranges from 0.17 to 3 [35,63,65]. Based on a preliminary study, it was observed that, the ratio of alkali to fly ash as 0.55, ratio of Na_2SiO_3/NaOH as 2.5 and a curing temperature of 100 °C yields good strength properties in geopolymer concrete. Hence, to start with, the above values were kept constant in M1

group of mixtures. The total aggregate content was varied from 60% to 75% of the volume of concrete. Further, for each value of the total aggregate content, the ratio of the mass of fine aggregate to total aggregate was varied from 0.2 to 0.4. A total of 20 mixtures were cast under M1 group and Table B.1 in APPENDIX B presents the various quantities of materials required for making one cubic meter of geopolymer concrete under group M1.

Based on test conducted on M1 group of specimens, the aggregate content that yields maximum compressive strength in geopolymer concrete has been arrived.

Having fixed the aggregate content, the influence of the ratios of sodium silicate to sodium hydroxide on the strength properties of gepolymer concrete for different alkali to fly ash ratios has been investigated in M2 group of mixtures. The total aggregate content (70% of volume of concrete), mass ratio of the fine aggregate to total aggregate (0.35) and a curing temperature (100 °C) were kept constant in all the mixtures considered under M2 group. Table B.2 in APPENDIX B presents the details of various mixtures considered under M2 group.

After testing M2 group of specimens, the ratio of sodium silicate to sodium hydroxide that yields maximum compressive strength in geopolymer concrete has been determined.

The third group of mixtures, namely M3 was prepared to study the influence of the ratio of water to geopolymer solid on the strength properties of geopolymer concrete for different alkali to fly ash ratios. The ratio of water to geopolymer solids was varied from 0.20 to 0.32. The parameters kept constant in this group include total aggregate content (70%), mass ratio of the fine aggregate to total aggregate (0.35), ratio of sodium silicate to sodium hydroxide (2.50) and curing temperature (100 °C). The quantity of materials used for making one cubic meter of concrete under this group is given in Table B.3 of APPENDIX B

Having fixed the values of various parameters, the influence of curing temperature and curing period on the strength of GP concrete has been investigated. Accordingly the parameters that are kept constant for the study include total aggregate content (70%), mass ratio of the fine aggregate to total aggregate (0.35), ratio of Na_2SiO_3 to NaOH (2.50) and the ratio of water to geopolymer solid (0.25). The curing

temperature was varied from ambient (28 °C) to 120 °C and curing period was varied from 6 hours to 72 hours.

Further, by keeping all other parameters at their arrived values, the influence of the molarity of NaOH on the strength of GP concrete has been studied. In this case, the parameters that were kept constant include the total aggregate content (70%), mass ratio of the fine aggregate to total aggregate (0.35), ratio of Na_2SiO_3 to NaOH (2.50) , ratio of water to geopolymer solid (0.25) and curing temperature (100 °C). The molarity of NaOH was then varied from 8 to 16.

4.3 MIXING, CASTING AND CURING

The method of mixing, casting and curing of specimens has already been discussed in section 3.3 of chapter 3.

4.4 ANALYSIS OF THE TEST RESULTS

Each value of the result discussed or presented in tables and figures is the mean of 3 test results. Further, individual strength test results were well within the range of $\pm$15% of the mean value [138].

4.4.1 Workability

Due to the high cohesive nature of geopolymer concrete, no appreciable slump value could be obtained. As a result, the compacting factor [137] has been considered for comparing the workability of geopolymer concrete. A typical comparison of the compacting factor with different ratio of water to geopolymer solid is shown in Fig. 4.1.

It could be seen from Fig. 4.1 that the compacting factor increases almost linearly with the ratio of water to geopolymer solid. Further, as expected, the compacting factor is higher for a higher alkali to fly ash ratio.

4.4.2 Compressive Strength

Variation of the strength of geopolymer concrete with age after the period of temperature curing is presented in Table 4.1 for different total aggregate content.

It can be seen from Table 4.1 that, the rate of strength development of geopolymer concrete beyond 7^{th} day is marginal, unlike OPC (OPC A67R29) concrete.

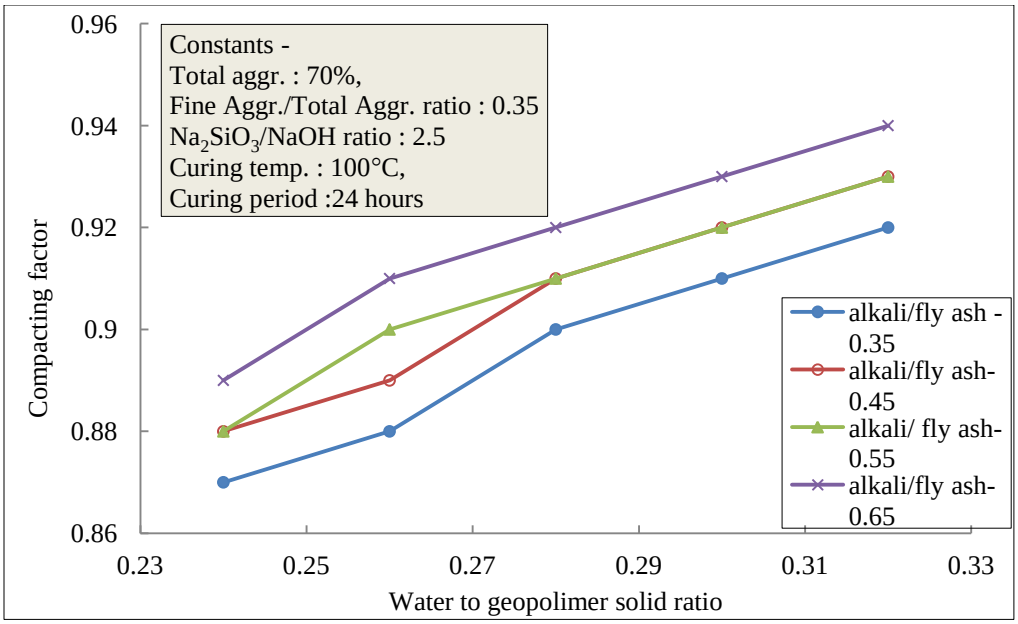

Fig 4.1. Variation of compacting factor with the ratio of water to geopolymer solid.

Table 4.1. Variation of cube compressive strength of geopolymer and OPC concrete with age

S l. No.	Mix ID	Total Aggr. Content (%)	Cube compressive strength (MPa)		
			3^{th} day	7^{th} day	28^{th} day
1	M1A60R35*	60	42	43	45
2	M1A65R35*	65	45	46	47
3	M1A70R35*	70	52	54	56
4	M1A75R35*	75	45	48	49
5	OPC A67R29	67	45	51	58
	* Curing temperature: 100 ºC; curing period: 24 h; ratio of alkali to fly ash: 0.55; ratio of Na_2SiO_3 to NaOH: 2.5; and ratio of fine aggregate to total aggregate: 0.35.				

The influence of aggregate content on the compressive strength of geopolymer concrete is presented in Fig. 4.2 and 4.3. Details of the test results are presented in Table B.4 of APPENDIX B. While Fig. 4.2 shows the influence of total aggregate

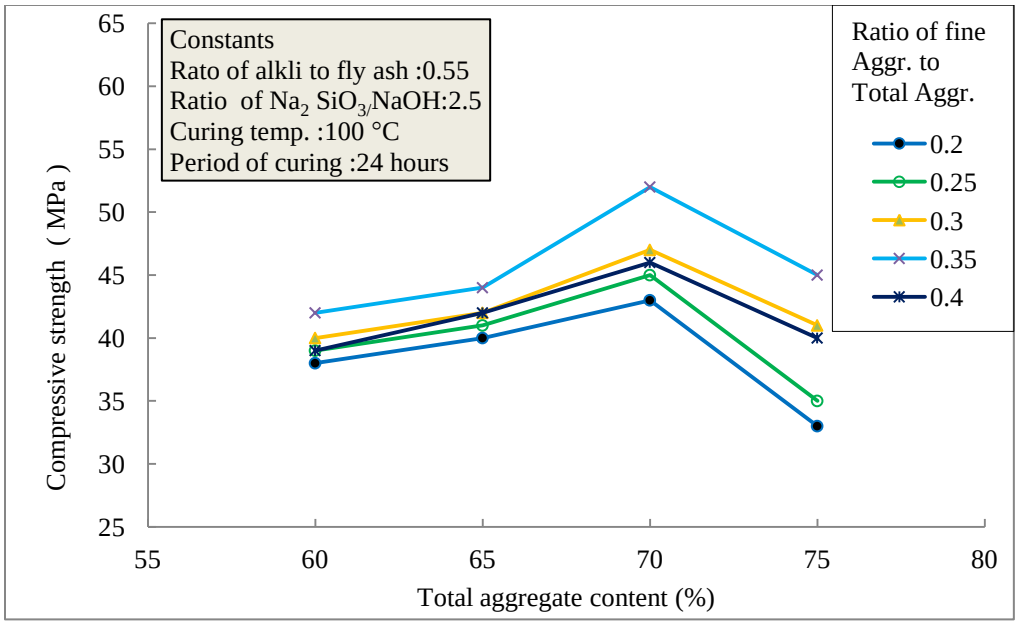

Fig. 4.2. Variation of 7th day compressive strength with total aggregate content.

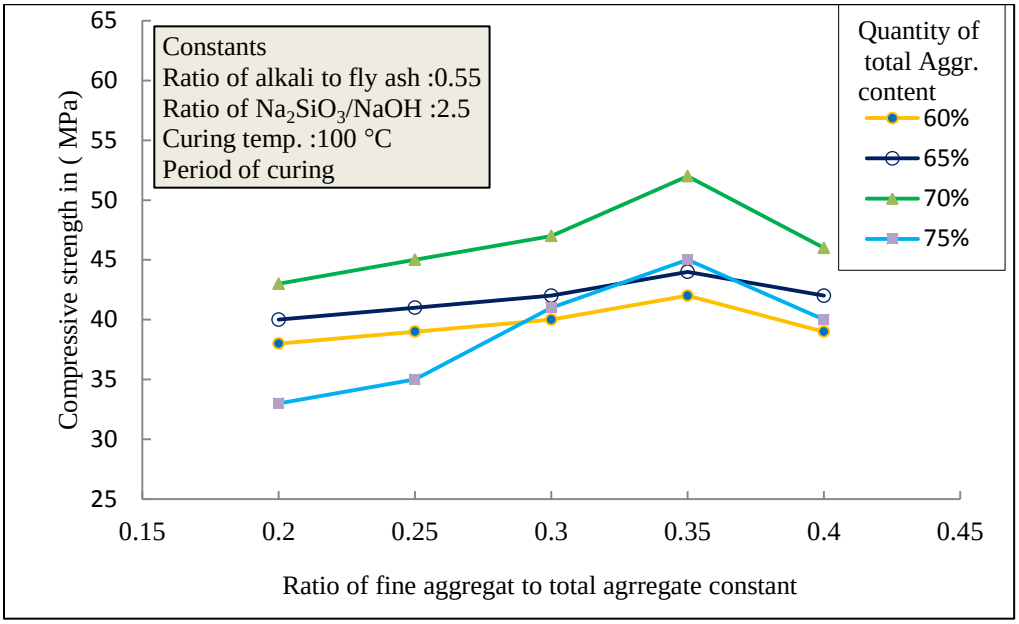

Fig. 4.3. Variation of 7th day compressive strength with ratio of fine aggregate to total aggregate content

content on compressive strength, Fig 4.3 shows the variation of the ratio of fine aggregate to total aggregate on 7th day compressive strength of geopolymer concrete. The constant parameters considered in these figures have been decided based on a preliminary study

(explained in section 4.2, page 59). It could be observed from Fig. 4.2 that, the compressive strength of geopolymer concrete increases with increase in total aggregate content up to a value of 70% and then it decreases. This phenomenon is true for all values of the ratio of fine aggregate to total aggregate

considered (0.20–0.40). From Fig. 4.3, it could be observed that the compressive strength of geopolymer concrete increases with an increase in the ratio of fine aggregate to total aggregate for a value up to 0.35 and then it decreases. This phenomenon is true for all the values of the total aggregate content in the mixture considered (60%–75% by volume).

So, it is evident that for a given type of fine and coarse aggregate, there is a definite proportion of total aggregate and fine aggregate that gives maximum compressive strength for geopolymer concrete. This behaviour is similar to that of conventional concrete and is due to the fact that the optimum proportion of fine aggregate and coarse aggregate yields efficient binding by geopolymer.

Having obtained the proportion of aggregates for maximum strength, the other mechanical properties like split tensile strength, flexural strength, poissons's ratio and young's modulus were also determined by varying total aggregates content but by keeping the ratio of fine aggregate to total aggregate as 0.35. These test results are presented in Table 4.2.

Table 4.2. Mechanical properties of Group M1 mix concrete

S.l.No.	Mix ID	Tensile strength (MPa)		Poisson's ratio	Modulus of elasticity (MPa)
		Split tensile	Flexural strength		
1	M1A60R35*	3.10	3.79	0.192	42369
2	M1A65R35*	3.34	3.82	0.202	45082
3	M1A70R35*	3.45	4.74	0.242	59068
4	M1A75R35*	4.51	4.95	0.195	47519
5	OPC A67R29**	4.39	4.79	0.203	51623

*Strength results on 28th day. Curing temperature: 100; curing period: 24 h; ratio of alkali to fly ash: 0.55; ratio of Na_2SiO_3 to NaOH: 2.5; and ratio of fine aggregate to total aggregate: 0.35.
** Strength results on 28th day

More details about the test data are shown in Table B.5 to B.9 of APPENDIX B. From Table 4.2, it could be observed that the tensile strength of geopolymer concrete increases with the total aggregate content. Geopolymer concrete with 70% aggregate content gave a flexural strength higher by 37% than its corresponding split tensile strength. On the other hand, the corresponding ordinary concrete gave a flexural strength higher by only 9% than its split tensile strength. Further, geopolymer concrete with total aggregate content value other than 70% gave a flexural strength higher by 9% to 22% than the corresponding split tensile strength.

From Table 4.2, it could be seen that the modulus of elasticity of geopolymer concrete is the highest for total aggregate content of 70% with fine aggregate to total aggregate content of 35%. It has been reported elsewhere that the modulus of elasticity of geopolymer concrete is lower compared to that of normal concrete [35,65]. However from Table 4.2, it could be concluded that by proper proportioning of aggregate content in geopolymer concrete, it's modulus of elasticity can be brought to an even higher level than that of ordinary cement concrete. Table 4.2 also present the value of poisson's ratio of geopolymer concrete for different aggregate content. It is obvious that the concrete with the higher modulus of elasticity shows a higher poisson's ratio and the present study also proves the same.

Figure 4.4 shows the variation of 7^{th} day compressive strength of geopolymer concrete with the ratio of sodium silicate to sodium hydroxide for different values of alkali to fly ash ratios.

The total aggregate content and the ratio of fine aggregate to total aggregate in all these mixes were kept at a constant value of 70% and 0.35 respectively. Details of test results are shown in Table B.10, APPENDIX B.

From Fig. 4.4, it could be seen that the compressive strength of geopolymer concrete increases with the ratio of sodium silicate to sodium hydroxide up to a value of 2.5 and then it decreases. Further, up to a value of the ratio of alkali to fly ash 0.55, the compressive strength increases and beyond that it decreases. Increase in compressive strength is mainly due to the change in microstructure of geopolymer, which was influenced by the quantity of sodium silicate. On the other hand, the decrease in compressive strength is because of the fact that, at high ratios of sodium silicate to

sodium hydroxide, the quantity of sodium hydroxide is not sufficient for the completion of dissolution process during the formation of geopolymer [25,139].

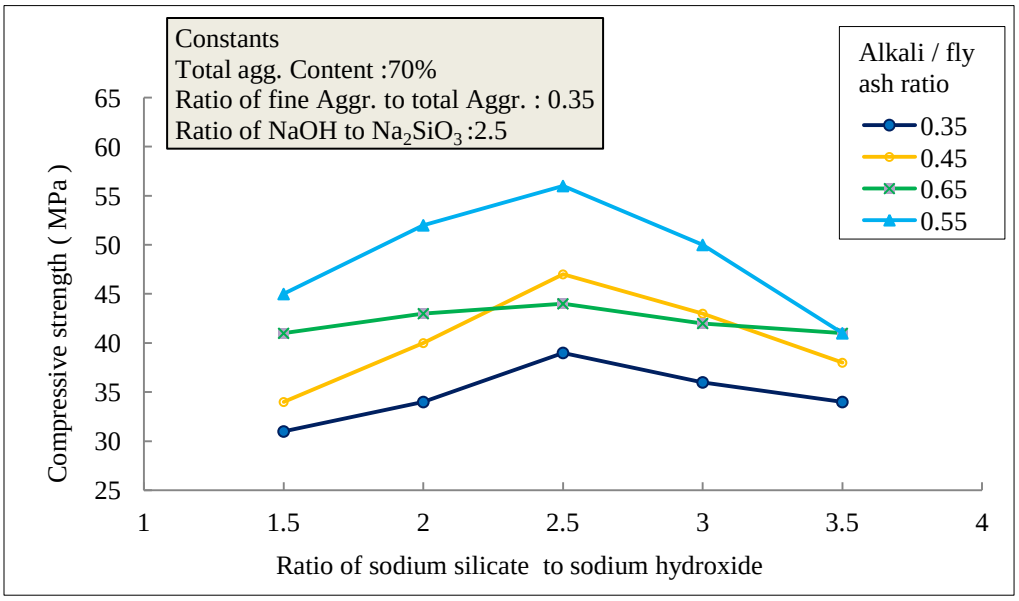

Fig. 4.4. Variation of 7th day cube compressive strength with ratio of sodium silicate to sodium hydroxide

The variation of the compressive strength with change in molarity of NaOH is depicted in Fig. 4.5. Table B.11 in APPENDIX B shows more details of the test result.

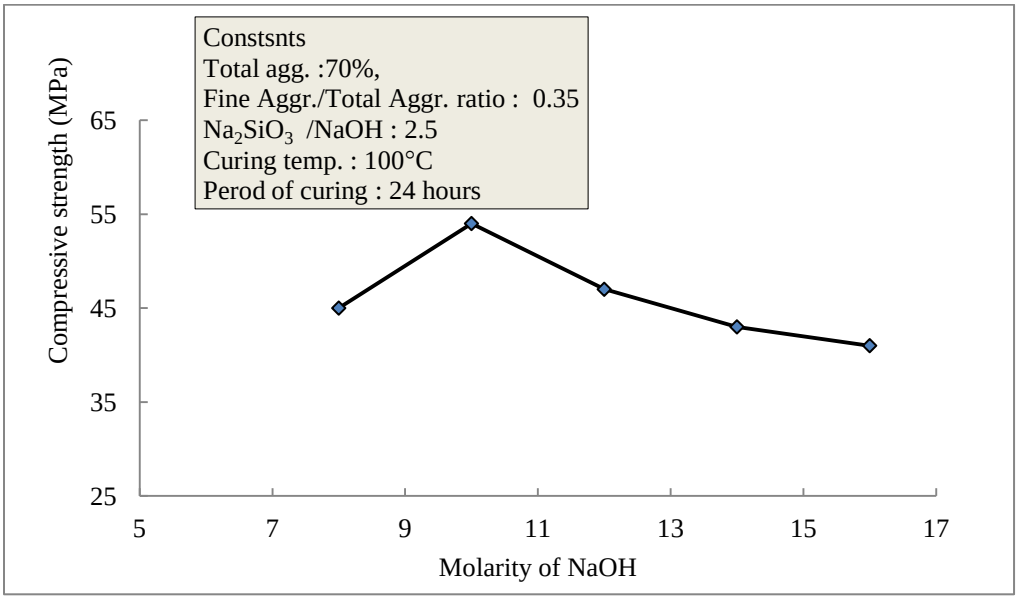

Fig. 4.5. Variation of 7th day cube compressive strength of geopolymer concrete with molarity of NaOH

It could be observed from Fig. 4.5 that, the compressive strength of geopolymer concrete increased with increase in molarity of NaOH up to a value of 10 and on further increase of molarity of NaOH, the compressive strength decreases. This behaviour is mainly due to the fact that the concentration of NaOH solution has a positive influence on dissolution, hydrolysis and condensation reactions but excess alkali concentration hinders the condensation of the silicate species [25, 43] a that formed during dissolution and hydrolysis. So, it could be observed that there is an optimum value for the ratio of sodium silicate to sodium hydroxide, ratio of alkali to fly ash and molarity of NaOH that yields maximum compressive strength for a geopolymer concrete.

Fig 4.6 shows the effect of curing temperature on cube compressive strength of geopolymer concrete (Test details are presented in Table B.12 of APPENDIX B).

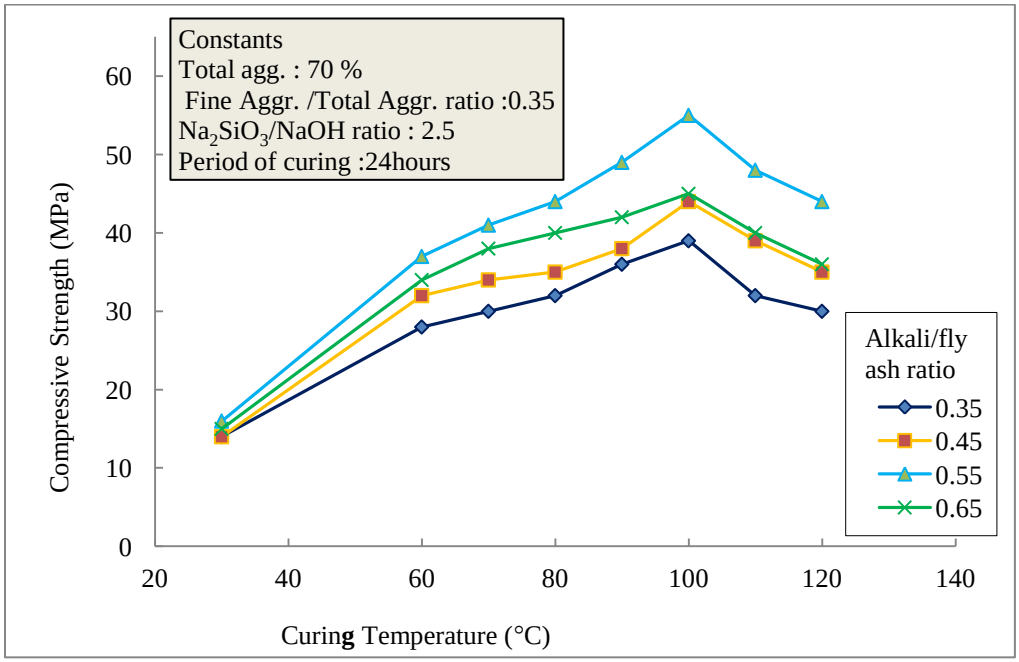

Fig. 4.6. Variation of 7th day cube compressive strength of geopolymer concrete with curing temperature

From Fig. 4.6, it could be seen that the compressive strength increases with increase in curing temperature up to 100 °C, and then it decreases. Further, the maximum compressive strength has been observed for the mixture having the ratio of alkali to fly ash as 0.55. The phenomenon of increase in strength of GP concrete with increase in

temperature is in line with the reported literature, although the curing temperature for maximum strength differs from 100 °C [56, 63].

The loss of strength beyond the curing temperature of 100 °C is due to the loss of moisture from the specimen. Even if sealed properly, at temperatures above 100 °C, the specimen may dry out and lead to a reduced strength. Even though similar observations were reported by investigators earlier [57, 63], a study on the shrinkage, cracking and durability may yield a better understanding on the actual behaviour of GP concrete.

Figure 4.7 shows the influence of the period on strength of geopolymer concrete for a curing temperature of 100 °C (test details are shown in Table B.13 of APPENDIX B).

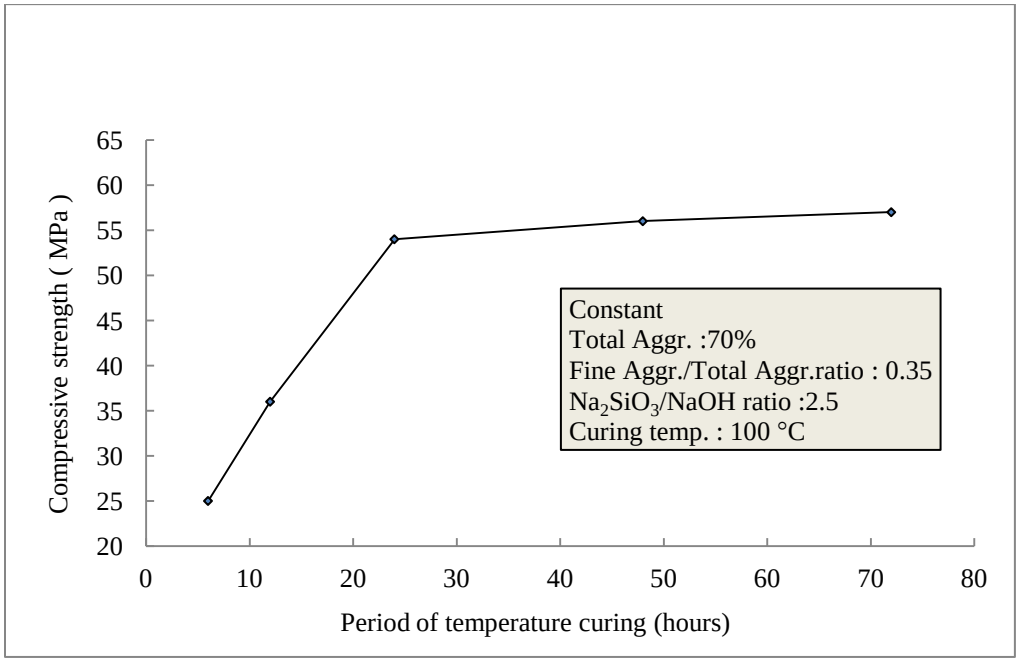

Fig. 4.7. Variation of 7th day cube compressive strength of geopolymer concrete with period of temperature curing.

From Fig. 4.7, it could be observed that, up to a curing period of 24 h, the strength gain of geopolymer is proportional to the period of curing and no appreciable strength gain could be obtained beyond 24 hours. This could be due to the reason that most of the polymerization would have been completed within 24 hours.

Variations in the compressive strength of geopolymer concrete with the ratio of total water to geopolymer solid is presented in Fig. 8 (test details are presented in Table B.14 of APPENDIX B).

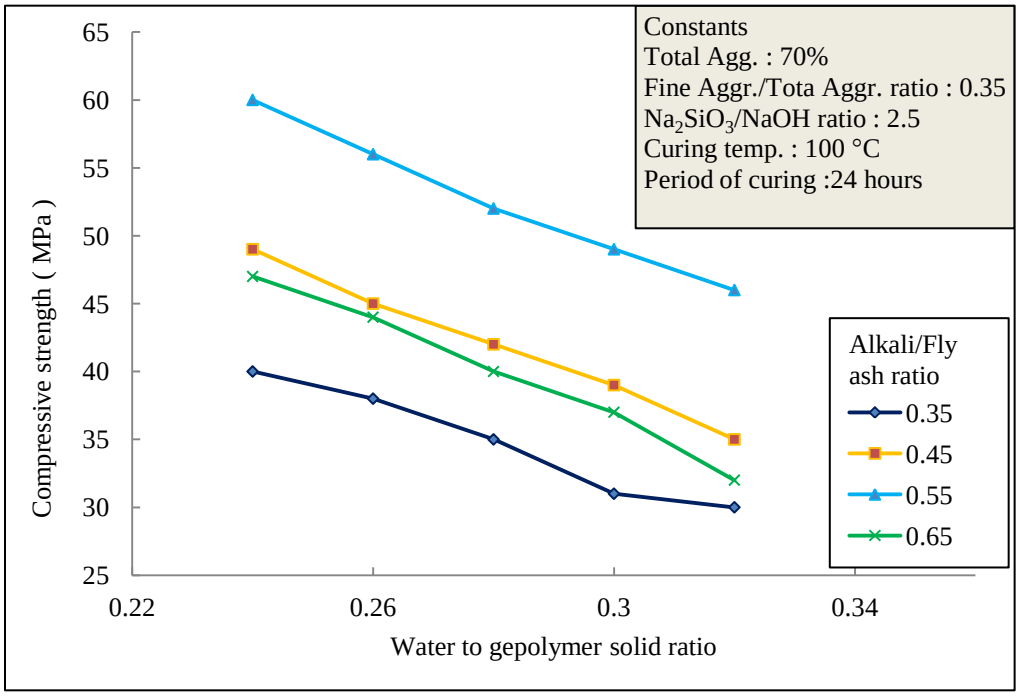

Fig. 4.8. Variation of 7th day cube compressive strength of geopolymer concrete with ratio of water to geopolymer solid

From Fig. 8, it could be seen that the compressive strength of geopolymer concrete decreases as the water to geopolymer solid ratio increases. The variation is almost linear for all values of alkali to fly ash ratios considered.

4.5 INTERFACE SHEAR STRENGTH OF GEOPOLYMER CONCRETE

Geopolymer concrete is best suited for pre-cast construction. The connective distress in pre-cast construction is primarily on the shear interfaces. However, limited study has been reported in the case of the interface behaviour of geopolymer concrete. Hence a preliminary study has been carried out to understand how geopolymer concrete behaves under similar condition.

Push -off specimens were prepared to study the influence of the aggregate content on the interface shear strength of geopolymer concrete. For preparing the GP concrete specimens, the ratio of fine aggregate to total aggregate (=0.35), ratio of alkali to fly ash (=0.55), molarity of NaOH (=10), ratio of Na_2SiO_3 to NaOH (=2.5), ratio of water to geopolymer solid (=0.25) were kept constant. The total aggregate content in the mixture was varied from 60% to 75% of the volume of GP concrete. A reference OPC concrete mixture proportion has also been arrived at based on a trial and error method, such that, its compressive strength is almost the same as that of the GP concrete that gave maximum compressive strength. Table 4.3 shows the quantity of materials required to produce $1m^3$of GP concrete and OPC concrete for making push- off specimens.

Table 4.3. Quantity of materials for 1 m^3 of geopolymer concrete

Sl.No.	Mix ID	Total Aggr. (% by vol.)	Fine Aggr./ Total Aggr.	Coarse Aggregate (kg)	Sand (kg)	Fly ash (kg)	Alkali content (kg)	Super plasticizer (kg)
1	M1A60R35*	60	0.35	1031.99	555.73	420.57	231.31	8.41
2	M1A65R35*	65	0.35	1117.99	602.04	365.16	210.84	7.3
3	M1A70R35*	70	0.35	1203.99	648.35	309.85	170.41	6.2
4	M1A75R35*	75	0.35	1289.99	694.66	254.54	139.99	5.1
5	OPC A65R29**	0.67	0.39	1279	500	-	-	1.9

The size of push-off specimen reported in published literature varies [128,130-132]. Hence, depending on the test facility available, 100 mm x 200 mm x 500 mm size push-off specimens has been considered for the present study. V-grooves of 4 mm depth were made on either sides of the specimen along the shear plane with the help of standard angles. The push-off specimens were cast with and without dowel bars. Two 8 mm diameter dowel bars (0.95% of concrete cross section) having yield strength of 435 MPa, were placed across the shear plane (0.99%), in the form of a link. Additionally, 10 mm diameter bars and 8 mm diameter stirrups were provided to prevent premature failure at

the loading points for all specimens. Schematic diagram of push- off specimen showing the dimensions and details of reinforcements is presented in Fig.4.9.

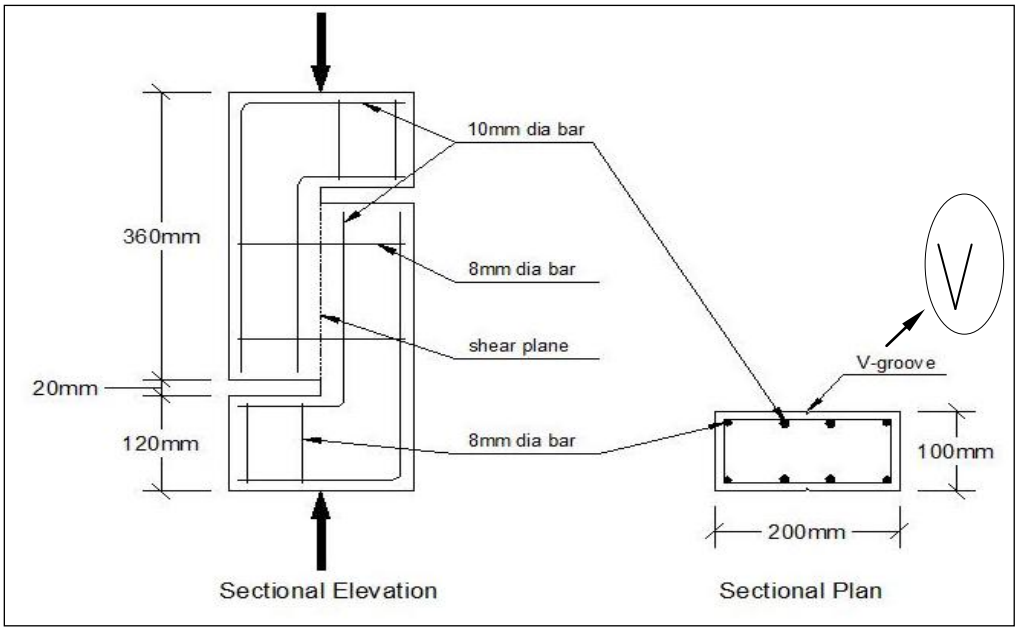

Fig. 4.9. Details of Push - off Specimen

4.5.1 Testing of push-off specimen

The experimental set up for the push-off specimen is presented in Fig. 4.10. Axial load was applied on push- off specimens at regular intervals until failure occurred. Average shear strength of the concrete was calculated on the basis of the area of shear plane. Dial gauges were used to measure the relative slip at the shear plane.

4.5.2 Analysis of Test Result

Figure 4.11 presents the variation of slip with interface shear stress in push-off specimens in which no shear reinforcement across the shear plane has been provided.

From this figure, it is clear that, for a given value of shear strength of geopolymer specimen, the slip is more with lower aggregate content. Further, as the aggregate content increases, the ultimate shear strength also increases. This is primarily due to the improvement of the cohesive strength of concrete and better aggregate interlocking at the interface with higher percentage of aggregate content. It has been reported that, for low steel ratios the cohesive stı ıgth of concrete has considerable influence on interface shear strength [127]

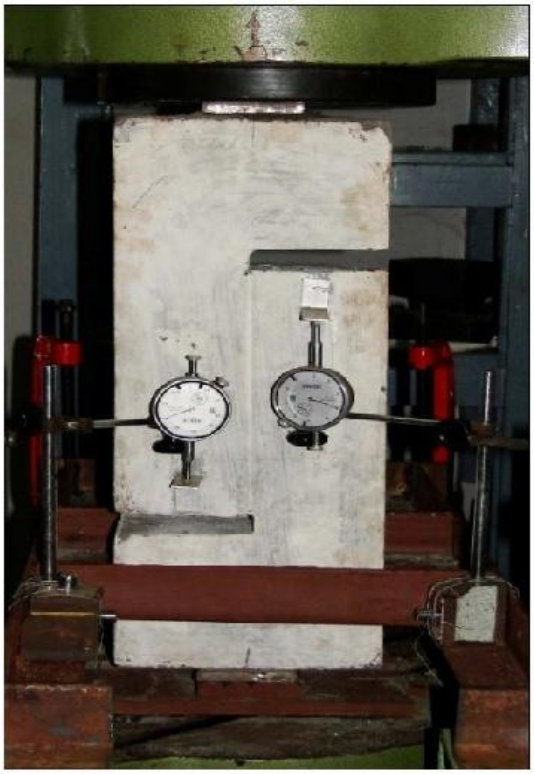

Fig. 4.10. Test Setup for slip measurement

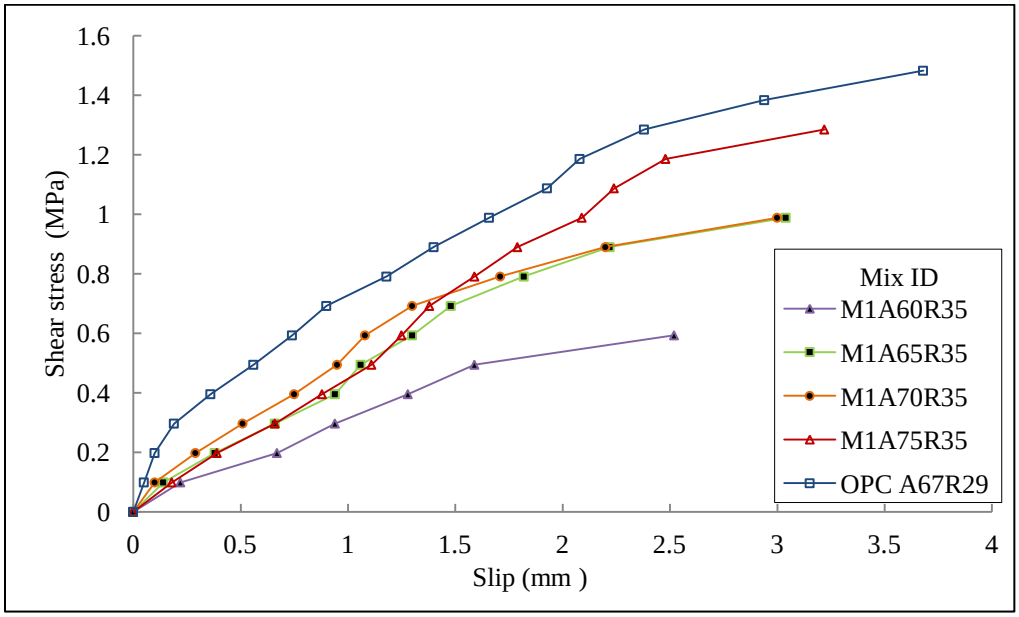

Fig. 4.11. Variation of slip with interface shear stress in specimen without shear reinforcement

From this figure, it is clear that, for a given value of shear strength of geopolymer specimen, the slip is more with lower aggregate content. Further, as the aggregate content increases, the ultimate shear strength also increases. This is primarily due to the improvement of the cohesive strength of concrete and better aggregate interlocking at the interface with higher percentage of aggregate content. It has been reported that, for low steel ratios the cohesive strength of concrete has considerable influence on interface shear strength [127]

Figure 4.12 depicts the variation of slip with shear stress in push- off specimen with 0.99% shear reinforcement. This figure also shows a similar behaviour as that of the specimen without shear reinforcement. Hence, it could be stated that, for a given interface shear stress, a GP concrete with an aggregate content less than 65% shows large slip values. It may be further noted from Fig. 4.11 and 4.12 that, for a given shear strength, the slip of GP specimen is more than that of the OPC specimen which has almost the

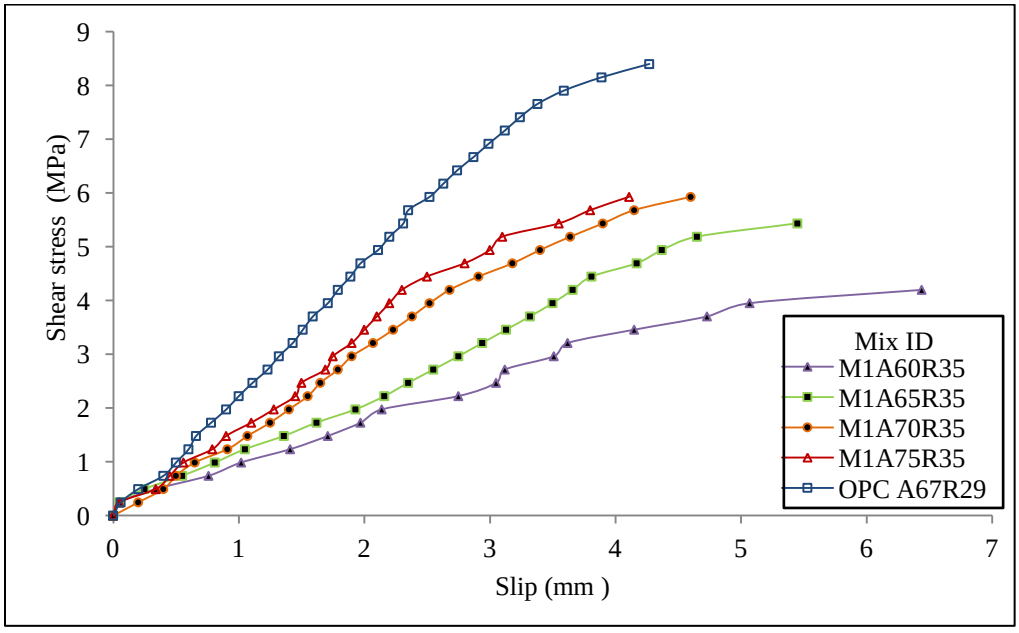

Fig. 4.12. Variation of slip with interface shear stress in specimen with shear reinforcement

same compressive strength of GP specimen (M1A70R35) in the case of specimens with and without shear reinforcement. The OPCA67R29 and M1A70R35 had respectively 67% and 70% total aggregate content. This clearly shows that the cohesive strength of

GP concrete is inferior to OPC concrete as far as the interface shear resistance is concerned.

The ultimate shear strength of specimens tested is presented in Table 4.4.

Table 4.4. Ultimate shear strength in Push-off specimen

Specimen ID	Unreinforced specimen		Reinforced specimen	
	Ultimate Load (kN)	Ultimate shear Strength (MPa)	Ultimate Load (kN)	Ultimate shear Strength (MPa)
M1A60R35	12	0.59	85	4.19
M1A65R35	19	0.94	110	5.43
M1A70R35	20	0.99	120	5.92
M1A75R35	26	1.28	120	5.92
OPC A767R29	30	1.48	170	8.34

From this table, it could be observed that, the shear strength of both the types of GP specimens (unreinforced and reinforced) is very much low when the total aggregate content is lower than 65%. Further, while the unreinforced GP specimen shows an increase in shear strength with increase in aggregate content, the GP specimen with shear reinforcement shows no significant variation (about 8% only) in shear strength for an aggregate content more than 65%. This proves that, the contribution of cohesive strength in the development of ultimate interface shear resistance of GP concrete is negligible (one of the assumptions in the development of interface shear friction theory) if its aggregate content is more than 65%. From Table 4.4, it could be observed that with 0.99 %, shear reinforcement, the ultimate shear strength of OPC specimen is increased by about 4.5 times and that of the corresponding geopolymer concrete (M1A70R35) is increased by about 5 times. The other GP concrete specimen had an average increase in ultimate shear strength by about 4.5 times when shear reinforcement is provided.

Comparing OPC concrete that has almost same compressive strength of GP concrete (M1A70R35), it could be observed from Table 4.4 that, the ultimate interface shear strength of GP concrete is inferior to OPC concrete. For the present study, compared to OPC concrete, a reduction in the strength by 33% and 29% was observed for unreinforced and reinforced GP specimens respectively. Hence, the equations available to

calculate interface shear capacity of OPC concrete may overestimate the interface shear capacity of GP concrete.

Table 4.5 compares the experimental interface shear capacity of reinforced specimen with the empirical formula available in literature [127,129,130]. From this table, it may be observed that the empirical formula proposed for OPC concrete, when used in GP concrete overestimates the interface shear capacity for GP concrete if its aggregate content is equal to and less than 65%. In the present study, while Mast [127] overestimates the shear strength by about 43% for 60% aggregate content (M1A65R35), the value is only about 2% for GP concrete with 75% aggregate content (M1A70R35). On the other hand, the interface shear strength of OPC concrete specimen is underestimated by about 28% to 32% when different formulae are used to predict the interface shear strength. Since no equation is available for the prediction of interface shear strength of GP concrete it is recommended that, only 50% of the predicted

Table 4.5. Comparison of Shear capacity of reinforced concrete with the calculated value using empirical formula

Specimen I D	Ultimate load Experimental value Pu_{exp} (kN)	Ultimate load Theoretical value P_{Uth} (kN)			Pu_{exp}/ Pu_{th}		
		Mast	Mattock	ACI	Mast	Mattock	ACI
M1A60R35	85	122	119	116	0.69	0.71	0.73
M1A65R35	110	122	119	116	0.90	0.92	0.94
M1A70R35	120	122	119	116	0.98	1.00	1.03
M1A75R35	120	122	119	116	0.98	1.00	1.03
OPC A67R29	170	122	119	116	1.41	1.42	1.46

interface shear strength based on the available equations can be considered as the shear strength of GP concrete which has an aggregate content above 65%. However, further study has to be carried out to propose a more refined estimation of interface shear strength of geopolymer concrete.

4.6 CONCLUSIONS

Following conclusions could be derived based on the discussions carried out in this chapter.

1. The compressive strength of fly ash based geopolymer concrete increases with increase in curing temperature up to a value of 100 °C, beyond which it decreases.
2. An early strength development in geopolymer concrete could be achieved by the proper selection of curing temperature and the period of curing. With 24 hours of curing at 100 °C, 96.4 % of 28th day cube compressive strength could be achieved in 7 days according to the present study.
3. Modulus of elasticity as well as the Poisson's ratio of geopolymer concrete can be brought equal to or even higher than that of the corresponding ordinary portland cement concrete by the proper selection of total aggregate content and ratio of fine aggregate to total aggregate content in geopolymer concrete. In the present study, compared to ordinary portland cement concrete, 14.4% enhancement in modulus of elasticity and 19.2% enhancement in Poisson's ratio could be achieved in geopolymer concrete having 70% total aggregate content and the ratio of fine aggregate to total aggregate as 0.35.
4. The tensile strength of geopolymer concrete increases with increase in the total aggregate content. In the present study, as the total aggregate content varied from 60% to 75% (with a constant ratio of fine aggregate to total aggregate 0.35), the split and flexural tensile strength increased by 45.5% and 30.6%, respectively.
5. Based on the present study, a geopolymer concrete with total aggregate content of 70% by volume, ratio of fine aggregate to total aggregate of 0.35, NaOH molarity 10, Na_2SiO_3/NaOH ratio of 2.5 and alkali to fly ash ratio of 0.55, cured for 24 hours at 100 °C gave an average cube compressive strength of 54 MPa after 7 days (56 MPa after 28th day). This geopolymer concrete gave a higher value of Poisons ratio and modulus of elasticity compared to ordinary cement concrete having almost the same cube compressive strength as that of geopolymer concrete.
6. For a given interface shear stress, geopolymer concrete specimen shows more slip compared to OPC concrete specimen.

7. The interface shear strength of geopolymer concrete is inferior to OPC concrete. In the present study, compared to OPC concrete, a reduction in the strength by 33% and 29% was observed for unreinforced and reinforced geopolymer specimens respectively.
8. When the total aggregate content is lower than 65%, the interface shear strength of both unreinforced and reinforced geopolymer specimens becomes very much low.
9. The enhancement in interface shear strength of reinforced (with 0.99% steel) geopolymer concrete specimen is not significant (about 8% only) for an aggregate content above 65%.
10. The equations available to calculate interface shear capacity of OPC concrete very much overestimate the interface shear capacity of geopolymer concrete if its aggregate content is less than 65%.
11. Approximate value of the interface shear strength of geopolymer concrete (that has an aggregate content above 65%) could be predicted by considering 50% of the value. obtained based on the prediction equations available (Mattock and ACI) for the calculation of the interface shear capacity of OPC concrete.
12. Further study is needed to have a better estimation of the interface shear strength of geopolymer concrete.

****

CHAPTER 5

ENGINEERING PROPERTIES OF GEOPOLYMER CONCRETE AFTER EXPOSURE TO ELEVATED TEMPERATURES

5.1 INTRODUCTION

Even though much study has been carried out on the behaviour of concrete exposed to elevated temperatures, to the best of the author's knowledge, no systematic study has been reported to understand how the geopolymer concrete behaves when exposed to elevated temperatures. Only limited information is available about the behaviour of geopolymer concrete when exposed to elevated temperatures.

This Chapter presents the engineering properties of fly ash based geopolymer concrete after exposure to elevated temperatures and compares the corresponding results with those of conventional concrete.

The details of SEM analysis of GP mortar and XRD, FTIR spectrum and TGA analysis of geopolymer paste after exposure to elevated temperatures are also discussed in this chapter.

5.2 MIXTURE PROPORTION

The quantity of different constituents of the mixture that give maximum compressive strength and other mechanical properties like tensile strength, flexural strength, modulus of elasticity and poisson's ratio have been arrived in chapter 4. The mixture proportion has been considered for further study. Accordingly, following parameters have been considered for the of GP concrete.

Aggregate content by volume = 70%

Mass ratio of fine aggregate to total aggregate = 0.35

Ratio of alkali to fly ashy by mass = 0.55

Molarity of NaOH = 10

Ratio of Na_2SiO_3 to NaOH = 2.5

Curing temperature = 100 °C

Temperature curing time = 24 hours

A reference OPC concrete mixture proportion has also been arrived at based on a trial and error method, such that, it's compressive strength is almost the same as that of the GP concrete. The quantity of materials required for producing $1m^3$ of GP concrete and OPC concrete based on the proportions considered is given in Table 5.1

Table 5.1. Quantity of materials required to produce $1m^3$ of GP and OPC concrete

Mix ID	Cement (kg)	Fly ash (kg)	Coarse Aggr. (kg)	Fine Aggr. kg)	NaOH solution (kg)	Na_2SO_3 (kg)	Super Plasticizer (kg)
GP concrete	----	310	1204	648	48.7	121.7	6.2
OPC concrete	475	-----	1279	500	-----	-----	1.9

The specimens prepared were subjected to elevated temperatures at different levels, namely 200 °C, 400 °C, 600 °C and 800 °C on the 28^{th} day. The method of temperature exposure and cooling has been discussed in section 3.3 of chapter 3.

5.3 ANALYSIS OF RESULTS

5.3.1 Compressive Strength

Table 5.2 gives the compressive strength of GP and OPC concrete after exposure to elevated temperatures (test details are presented in Table C.1 of APPENDIX C).

Table 5.2. Cube compressive strength of GP and OPC specimens after exposure to elevated temperatures

Exposure Temperature (°C)	GP Concrete				OPC Concrete			
	Air cooled		Water cooled		Air cooled		Water cooled	
	Comp. strength (MPa)	SD*	Comp. strength (MPa)	SD*	Comp. strength (MPa)	SD*	Comp. strength (MPa)	SD*
Ambient (28)	57.30	0.45	-	-	59.85	0.68	-	-
200	42.52	0.68	39.40	0.68	59.60	1.17	54.37	0.88
400	37.33	0.45	35.85	0.44	42.66	0.44	39.85	1.14
600	30.82	0.67	28.00	0.94	32.44	0.84	31.48	0.54
800	32.88	0.38	31.30	0.31	21.00	0.31	19.55	0.62
* SD - Standard deviation								

From Table 5.2, it could be observed that, compared with OPC concrete, there is a higher strength loss for GP concrete during the early stages of temperature rise, even though both have almost the same compressive strength. In the present study, at 200 °C , while air cooled and water cooled OPC concrete had a strength loss of about 0.4 % and 9% respectively, the corresponding loss of strength of GP concrete is about 26 % and 31% respectively.

The reasons for a higher strength loss in GP concrete during the early stages of temperature exposure, are due to the reduction in bonding force and decrease in chain length in Si-O-Al and Si-O-Si regions (explained in section 5.3.6), and due to the expulsion of most of the water present in the geopolymer and also due to the result of microcrack formation (explained in section 5.3.8 and 5.3.5).

In the case of OPC concrete, even though the free water in concrete gets removed, the strength gained due to the hydration of unreacted cement particles as a result of the heating compensates the strength loss due to other parameters in concrete when heated up to about 200 °C; a behaviour well accepted by many researchers [91,140].

Figure 5.1 shows the residual compressive strength of the test specimen (in percentage of strength at ambient temperature) after exposure to different temperatures and tested after cooling by air and water cooling methods.

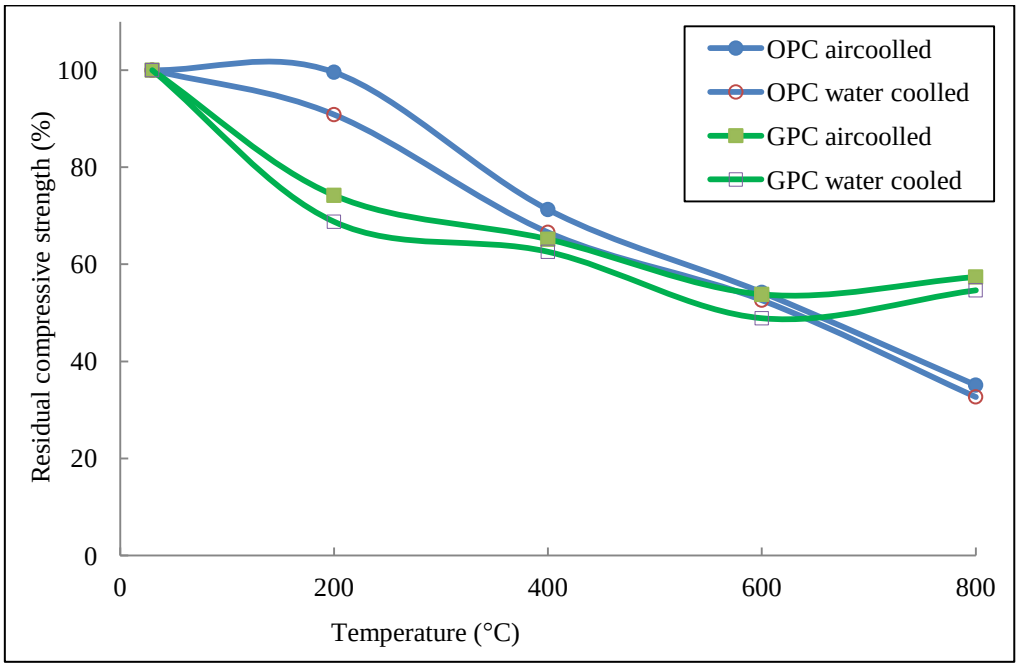

Fig. 5.1. Residual cube compressive strength of GP and OPC concrete after exposure to elevated temperatures

From Fig.5.1, it could be observed that, the air cooled OPC specimen does not experiences much strength reduction up to 200 °C beyond which, there is more or less a constant rate of strength reduction up to 800 °C .

Compared to air cooled OPC specimen, even though there is a higher rate of strength reduction for GP concrete up to a temperature exposure of 200 °C, the rate of strength reduction between 200 °C and 400 °C is less for GP concrete and the percentage of residual strength is almost the same for both the types of concrete at 400 °C. It may further be noted that, while the rate of strength loss is almost the same for both the types of concrete between 400 °C and 600 °C, GP concrete shows a strength gain beyond 600 °C. The reason for strength gain, as explained in FTIR analysis presented in section 5.3.6 is due to the polymerization of initially unreacted material beyond 600 °C resulting in an increase in the amorphous phase content (details are explained in section 5.3.7 of XRD analysis).

It could be observed that, water cooled OPC specimens showed a lower strength at all exposure temperatures compared to the strength of air cooled specimens. A similar behaviour has been reported by other investigators also (141-144]. For the present investigation, water cooled OPC specimen showed a lower strength in the range between 3% and 9% compared to the corresponding strength of air cooled specimen after the exposure to elevated temperatures. The water cooled GP concrete specimens also show a lower strength compared to air cooled GP specimens (4% to 9% lower strength).

It may be concluded that, the effect of water spray on specimen exposed to elevated temperatures is more or less the same for both GP and OPC concrete.

The strength reduction in OPC concrete when exposed to high temperatures is primarily due to the decomposition of the cement paste and the corresponding loss of adhesion [145]. Further, the reason for a lower compressive strength of water cooled OPC specimen compared to air cooled specimen is due to the micro cracks developed subsequent to the thermal shock induced [94,106].

Many investigators have proposed equations, available in literature, for the prediction of properties of conventional concrete (compressive and tensile strengths, modulus of elasticity, etc.) when exposed to elevated temperatures [95-98]. The

present experimental results have been used to check whether these prediction equations are applicable in the case of geopolymer concrete.

Figure 5.2 shows the prediction of cube compressive strength of GP concrete specimen after exposure to different temperature levels based on the available

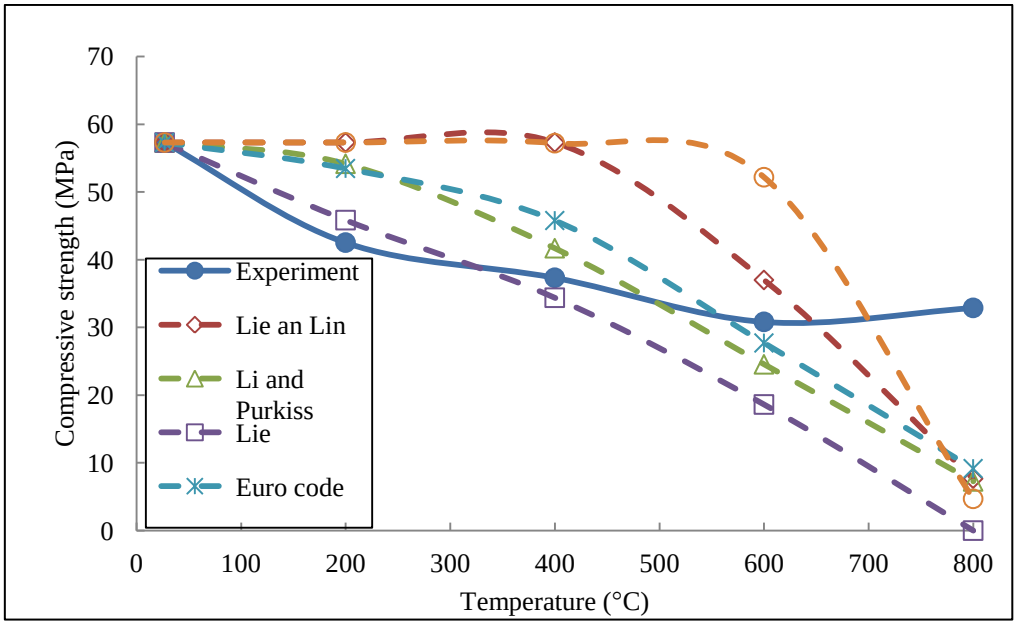

Fig. 5.2. Comparison of cube compressive strength of GP concrete at elevated temperatures with the predicted values based on available equations for OPC concrete.

equations for the strength prediction of OPC concrete. It could be seen from Fig. 5.2 that, none of the equations is suitable for predicting the compressive strength of GP concrete after exposure to elevated temperatures. Hence, based on the available data, the following equations have been proposed to predict the cube compressive strength of GP concrete after exposure to elevated temperatures.

$f_{ckT} = f_{ck}\,[\,1.055 - 2.21\,(T/1000) + 3\,(T/1000)^2\,]$ for $28 \le T \le 400$ ---------- (5.1)

$f_{ckT} = f_{ck}\,[\,1.327 - 2.26(T/1000) + 1.65(T/1000)^2\,]$ for $400 < T \le 800$ ---------- (5.2)

These equations have been proposed based on a limited test data. Since no such equation is available, these equations can be used for an approximate prediction of the compressive strength of geopolymer concrete after exposure to elevated temperatures. More data are required to have refined prediction equations.

5.3.2. Tensile Strength

Tables 5.3 and 5.4shows the split tensile strength and flexural strength of GP and OPC specimens respectively, tested after exposure to elevated temperatures (test details are given in Table C.2 and C.3 of APPENDIX C). Figures 5.3 and 5.4 present

the corresponding split tensile and flexural strength, in terms of the percentage residual strength, of GP and OPC concrete respectively.

From Tables 5.3 and 5.4 as well as from Figs.5.3 and 5.4, it could be observed that, both split and flexural tensile strength of GP concrete is slightly lower than the corresponding values of OPC concrete up to a temperature of 400 °C. However, beyond this temperature, GP concrete behaves better. Further, similar to the compressive strength, beyond 600 °C, there is a strength gain for GP concrete in both

Table 5.3. Split tensile strength of GP and OPC specimens after exposure to elevated temperatures

Exposure Temperature (°C)	GP Concrete				OPC Concrete			
	Air cooled		Water cooled		Air cooled		Water cooled	
	Split tensile strength (MPa)	SD*	Split tensile strength (MPa)	SD*	Split tensile strength (MPa)	SD*	Split tensile strength (MPa)	SD*
Ambient (28)	5.44	0.76	-	-	5.47	0.46	-	-
200	4.17	0.38	3.89	0.49	4.45	0.63	4.30	0.92
400	2.61	0.89	2.47	0.69	3.04	0.87	2.89	0.43
600	1.76	0.86	1.37	0.55	1.48	0.64	1.45	0.78
800	1.94	0.75	1.58	0.69	1.06	0.57	0.95	1.10
* SD - Standard deviation								

Table 5.4. Flexural strength of GP and OPC specimens after exposure to elevated Temperatures

Exposure Temperature (°C)	GP Concrete				OPC Concrete			
	Air cooled		Water cooled		Air cooled		Water cooled	
	Flexural strength (MPa)	SD*	Flexural strength (MPa)	SD*	Flexural strength (MPa))	SD*	Flexural strength (MPa))	SD*
Ambient (28)	5.30	0.68	-		5.44	0.45	-	-
200	4.23	0.53	4.10	0.68	4.53	0.67	4.40	0.38
400	2.89	1.21	2.61	0.86	3.36	0.77	3.19	0.82
600	1.86	0.87	1.52	0.58	1.72	0.83	1.49	0.89
800	1.90	0.47	1.65	0.96	0.72	0.66	0.61	0.87
* SD - Standard deviation								

split and flexural strength. In the present investigation, the residual split tensile strength of air cooled GP concrete (Table 5.3) exposed to 600 °C is 32.3% and that in OPC concrete is 27.0%. However, the corresponding values at 800 °C exposure temperature are respectively 35.6% and 19.3%. Also, the rate of strength reduction of both OPC and GP concrete is more or less the same up to 600 °C in the case of split tensile strength as well as flexural strength

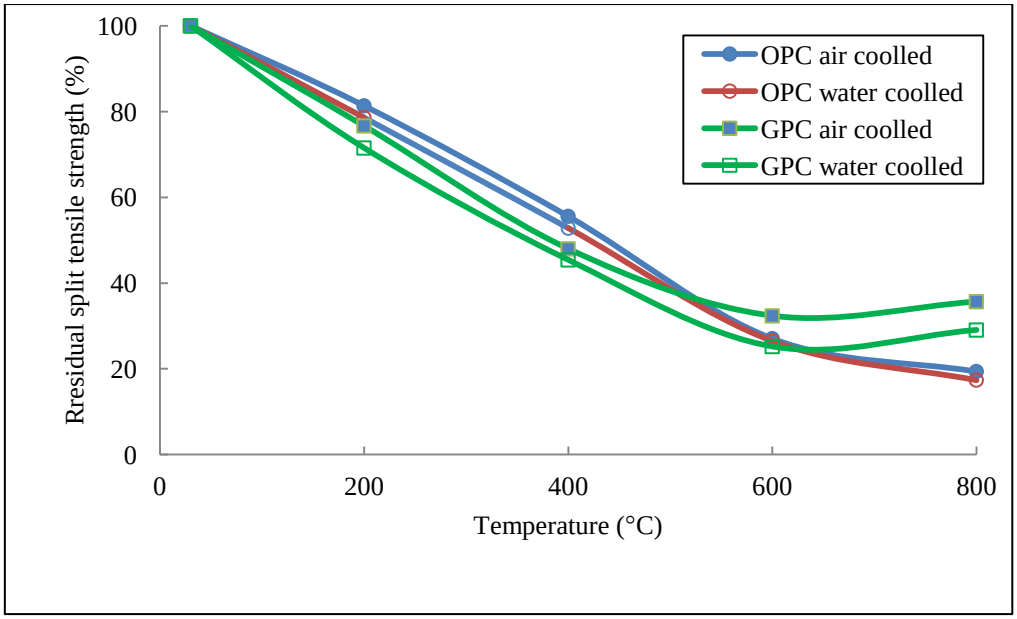

Fig. 5.3. Residual split tensile strength of GP and OPC concrete after exposure to elevated temperatures

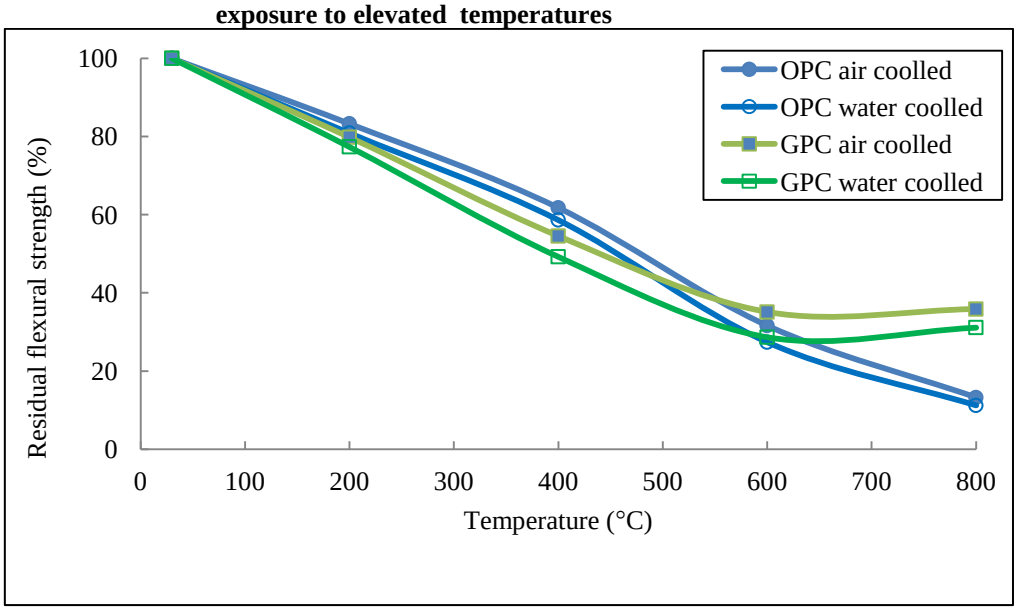

Fig. 5.4. Residual flexural strength of GP and OPC concrete after exposure to elevated temperatures

Figure 5.5 shows the prediction of split tensile strength of GP concrete at elevated temperatures using the equations available for OPC concrete. From Fig. 5.5, it is clear that, the available equations cited (for OPC concrete) are not suitable to predict the split tensile strength of GP concrete after exposure to elevated temperatures. Hence, the following equations have been proposed to predict the split tensile strength of air cooled GP concrete exposed to elevated temperatures.

$f_{tT} = ft\,[1.036 - 1.3(T/1000) - 0.24(T/1000)^2]$ for $28 \le T \le 400$ ---------- (5.3)

$f_{tT} = ft\,[1.36 - 3.1(T/1000) + 2.3(T/1000)^2]$ for $400 < T \le 800$ ---------- (5.4)

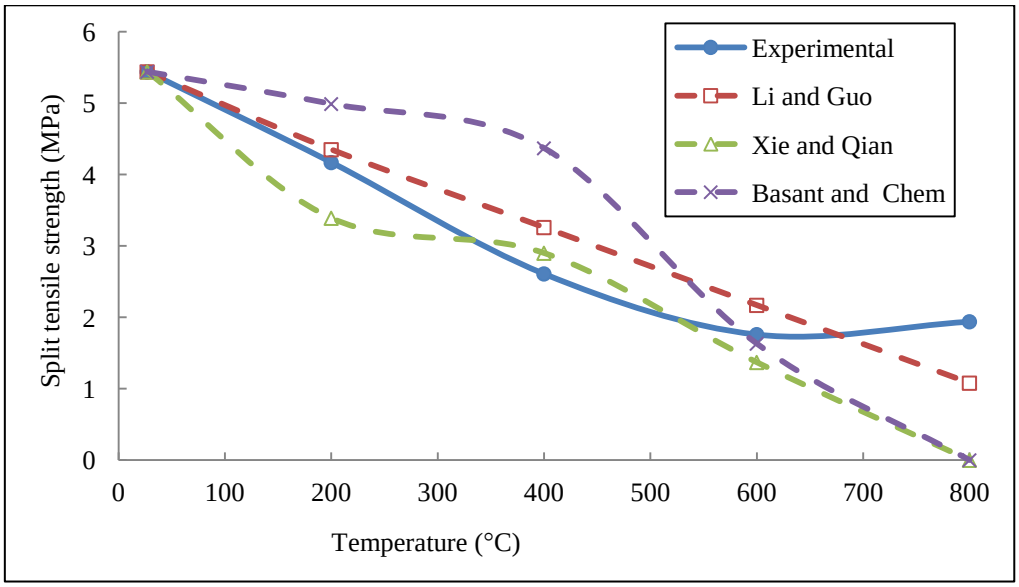

Fig. 5.5. Comparison of the split tensile strength of GP concrete at elevated temperatures with the predicted values based on available equations for OPC concrete

5.3.3. Modulus of Elasticity

The slope of the secant drawn at one third of the cube compressive strength of concrete has been considered as the modulus of elasticity of concrete. Standard cylinder specimens have been used to determine the modulus of elasticity.

Figure 5.6 shows the variation of the modulus of elasticity (%) of GP and OPC concrete after exposure to elevated temperatures and cooled to room temperature by both the methods (test details are presented in Table C.4 of APPENDIX C).

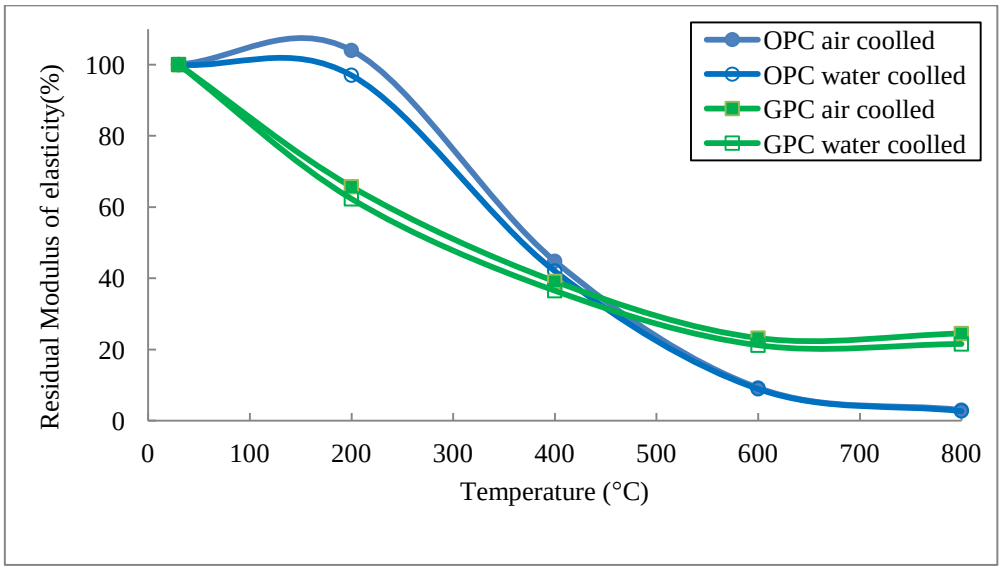

Fig. 5.6. Residual modulus of elasticity of GP and OPC concrete after exposure to elevated temperatures

From Fig. 5.6, it could be observed that, compared to OPC concrete, GP concrete shows a lower residual modulus of elasticity up to about 450 °C, and higher values for temperatures above 450 °C. Further, unlike OPC concrete, GP concrete does not undergo any additional reduction in modulus of elasticity beyond 600 °C, a behaviour similar to that of the strength of GP concrete. For the present study, at 600 °C while air cooled GP had a residual modulus of elasticity of 23.2%, OPC had only 9.2% residual modulus of elasticity value. On the other hand, at 800 °C, air cooled GP concrete had a residual modulus of elasticity of 24.5% and the corresponding value of air cooled OPC concrete is only 2.9%.

Figure 5.7 shows the prediction of the modulus elasticity of GP concrete after exposure to elevated temperature using the equations available for cement concrete.

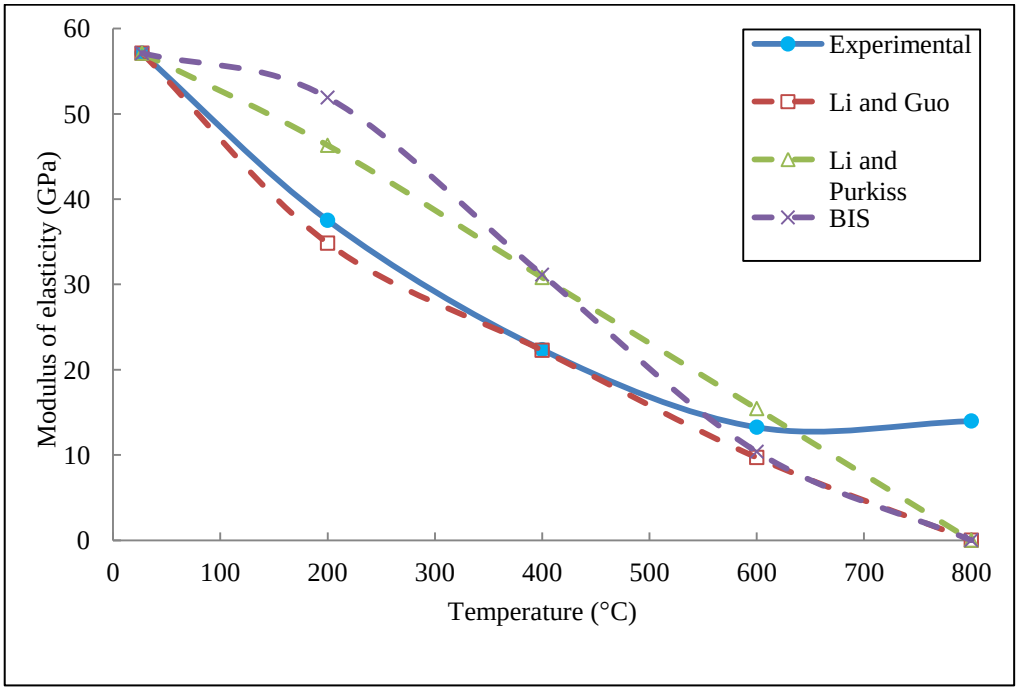

Fig. 5.7. Comparison of the modulus of elasticity of GP concrete at elevated temperatures with the predicted values based on available equations for OPC concrete

From Fig. 5.7, it could be observed that, in the case of GP concrete, the equation proposed by Li and Guo agrees with the experimental value only up to a temperature of about 500 °C and beyond which, it underestimates the modulus of elasticity value. It is to be noted that, none of the available equations for OPC concrete could be used

to predict the modulus of elasticity of GP concrete beyond an exposure temperature of about 500 °C.

Based on the present study, the following equations have been proposed to predict the modulus of elasticity of air cooled GP concrete at elevated temperatures based on the modulus of elasticity at ambient temperature (28 °C).

$E_{cT} = E_{cG}[1.065 - 2.4(T/1000) + 1.8(T/1000)^2]$ for $28 \leq T \leq 400$ ---------- (5.5)

$E_{cT} = E_{cG}[1.225 - 2.95(T/1000) + 2.15(T/10)^2]$ for $400 < T \leq 800$ ---------- (5.6)

5.3.4. Surface Crack

The surface crack pattern has been observed on cube specimens after they were exposed to different temperature levels and cooled to ambient temperature by air cooling. It could be observed that, the GP concrete specimen did not show any visible surface crack up to an exposure temperature of 600 °C and developed only one or two minor cracks at 800 °C.

On the other hand, OPC specimens started developing hair line cracks at 400 °C itself and when the temperature was increased to 800 °C, an increased number of wider and distributed cracks developed. Figure 5.8 to 5.10 depict the cracking behaviour of GP and OPC concrete specimens after they were exposed to different temperature levels (400 °C, 600 °C and 800 °C) and cooled to ambient temperature by air cooling.

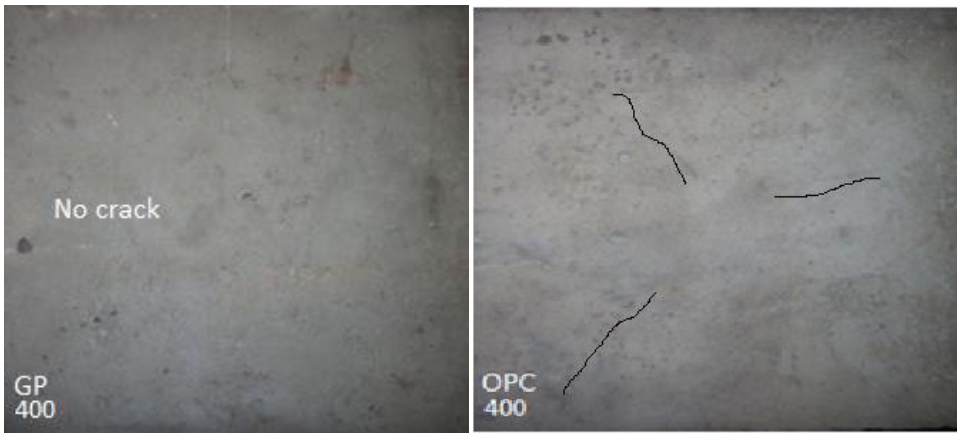

Fig. 5.8. Cracking behaviour of GP and OPC concrete after a temperature exposure of 400 °C

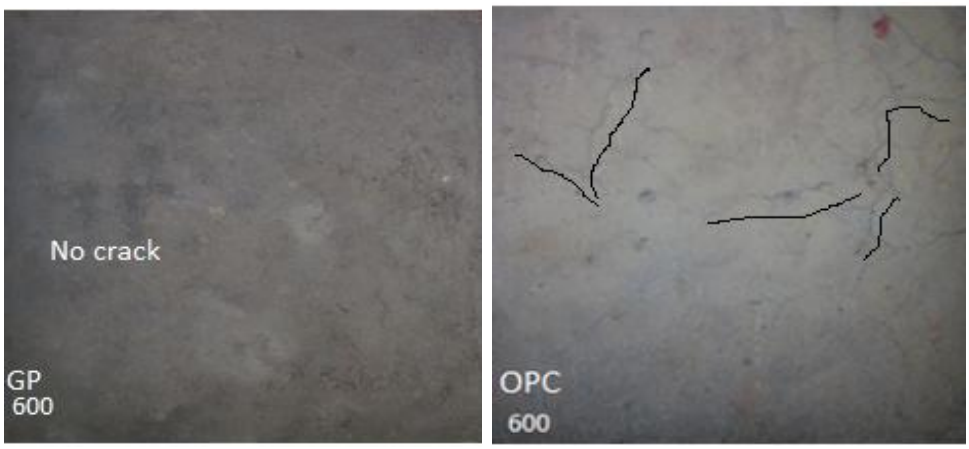

Fig. 5.9. Cracking behaviour of GP and OPC concrete after a temperature exposure of 600 °C

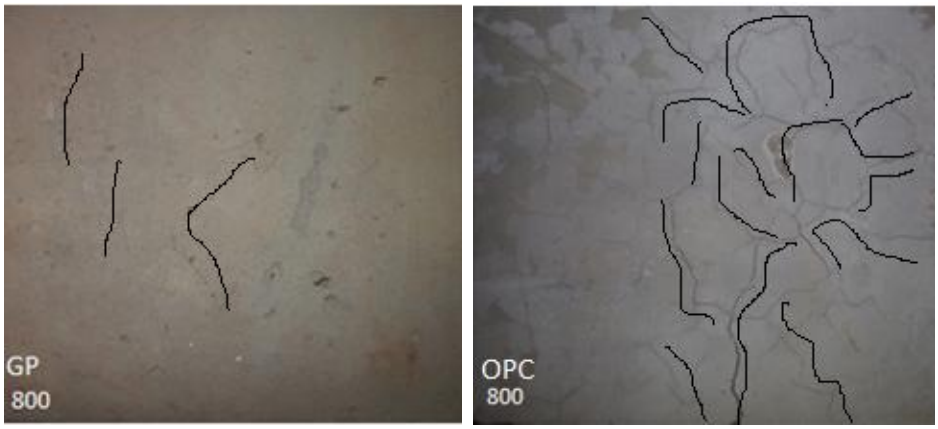

Fig. 5.10. Cracking behaviour of GP and OPC concrete after a temperature exposure of 800 °C

5.3.5. Scanning Electron Microscopy Analysis

The SEM Image analysis was carried out on GP mortar and cement mortar taken from their respective concrete samples. SEM Images of GP and cement mortar specimens exposed to 200 °C, 400 °C, 600 °C and 800 °C and air cooled are compared in Figs. 5.11 and 5.12 respectively.

Even though there was no visible crack on both GP and OPC specimen at a temperature exposure of 200 °C, SEM analysis of specimens exposed to 200 °C shows the development of microcracks in both the specimens. However, from the Fig. 5.11 and 5.12, it could be observed that, at a temperature exposure of 200 °C, GP mortar specimen experiences very low crack width (400 nm), compared to the crack width of cement mortar (2.33 µm wide cracks, which is about 480% higher than that of the GP specimen). At 800 °C, even though GP mortar experiences lower crack

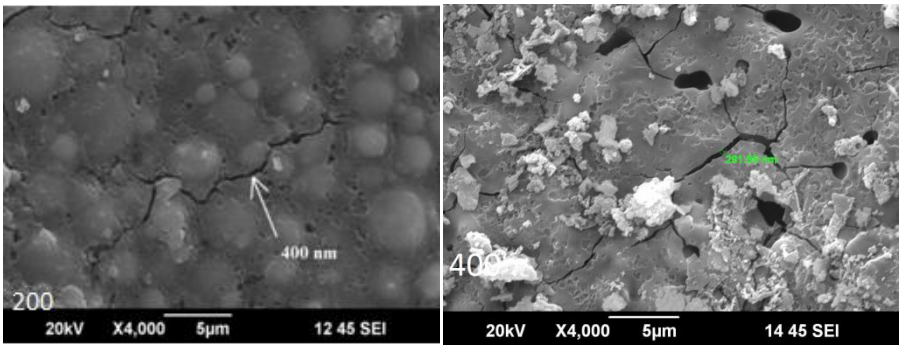

(a) 200 °C (b) 400 °C

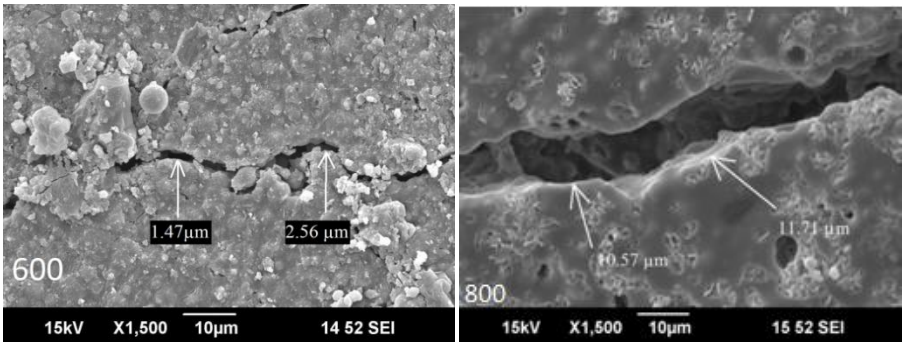

(c) 600 °C (d) 800 °C

Fig. 5.11. SEM image of geopolymer mortar specimens after exposure to different temperatures

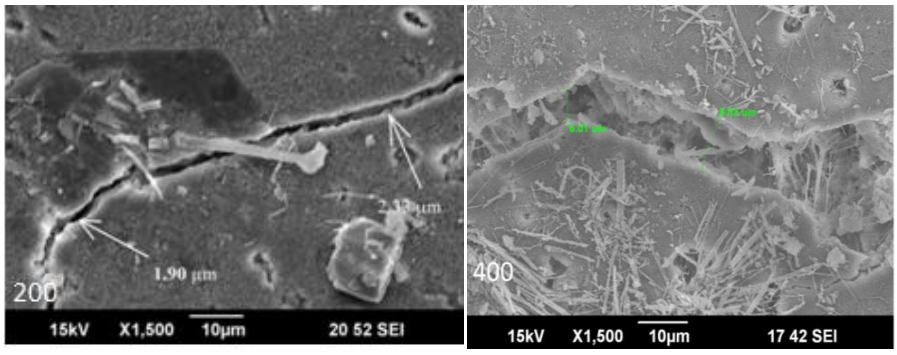

(a) 200 °C (b) 400 °C

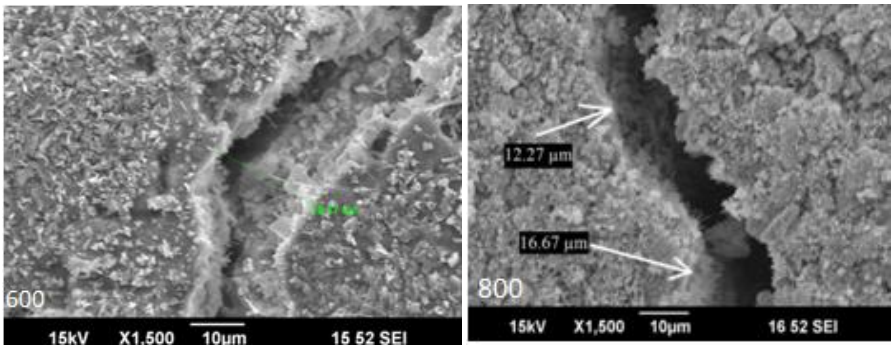

(c) 600 °C (d) 800 °C

Fig. 5.12. SEM image of OPC mortar specimens after exposure to different temperatures

width, the crack width variation of OPC mortar specimen is only about 40% higher than that of the GP specimen. It may also be noted that only one or two minor visible cracks developed in GP specimen at 800 °C. This confirms that the aggregate content in GP concrete influences the visible crack pattern of GP concrete.

5.3.6 Fourier Transforms Infrared Spectroscopy Analysis

Figure 5.13 shows the comparison of FTIR spectrum of fly ash with that of GP paste at ambient temperature.

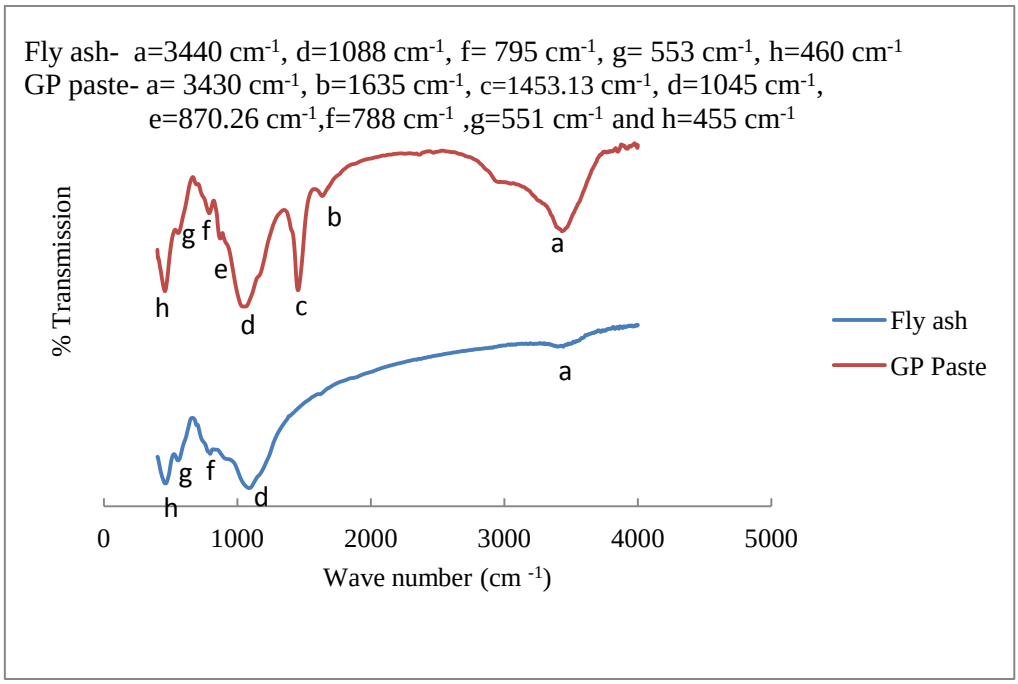

Fig. 5.13. FTIR of fly ash and geopolymer paste at ambient temperature

FTIR spectrum of fly ash has four distinct bands (h, g, f and d). The wave number corresponding to 1088 cm $^{-1}$ (d) and 460cm^{-1} (h) represents the Si-O/Al-O stretching vibration and in plane bending vibration respectively. The wave number 795cm^{-1} (f) indicates the tetrahedral linkage of Si-O-Al [20,30,146,147].

The FTIR spectrum of geopolymer paste shows higher peaks corresponding to wave numbers 795 cm^{-1} (f), 1088 cm^{-1}(d) and 460 cm^{-1}(h) compared to the FTIR of fly ash. This phenomenon indicates an increase in chain length and formation of alumino- silicate compound due to polymerisation [55]. The FTIR spectra of GP paste shows an increased peak in the wave number corresponding to water molecule (3430 cm^{-1}) when compared to fly ash. New band (1635 cm^{-1}) showing formation of water molecule is also visible in the FTIR of GP paste. These bands are due to weakly bound water molecules which were adsorbed on the surface or trapped in the large

cavities between the geopolymeric products [148]. Wave number corresponding to the 1453 cm^{-1} (c) and 870 cm^{-1} (e) represent the presence of Na_2CO_3 and that might be formed due to the carbonation of unreacted sodium silicate and /or sodium hydroxide [30].

The FTIR spectrum analysis of GP paste exposed to elevated temperatures is presented in Fig. 14. Figure 14 shows a substantial reduction of the peak in Si-O-Al and Si-O-Si regions (h to d - wave number 460cm^{-1} to 1088cm^{-1}) at a temperature

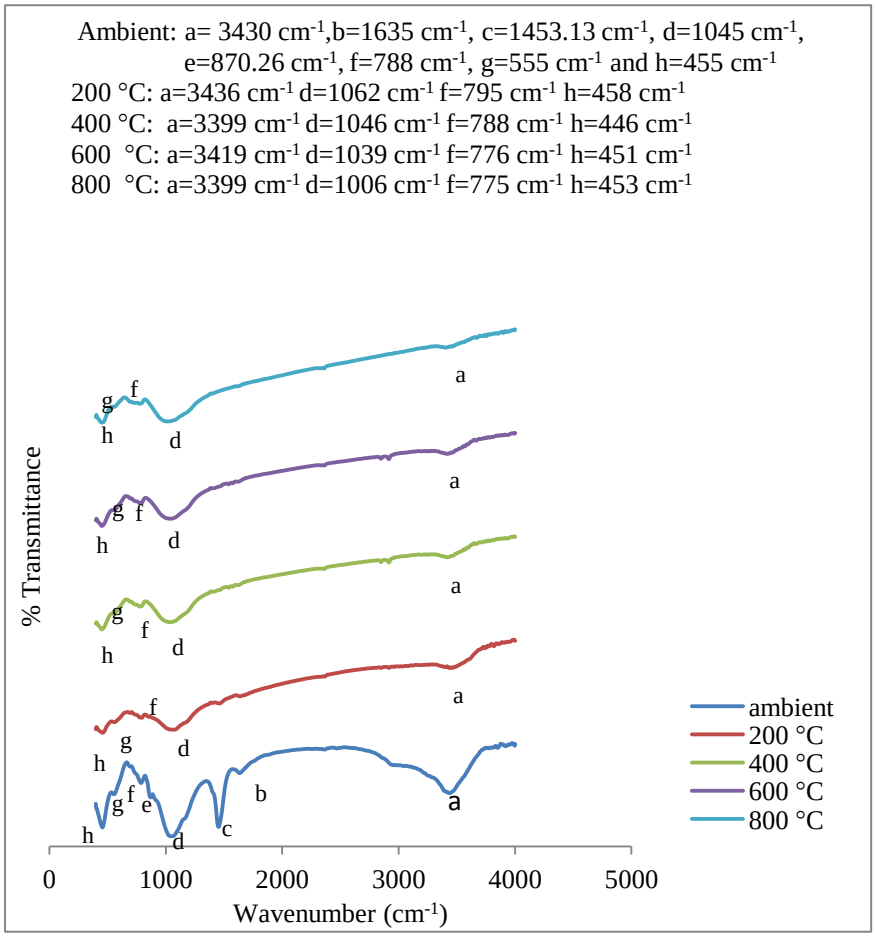

Fig. 5.14. FTIR of Geopolymer paste exposed at different temperature

exposure of 200 °C, indicating a reduction in their bonding force and decrease in chain length [42 ,48].

Also, the band representing water molecule (hydroxyl groups) in GP paste shows a marked decrease in its peak at a temperature exposure of 200 °C and further increase in exposure temperature do not cause any significant decrease in these peaks (wave number 3440 cm^{-1}). This means that, most of the weakly bound water molecules that were either adsorbed on the surface or trapped in the large cavities between the geopolymeric products get expelled at about 200 °C. The combined result of the

above may lead to a reduced strength in GP concrete compared to OPC concrete during the initial heating process.

Moreover while the FTIR spectrum of GP paste shows only marginal reduction in the peak intensities over the Si-O-Al and Si-O-Si region (h-d) for the temperature exposure between 200 °C and 600 °C, the peak intensity corresponding to Si-O-Si linkage increases slightly beyond 600 °C, confirming the polymerization of initially unreacteted materials beyond 600 °C.

5. 3.7. X-Ray Powder Diffractometer Analysis

Figure 5.15 shows the XRD diagram of GP paste after exposure to elevated temperatures.

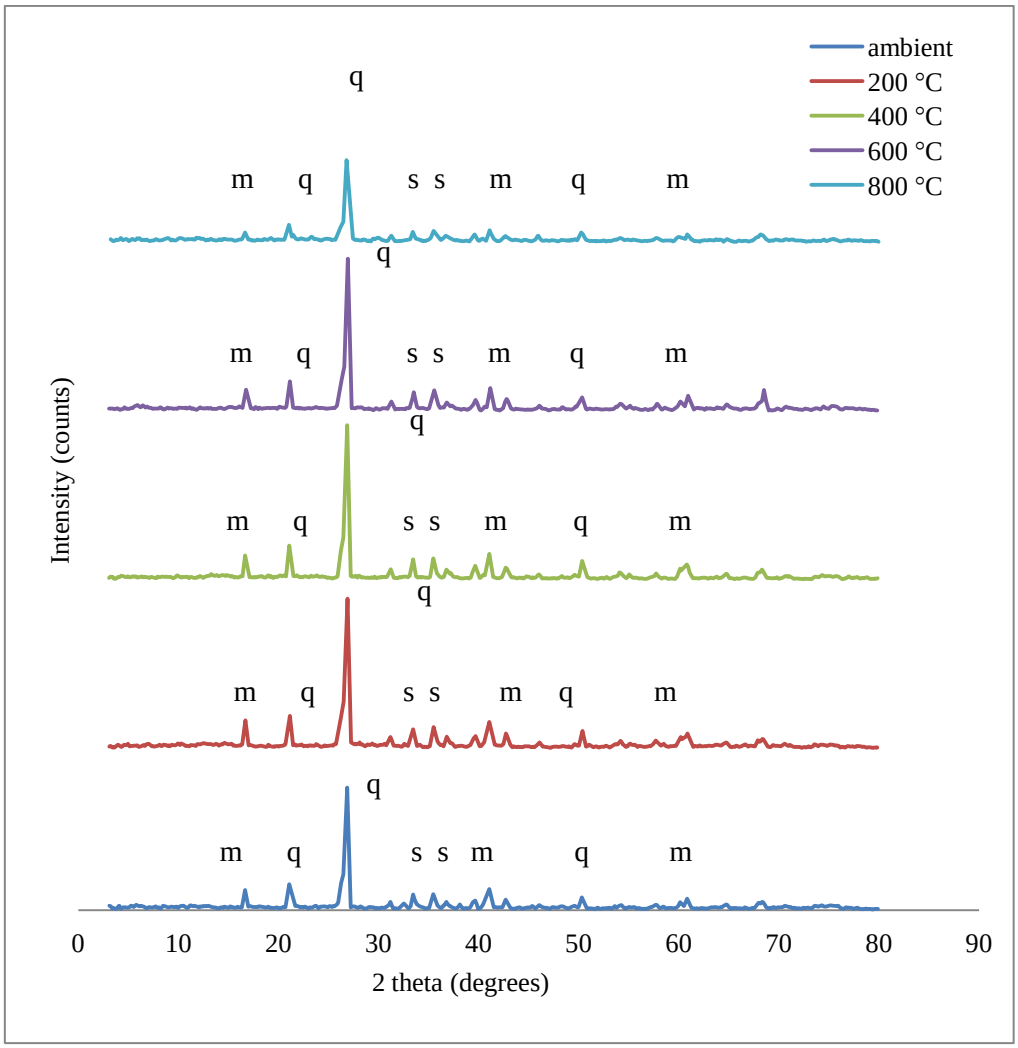

Fig. 5.15. XRD diagram of geopolymer paste after exposure to different temperatures

The peaks in the diagram represent crystalline materials, whereas non peak represent amorphous material. The amorphous phase in GP paste, as per XRD

analysis was 78% while that in fly ash was 41%. This is to say that the geopolymer is more amorphous than the fly ash used in it and this observation is consistent with the observations reported elsewhere [46]. Furthermore, from the Fig 5.15 it is evident (existence of the peaks of quartz, mullite and Sellmanite) that, complete dissolution of fly ash due to alkali activation has not taken place (presence of peak in XRD diagram).

From Fig. 5.15, it could be seen that the crystalline materials present in the GP paste has not undergone any significant change in its phase up to an exposure temperature of 600 °C. However, at 800 °C, an increase in the amorphous phase content could be observed. This additional increase in the amorphous phase may cause further polymerization of initially unreacted material. This could be one of the reasons for improved engineering properties of GP concrete beyond 600 °C temperature exposure.

5.3.8 Thermo Gravimetric Analysis

Figure 5.16 shows the result of the Thermo gravimetric Analysis (TGA) of GP paste.

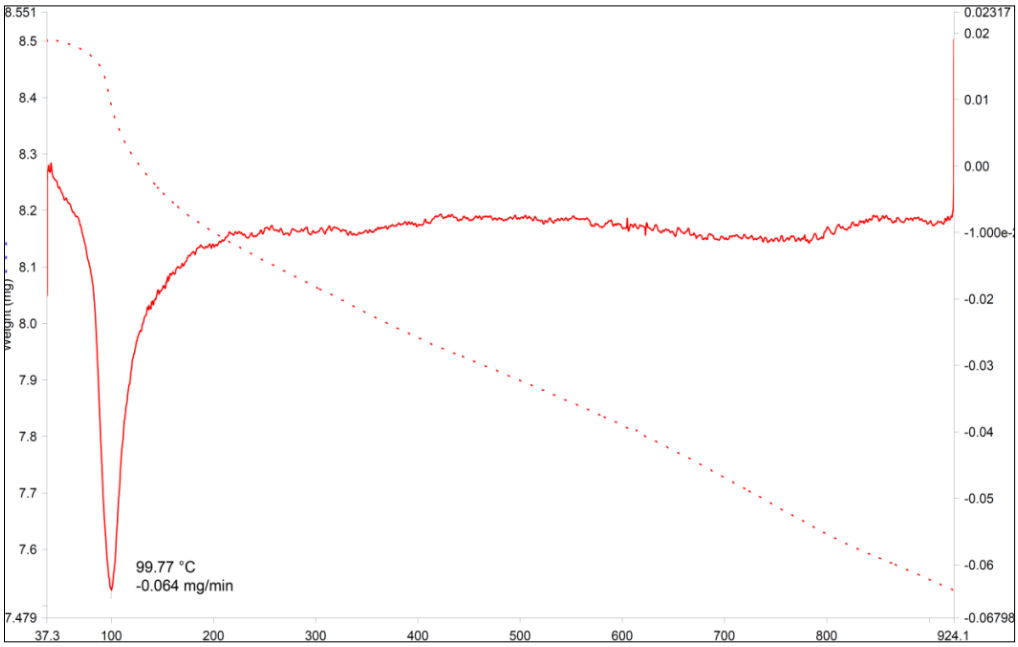

Fig. 5.16. TGA diagram of geopolymer paste

It could be seen from Fig.5.16 that, the rate of change of mass loss is maximum at around 100 °C and beyond the temperature of about 200 °C, it is more or less constant. It could be observed that, most of the free water and weakly adsorbed

water within the geopolymer paste escape at a temperature below 200 °C. This observation is in line with the published literatures [101,102] and FTIR analysis also confirms this fact.

It may be noted that, the chemical and structural changes that are taking place during the heating regime is entirely different for GP and OPC concrete.

It has been reported elsewhere [109] that the TGA of OPC has three major parts like loss of water due to dehydration of C-S-H up to 200 ºC, dehydration of portlandite causing major weight loss at 450 ºC-500 ºC and decarbonation of Ca_2CO_3 at 750 ºC.

5.5 CONCLUSIONS

Following conclusions could be derived from the study conducted on GP concrete after exposure to elevated temperatures.

1. Fly ash based geopolymer concrete undergoes a high rate of strength loss (compressive strength, tensile strength and modulus of elasticity) during its early heating period (up to 200 °C) compared to that of OPC concrete.
2. High rate of strength loss in geopolymer concrete at its early heating period is primarily due to the chemical restructuring of Si-O-Al (alumino silicate) and Si-O-Si compound and due to the formation of micro crack as a result of the removal of water (weakly bound and free water) from the geopolymer matrix.
3. At a temperature exposure beyond 600 °C, unreacted crystalline materials in geopolymer concrete get transformed into amorphous state and undergo polymerization. As a result, there is no further strength loss (compressive strength, tensile strength and modulus of elasticity) in geopolymer concrete. On the other hand, OPC concrete continues to lose its strength properties at a faster rate beyond 600 °C temperature exposure.
4. For the present study, after a temperature exposure of 600 °C, geopolymer and OPC concrete (both air cooled) had about 54% residual cube compressive strength (compared to the strength at ambient temperature, which is almost the same for both geopolymer and OPC concrete). However, at 800 °C, while geopolymer concrete slightly gained its residual strength (57%), OPC concrete had only about 35% residual strength.
5. As the nature of strength loss of geopolymer concrete is different from OPC concrete at elevated temperatures, available equations for the prediction of

residual strength of OPC concrete are not suitable for the residual strength prediction of geopolymer concrete after exposure to elevated temperatures.

6. New equations have been proposed to predict the residual strengths (cube compressive strength, split tensile strength and modulus of elasticity) of geopolymer concrete after exposure to elevated temperatures (upto 800 °C). Theses equations could be used for material modeling until better refined equations are proposed.
7. The effect of thermal shock due to water cooling of geopolymer and OPC concrete is more or less similar. In the present study, both geopolymer and OPC concrete had a maximum strength loss of 10% due to water cooling.
8. Compared to OPC concrete, geopolymer concrete shows better resistance against surface cracking when exposed to elevated temperatures. In the present study, while OPC concrete started developing cracks at 400 °C, geopolymer concrete did not show any visible crack up to 600 °C and developed only minor cracks at an exposure temperature of 800 °C.

****

CHAPTER 6

FLEXURAL BEHAVIOUR OF GEOPOLYMER CONCRETE BEAMS EXPOSED TO ELEVATED TEMPERATURES

6.1 INTRODUCTION

The Flexural behavior, namely deformation characteristics, moment–curvature relationship and cracking of fly ash based geopolymer concrete beams exposed to elevated temperatures (200 °C, 400 °C, 600 °C and 800 °C) are presented in this chapter.

6.2 BEAM DETAILS

The mixture proportion used for casting beams was the same as that used for the study of engineering properties of GP concrete after exposure to elevated temperatures (Chapter 5). Accordingly, the following parameters have been considered for the preparation of GP concrete beams.

Aggregate content by volume	= 70%
Mass ratio of fine aggregate to total aggregate	= 0.35
Ratio of alkali to fly ashy by mass	= 0.55
Molarity of NaOH	= 10
Ratio of Na_2SiO_3 to NaOH	= 2.5
Curing temperature	= 100 °C
Temperature curing time	= 24 hours

Details of mixing, casting and heating of specimen are explained in section 3.3 of chapter 3. For the present study, the target temperatures selected were 200 °C, 400 °C, 600 °C and 800 °C.

Reinforced geopolymer beams of size 150 mm (W) x 200 mm (D) x1100 mm (L) were used for the present study. Figure 6.1 depicts the reinforcement details of the beam considered.

Two ribbed bars of 10 mm diameter (HYSD) were used as bottom reinforcement. 6 mm diameter ribbed bars (HYSD) were used for shear reinforcement. The shear reinforcement in the form of closed links was spaced at 80 mm center to center. The top hanger bar consists of two 8 mm diameter ribbed (HYSD) bars.

Three groups of beam were cast by varying the clear cover to the bottom reinforcement (20 mm, 30 mm and 40 mm). In each group, 5 beam specimens were cast. Air cooling was adopted to bring down the temperature to ambient after heating to target temperature (200 °C, 400 °C, 600 °C and 800 °C).

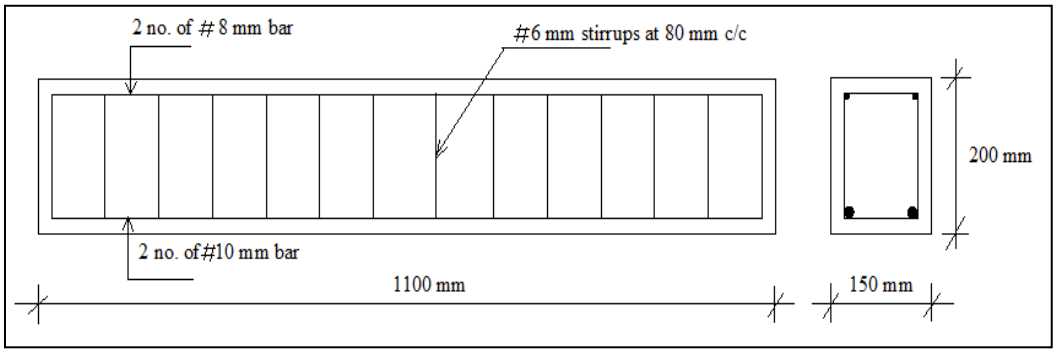

Fig. 6.1. Reiforcement detais of GP concrete beam

6.3 TESTING OF BEAMS

The beams were tested under two point load, applied at one third span. Figure 6.2 shows the experimental set up for testing GP concrete beam specimens.

Fig. 6.2. Experimetal set up for loading GP concrete beam

Demountable mechanical gauge (DEMEC) of 200 mm gauge length was used for measuring strain across the depth of the beam at the midspan of the specimen.

Loading on the beam was applied at an increment of 3 kN and for each increment of load, DEMEC gauge readings were taken. Observations like deflection, load at first crack, crack width, crack propagation etc. were also noted wherever applicable, at every load increment.

6.4 ANALYSIS OF RESULTS

Table 6.1 shows the load at first crack and ultimate load on GP concrete beam tested after exposure to different temperatures.

Table 6.1. Load at fist crack and ultimate load on geopolymer concrete beam

Temperature	Cube compressive strength of GP concrete (MPa)	Load at fist crack (kN)			Ultimate load (kN)		
		20 mm cover	30mm cover	40mm cover	20 mm cover	30mm cover	40mm cover
Ambient	57.30	45	43	40	101	99	98
200°C	42.52	42	42	36	94	95	92
400°C	37.33	36	39	33	92	92	78
600°C	30.82	33	36	33	85	90	75
800°C	32.88	30	33	30	68	75	66

From Table 6.1 it could be observed that the load at first crack for beam at ambient temperature reduces marginally with increase in clear cover to the reinforcement. However, for temperature above 200 °C GP concrete beam with a clear cover of 30 mm shows slightly higher load capacity against first crack compared to beams with 20 mm and 40 mm cover.

. The ultimate load on beams after exposure to temperatures above 200 °C is also slightly higher for the beam with 30 mm cover compared to that of the beam with 20 mm and 40 mm cover. However, considering the possible variations in the test results, it could be concluded that, the variation of cover to reinforcement up to 40 mm has no significant influence on the first crack load and on the ultimate load of GP beam after exposure to elevated temperatures.

It could be noted from Table 6.1 that, even though the cube strength of GP concrete is not reduced between 600 °C and 800 °C, the load caring capacity of beams reduces rapidly beyond 600 °C. This could be primarily due to the rapid strength reduction of reinforcing steel in the beam at these temperatures. Details of mechanical properties of GP concrete after being exposed to different temperatures are presented in

Table D.1 of APPENDIX D. Details of stress strain curve and strength of reinforcing steel after exposure to different temperatures are presented respectively in Table D.2 and Fig. D.1 to D.5 of APPENDIX D.

Figure 6.3 shows the typical load deflection graph of GP concrete beam after exposure to elevated temperatures (load deflection graph of all the beams are presented in Fig. D.6 to Fig. D.8 of APPENDIX D).

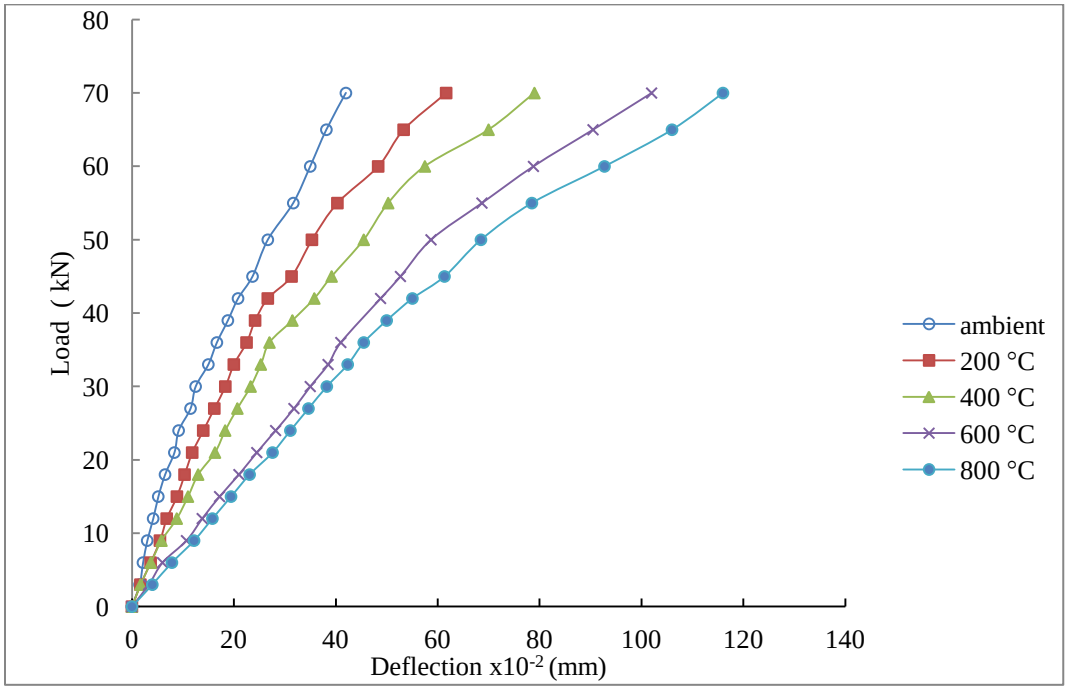

Fig. 6.3. Typical load deflection graph of GP concrete beam after exposure to elevated temperature

As expected, for a given load the deflection is more for a GP concrete beam exposed to higher temperature. Larger deformation with temperature increase is due to the development of more number of micro cracks as well as due to the reduced strength of materials (concrete and steel) at elevated temperatures. It may be noted from Fig. 6.3 that, the rate of increase of the deflection of beams slightly reduces when the temperature is increased from 600 °C to 800 °C, as against the rate of increase of deflection of beams exposed to a temperature up to 600 °C. This behaviour is more predominant after the initiation of crack and is primarily due to the slight strength gain of GP concrete beyond 600 °C.

Figure 6.4 shows the typical moment curvature (m-φ) relationship of GP concrete beam after exposure to elevated temperatures (m-φ relationship of all beams is shown in the Figs. D.9 to D.10 of APPENDIX D).

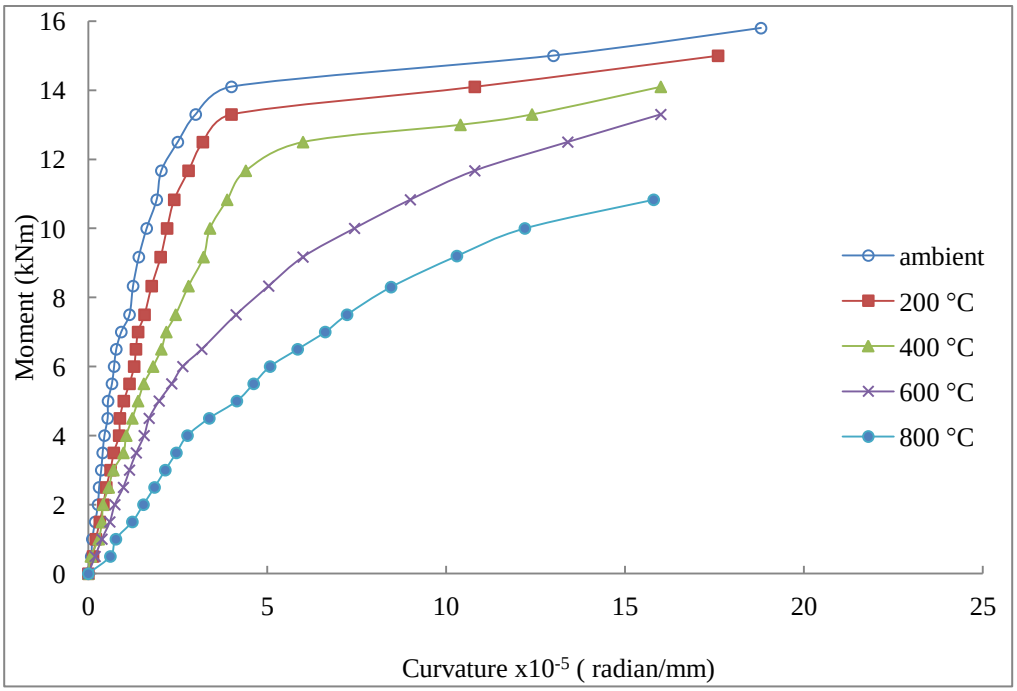

Fig. 6.4. Typical moment curvature curve of GP concrete beam after exposure to elevated temperatures

It could be seen from Fig.6.4 that, for lower temperature exposures, the m-φ relationship shows a bilinear curve, which is similar to that of RCC beams [149]. A definite yield stage could be observed for GP concrete beams when they are exposed to a temperature up to 400 °C. However, beyond 400 °C, the m-φ curve becomes multi-linear. Further, a clear yield stage of the beams is not visible in m-φ relationship for temperature exposure beyond 400 °C. The curvature of the beam also increases beyond 400 °C. This is due to the development of more number of internal cracks as well as due to the low residual strength of materials beyond 400 °C.

Figure 6.5 compares the experimental m-φ relationship of the beam with the theoretical values for two extreme temperature ranges as a typical case.

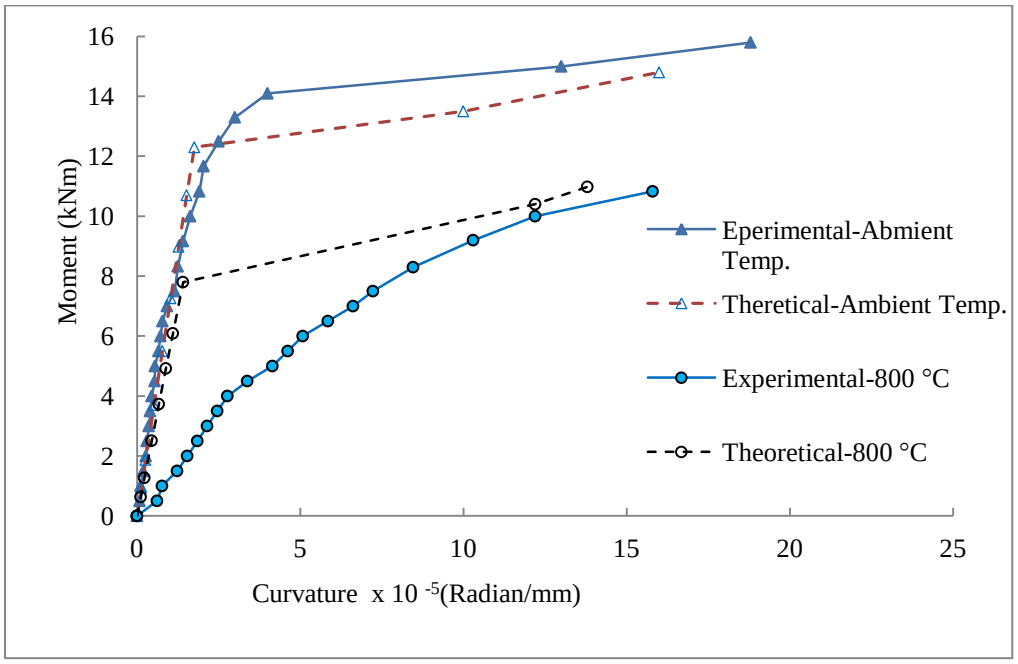

Fig. 6.5. Typical experimental and theoretical moment curvature curve of GP concrete beam after exposure to ambient and 800 °C temperatures

The theoretical m-φ curves have been obtained based on strain compatibility criteria and by considering the residual strength and modulus of elasticity of materials at the temperature considered. A sample calculation is presented in D.3 of APPENDIX D.

For the temperature exposure within the extreme temperatures presented (ambient and 800 °C) the m-φ relationship lies between these two extreme curves. These details are presented in Fig. D.11 APPENDIX D.

From Fig.6.5, it could be observed that, the experimental m- φ relationship of geopolymer concrete beams has been predicted correctly at ambient temperature. However, as the exposure temperature increases, the theoretical values underestimate the curvature up to the yield moment. While the theoretical curve shows a bilinear behaviour, the experimental curve (800 °C temperature exposure) shows a multi-linear variation. However, towards the ultimate moment, the theoretical curvature tends to meet the experimental value reasonably well.

Figure 6.6 compares the variation of curvatures at cracking and yielding stages of the beam exposed to different temperatures.

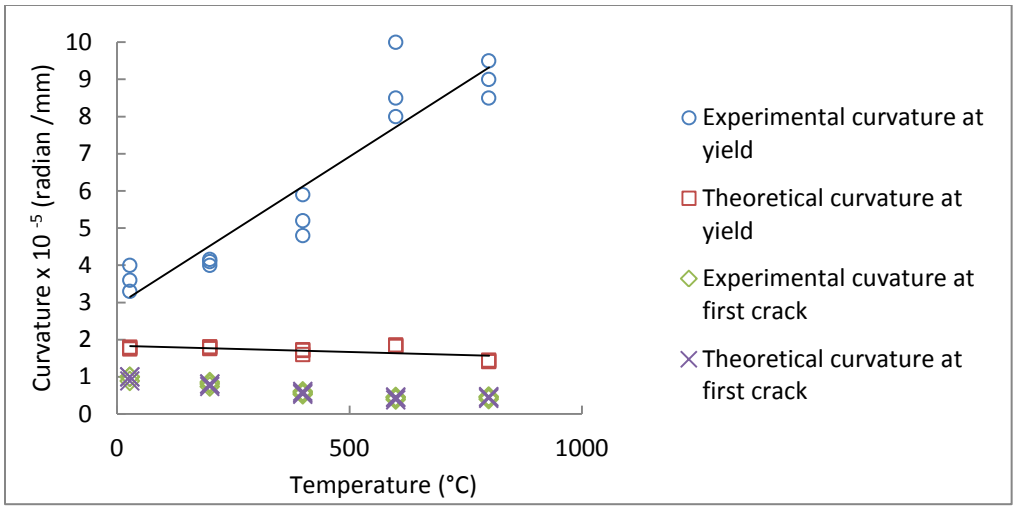

Fig. 6.6. Variation of experimental and theoretical curvature with different temperatures at first crack and yield point with different temperature

From this figure, it is clear that, the curvature varies linearly with temperature between cracking and yielding of reinforcement.

Ultimate moment of resistance of GP concrete has been calculated theoretically in a way similar to the calculation for R.C.C. beams and by considering the residual strength of steel and concrete at different exposure temperatures. The predicted value is only marginally lower than that of the experimental results (within 12%). Hence it could be concluded that, the m-φ relationship of the geopolymer concrete beam at ambient temperature behaves similarly to RCC beams and it could be predicted well by adopting strain compatibility criteria. However as the exposure temperature increases, the theoretical method very much underestimates the curvature between values corresponding to the first cracking and yielding.

Table 6.2 shows the ductility ratio of GP concrete beam (typical) after exposure to elevated temperatures. The ultimate curvature has been considered as the curvature

Table 6.2. Ductility ratio of GP concrete beam after exposed to different temperatures

Temp.	Mu (kNm)	My (kNm)	Mu/My	φu (radian/mm)	φy (radian/mm)	φu/φy
28	15.8	14.1	1.12	0.000188	0.00004	4.7
200	15.0	13.3	1.13	0.000176	0.00004	4.4
400	14.1	12.2	1.16	0.000165	0.000048	3.4
600	13.3	11.2	1.19	0.00016	0.00008	2.0
800	10.83	9.6	1.13	0.000158	0.000095	1.7

corresponding to 95 % of the ultimate load. From the Table 6.2 and Fig 6.4, it could be observed that, while the ratio of ultimate moment to yield moment does not vary much with temperature, the ductility of the GP concrete beam reduces as the exposure temperature increases. This is because of the fact that, while both ultimate moment (Mu) and yield moment (My) reduces more or less at a constant ratio with temperature, curvature at yield (φ_y) increases towards curvature at ultimate stage (φ_u) with increase in temperature.

Figure 6.7 shows typical crack pattern of GP concrete beam. It could be observed from Fig.6.7 that, the crack pattern is similar to that of R.C.C beam.

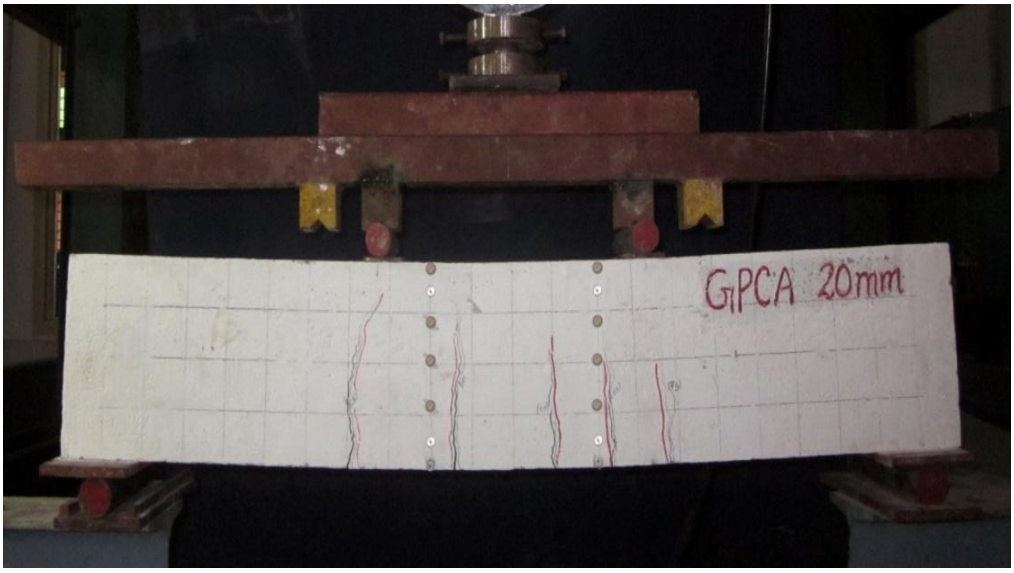

Fig. 6.7. Typical crack pattern of GP concrete beam

.

Different codes of practices propose different permissible maximum crack width based on the exposure conditions. These maximum permissible crack widths ranges from 0.1 mm to 0.3 mm in BS [120] and BIS [119] code of practices and ranges from 0.1mm (0.04 in) to 0.4 mm (0.16 in) in the case of ACI code [129].

Once the beams are exposed to elevated temperatures, existing cracks if any may widen under service load, leading to unacceptable serviceability conditions. So a beam after exposure to elevated temperature may have to have either reduced service load or to have additional protection, primarily corrosion protection to reinforcing bars. Hence it is important to understand the extent of the crack development at service load stage after beams are exposed to elevated temperatures.

So, the present study focuses on the cracking behaviour of GP concrete at service load and when exposed to elevated temperatures. For the present study, the service load has been assumed as 2/3rd of ultimate load of the reference beam that was not exposed to elevated temperature.

To the best of the author's knowledge, there is no equation available to predict the crack width of GP concrete beam after exposure to elevated temperatures. Hence the suitability of available equations for RCC beams has been checked for the prediction of crack width of geopolymer concrete beams. The equations proposed by different investigators and code of practices [119,121,124,125] have been considered in the present study. As these equations are proposed primarily for crack width calculation at ambient temperature, appropriate residual strength parameters of GP concrete and steel have been used in the equations for determining crack width at elevated temperatures.

Figures 6.8 and 6.9 illustrate a typical graph comparing the experimental results with the theoretically calculated crack width at different temperature exposure.

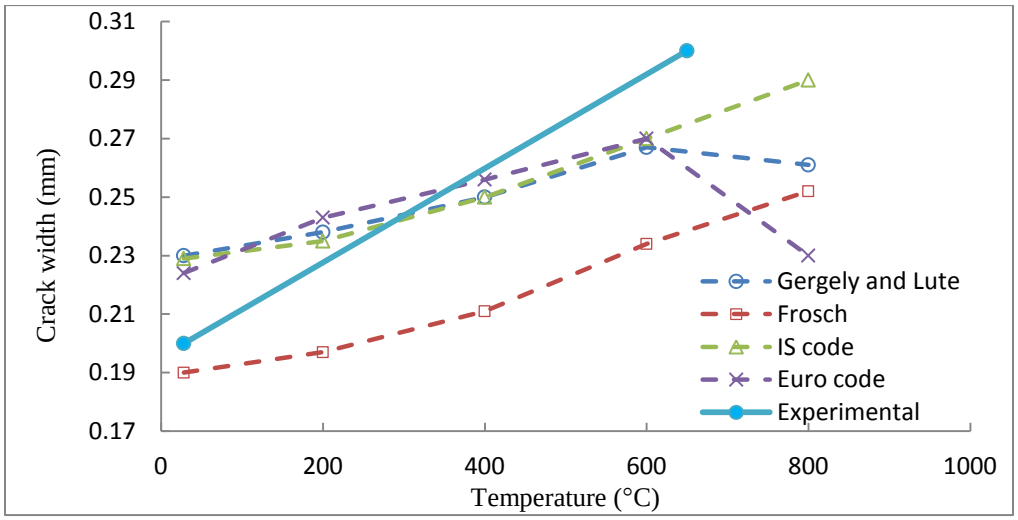

Fig. 6.8. Comparison of theoretical and experimental crack width at different temperature exposure (30 mm cover)

From these figures it could be observed that, while some equations underestimate the crack width of GP concrete at elevated temperatures, others overestimate it. However the rates of development of crack width with temperatures calculated based on the equations considered is more or less the same as that of the experimental curve.

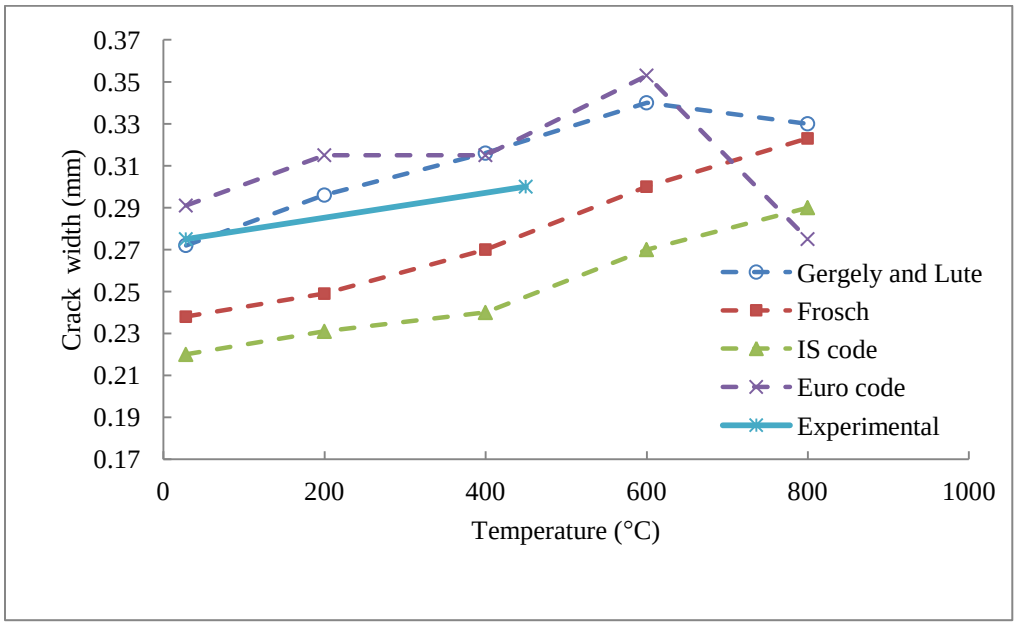

Fig. 6.9. Comparison of theoretical and experimental crack width at different temperature exposure(40 mm cover)

Figure 6.10 shows the variation of crack width with temperature for GP concrete beams at different load stages.

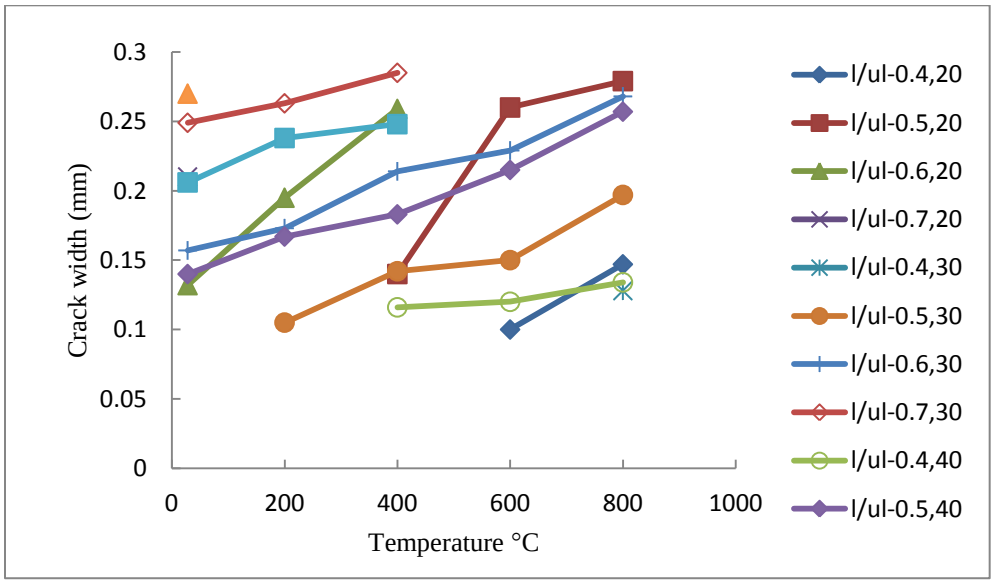

Fig. 6.10. Variation of crack width with temperature

The graph has been plotted considering the load stage in terms of the ultimate load (l/ul). The plot has been limited to the crack width between 0.1mm and 0.3 mm (serviceability condition).

From Fig. 6.10 it could be observed that, the development of crack width is almost in a linear pattern with temperature rise for all beams (with cover 20 mm to 40 mm) and under all load stage (l/ul from 0.4 to 0.7). The average slope of the curve depicted in Fig. 6.10 could be assessed as 1 in 1000.

Since the cracking pattern of GP concrete exposed to elevated temperatures is more or less in a linear pattern, the crack width at any temperature can be linearly interpolated. So, the total crack width of a cracked GP concrete beam exposed to elevated temperatures could be calculated by knowing the average slope of the curves and the initial crack width.

In order to get crack width corresponding to a particular load stage of GP concrete beams at ambient temperature, Fig. 6.11 has been plotted, which is a scattergram between crack width and (l/ul) for all the beams tested (beams with 20 mm, 30 mm and 40 mm cover). From this scatter diagram, it could be seen that, a linear equation could be proposed to predict the crack width of a GP concrete beam tested at ambient temperature. Accordingly, the following equation could be proposed for the determination of crack width (between 0.1 mm and 0.3mm) of the GP concrete beam subjected to load (l/ul) at ambient temperature.

$C_{wa} = (6667/10000)(l/ul) – (2274/10000) \quad 0.4 < (l/ul) < 0.8$ ……. …….. (6.1)

Where, C_{wa} is the crack width at ambient temperature in mm and is valid for crack width between 0.1mm and 0.3mm.

Since the slope of the curves showing the variation of crack width of GP concrete beam after exposure to elevated temperatures comes to about 1in 1000, the crack width of GP concrete caused due to an increase in temperature of T can be calculated as (T/1000). Hence the following equations have been proposed to assess the crack width of GP concrete beam exposed to elevated temperatures.

$C_{wt} = C_{wa} + (T/10000), \quad 28 < T \leq 800 \ \& \ 0.4 < l/ul < 0.8$ ….....…….. ……. (6. 2)

Where, C_{wt} is the crack width in mm at a temperature exposure of T °C.

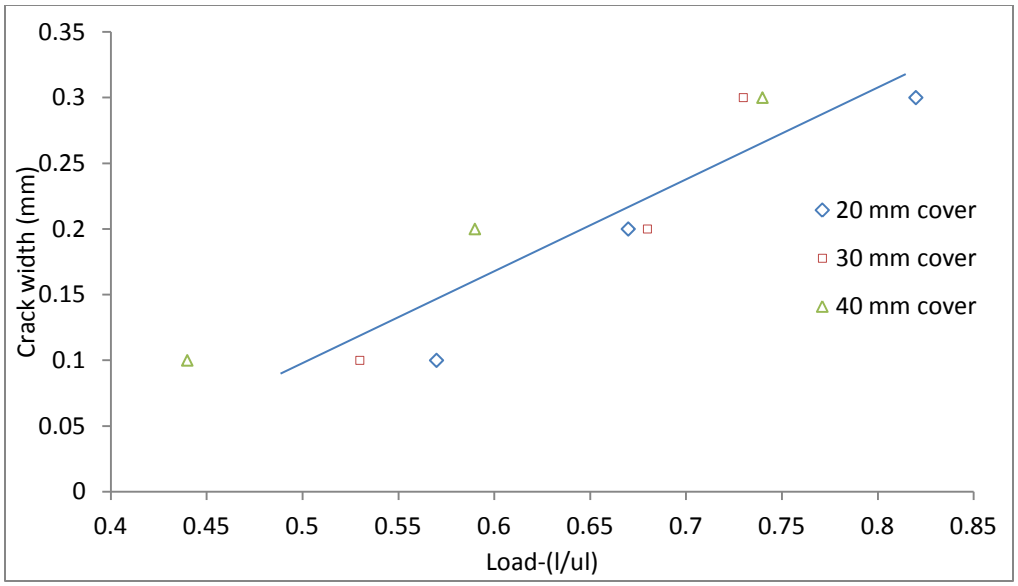

Fig. 6.11. Variation of crack width with l/ul of beams tested at ambient temperature

So, using equations 6.1 and 6.2, the service load on GP concrete beams exposed to elevated temperatures could be predicted for a limiting value of crack width (between 0.1 mm and 0.3mm) or vice versa.

6.5 CONCLUSIONS

Following conclusions could be made based on the results presented and discussions carried out in this chapter.

1. Once exposed to elevated temperatures, geopolymer concrete beams develop cracks at an early load stage.
2. The load carrying capacity of geopolymer concrete beam reduces rapidly beyond temperature exposure of 600 °C, even though its corresponding cube compressive strength is not affected by the temperature exposure beyond 600 °C.
3. With temperature, both ultimate moment and yield moment of geopolymer concrete beams reduces more or less at in a constant rate. However with increase in temperature, the curvature at yield of geopolymer concrete beam increases and there by a reduced ductility has been observed. For the present study, compared to the ductility at ambient temperature, the ductility of geopolymer concrete beams exposed to 800 °C reduces by 63.8%.

4. Appropriate equations have been proposed to predict the crack width of geopolymer concrete beams exposed to elevated temperatures. These equations could be used to limit the service load on GP concrete beams exposed to elevated temperature (up to 800 °C) for a pre defined crack width (0.1 mm to 0.3 mm) or vice versa.
5. The moment-curvature relationship of geopolymer concrete beams at ambient temperature is similar to that of RCC beams and this could be predicted using strain compatibility approach.
6. Once the beams are exposed to elevated temperatures, the strain compatibility approach underestimates the curvature of geopolymer concrete beams between first cracking and yielding point.

****

CHAPTER 7

SUMMARY AND CONCLUSIONS

7.1 SUMMARY

A systematic experimental study has been conducted to understand the behaviour of geopolymer concrete subjected to elevated temperatures.

The influence of parameters like aggregate content, fine aggregate to total aggregate ratio, ratio of alkali to fly ash, ratio of sodium silicate to sodium hydroxide, molarity of sodium hydroxide, curing temperature and curing time on mechanical properties of geopolymer concrete has been investigated.

A basic study on the interface shear strength of geopolymer concrete has been carried out.

The mechanical properties of specimens have been studied after they were subjected to elevated temperatures (200 °C, 400 °C, 600 °C, 800 °C) and cooled under air cooling and water cooling methods. Residual mechanical properties like compressive strength, tensile strength split tensile strength, flexural strength and modulus of elasticity of geopolymer concrete have been discussed.

Flexural behaviour like deflection, ductility, moment-curvature and cracking behaviour of geopolymer concrete beams after exposure to elevated temperatures have been studied.

7.2 CONCLUSIONS

The following important conclusions could be derived based on the present investigation carried out.

1. Based on the present study, it is observed that a geopolymer concrete with total aggregate content of 70% by volume, ratio of fine aggregate to total aggregate of 0.35, NaOH molarity 10, Na_2SiO_3/NaOH ratio of 2.5 and alkali to fly ash ratio of 0.55 gives maximum compressive strength.

2. The curing temperature of 100 °C yields maximum compressive strength for the geopolymer concrete.
3. An early strength development in geopolymer concrete could be achieved by the proper selection of curing temperature and the period of curing. With 24 hours of curing at 100 °C, 96.4% of the 28th day cube compressive strength could be achieved in 7 days in the present study.
4. The interface shear strength of both unreinforced and reinforced geopolymer specimens is influenced by the aggregate content. The interface shear strength reduces rapidly when the total aggregate content becomes less than 65%, whereas the enhancement in interface shear strength is not significant for aggregate content above 65%.
5. The interface shear strength of geopolymer concrete is lower to that of OPC concrete. Compared to OPC concrete, a reduction in the interface shear strength by 33% and 29% was observed for unreinforced and reinforced geopolymer specimens respectively.
6. The interface shear strength of geopolymer concrete can be approximately estimated as 50% of the value obtained based on the available equations for the calculation of interface shear strength of ordinary portland cement concrete (method used in ACI).
7. Fly ash based geopolymer concrete undergoes a high rate of strength loss (compressive strength, tensile strength and modulus of elasticity) during its early heating period (up to 200 °C) compared to OPC concrete.
8. At a temperature exposure beyond 600 °C, the unreacted crystalline materials in geopolymer concrete get transformed into amorphous state and undergo polymerization. As a result, there is no further strength loss (compressive strength, tensile strength and modulus of elasticity) in geopolymer concrete, whereas, OPC concrete continues to lose its strength properties at a faster rate beyond a temperature exposure of 600 °C.
9. Effect of thermal shock due to water cooling on geopolymer and OPC concrete after exposure to elevated temperatures is more or less similar. In the present

study, both geopolymer and OPC concrete had a maximum strength loss of 10% due to water cooling.

10. New equations have been proposed to predict the residual strengths (cube compressive strength, split tensile strength and modulus of elasticity) of geopolymer concrete after exposure to elevated temperatures (upto 800 °C). These equations could be used for material modelling until better refined equations are available.
11. Compared to OPC concrete, geopolymer concrete shows better resistance against surface cracking when exposed to elevated temperatures. In the present study, while OPC concrete started developing cracks at 400 °C, geopolymer concrete did not show any visible cracks up to 600 °C and developed only minor cracks at an exposure temperature of 800 °C.
12. Geopolymer concrete beams develop crack at an early load stages if they are exposed to elevated temperatures.
13. Even though the material strength of the geopolymer concrete does not decrease beyond 600 °C, the flexural strength of corresponding beam reduces rapidly after 600 °C temperature exposure, primarily due to the rapid loss of the strength of steel.
14. With increase in temperature, the curvature at yield point of geopolymer concrete beam increases and thereby the ductility reduces. In the present study compared to the ductility at ambient temperature, the ductility of geopolymer concrete beams reduces by 63.8% at 800 °C temperature exposure.
15. Appropriate equations have been proposed to predict the service load crack width of geopolymer concrete beam exposed to elevated temperatures. These equations could be used to limit the service load on geopolymer concrete beams exposed to elevated temperatures (up to 800 °C) for a predefined crack width (between 0.1mm and 0.3 mm) or vice versa.
16. The moment-curvature relationship of geopolymer concrete beams at ambient temperature is similar to that of RCC beams and this could be predicted using strain compatibility approach

17. Once exposed to an elevated temperature, the strain compatibility approach underestimates the curvature of geopolymer concrete beams between the first cracking and yielding point.

7.3 SCOPE FOR FUTURE STUDIES

1. Fly ash from different sources in India has different chemical and physical properties and this affects the strength and other properties of geopolymer concrete. A study on the influence of source of fly ash on properties of geopolymer concrete will help in arriving at a better mixture design procedure of geopolymer concrete.
2. Further study on geopolymer concrete beams after exposure to elevated temperature can refine the proposed prediction equations based on the present study.
3. The shear behaviour of geopolymer concrete beam after exposure to elevated temperatures can be studied.
4. Study on interface shear strength of geopolymer concrete with different quantities of reinforcement and after exposure to elevated temperature can be conducted for developing better equations to predict the interface shear strength of geopolymer concrete after exposure to elevated temperatures.
5. Study on thermal properties of geopolymer paste, mortar and concrete are other areas to be explored.
6. Fire test on geopolymer concrete beams and other structural elements can be conducted for better understanding of fire endurance of geopolymer concrete structural members.

****

REFERENCES

[1] Choate, W.T. (2003). "Energy and Emission Reduction Opportunities for the Cement Industry", *Report: Industrial Technological Program, Energy Efficiency and Renewable Energy*, US Department of Energy, USA.

[2] Davidovits, J. (1994). "High-Alkali Cements for 21st Century Concretes", *ACI Special Publication*, 144, 383-398.

[3] Malhotra, V. M. (1999). "Making Concrete "Greener" With Fly Ash." *Concrete International*, 21(5), 61-66.

[4] Cembureau. (2014). "Quarterly Economic reports-Keyfacts & Figures", *http://www.cembureau.be/about-cement/key-facts-figures*, visited on 3.8.2015.

[5] India Brand Equity Foundation. (2015). "Indian Cement Industry Analysis", *http://www.ibef.org/industry/cement-presentation*, visited on 3.8.2015.

[6] Worrell, E., Price, L., Martin, N., Hendriks, C., and Meida, L.O. (2001). "Carbon Dioxide Emissions From The Global Cement Industry", *Annual Review of Energy and Environment*, 26(November), 303–329.

[7] Central Electricity Authority. (2014). "Report on Fly ash generation at Coal/Lignite Based Thermal Power Stations And Its Utilization In The Country, For The Years 2011-12 And 2012-13", *Central Electricity Authority* ,Government of India, New Delhi.

[8] Lokeshappa, B., and Dikshit, A.K. (2011). "Disposal and Management of Flyash", *IPCBEE* , 3(January), 11-14.

[9] Ken, P.W., Ramli, M., and Ban, C.C. (2015). "An overview on the influence of various factors on the properties of geopolymer concrete derived from industrial by-products", *Construction and Building Materials*, 77(February), 370–395.

[10] Olivia, M., and Nikraz, H.R., (2011). "Strengthand Water Penetrability of Fly Ash Geopolymer Concrete", *ARPN Journal of Engineering and Applied Sciences*, 6(7), 70-78.

[11] Rangan, B.V. (2011). "Fly Ash-Based Geopolymer Concrete", *Proceeding of the International Workshop on Geopolymer Cement and Concrete*, Allied Publishers Private Limited, Mumbai, India, 68-106.

[12] Davidovits, J., Francisco, A. (1981). "Fabrication of stone objects, by geopolymeric synthesis, in the pre-incan Huanka civilization (Peru)", *Proceedigs of the 21st Symposium for Archaeometry at Brookhaven national Laboratory*, New York, USA.

[13] Davidovits, J. (1984). "X-Ray Analysis and X-Ray Diffraction of Casing Stone From the Pyramids of Egypt, and the Lime Stone of the Associated Quarries", *Proceedings of the Science in Egyptology Symposia*, Manchester, U.K., 511-520

[14] Jana, D. (2007). "The Great Pyramid debate: evidence from detailed petrographic examinations of casing stones from the Great Pyramid of Khufu, a natural limestone from Tura, and a man-made (geopolymeric) limestone, *Proceedings of the 29th Conference on Cement Microscopy*, Quebec City, PQ.

[15] Davidovits, F., Nasso, F., and Davidovits, J. (1999). "The making of Etruscan ceramic (Bucchero Nero) in VII-VIII century B.C", *Proceedings of the Geopolymer 99, 2nd International Conference on Geopolymers*, Geopolymer Institure, Saint-Quentin, France.

[16] Geopolymer Institute. (2012). "Archaeological Analogues (RomanCements)", *http://www.geopolymer.org/applications/archaeological-analogues-roman-cements*, visited on 4.8.15.

[17] Pacheco-Torgal, F., Castro-Gomes, J., and Jalali, S. (2008). "Alkali-activated binders: A review Part 1. Historical background, terminology, reaction mechanisms and hydration products", *Construction and Building Materials*, 22(7), 1305–1314.

[18] Roy, D.M. (1999). "Alkali-activated cements Opportunities and challenges", *Cement and Concrete Research*, 29(2), 249–254.

[19] Sofi, M., Van Deventer, J.S.J., Mendis, P.A., and Lukey G.C. (2007). "Engineering properties of inorganic polymer concretes", *Cement and Concrete Research*, 37(2), 251-257.

[20] Palomo, A., Grutzeck, M.W., and Blanco, M.T. (2008). "Alkali-activated fly ashes A cement for the future", *Cement and Concrete Research*, 29(8), 1323–1329.

[21] Davidovits, J. (1981). "The Need to Create a New Technical Language for the Transfer of Basic Scientific Information", *Proceedings of the Transfer and Exploitation of Scientific and Technical Information Symposium*, Luxembourg .

[22] Davidovits, J. (1994). " GEOPOLYMERS: Man-made rock Geosynthesis and the resulting Development of Very Early high Strength Cement", *Journal of Material Education*, 16(2&3), 91-139.

[23] Davidovits, J. (1991). "Geopolymers:Inorganic polymerie new materials", *Journal of Thermal Analysis*, 37(8), 1633-1656.

[24] Xu, H., and Van Deventer, J.S.J. (2000). "The geopolymerisation of alumino-silicate minerals", *International Journal of Mineral Process*, 59(3), 247–266.

[25] Weng, L., and Sagoe-Crentsil, K. (2007). "Dissolution Processes, hydrolysis and condensation reactions during geopolymer synthesis: Part I- Low Si/Al ratio systems", *Journal of Material Science*, 42(9), 2997-3006.

[26] Rahier, H., Wastiels, J. Biesemans, M, Willlem, R., Van Assche, G., and Van Mele, B. (2007). "Reaction mechanism, kinetics and high temperature transformations of geopolymers", *Journal of Materialscience*, 42(9), 2982–2996.

[27] Davidovits, J. (2002). "30 Years of Successes and Failures in Geopolymer Applications. Market Trends and Potential Breakthroughs*", Proceedings of the Geopolymer 2002 Turning potential into profit Third International Conference*, Melbourne, Australia.

[28] Shetty, M.S. (2008). "Concrete Technology", *S Chand and company Ltd.*, New Delhi, India.

[29] Pellenq, R.J.M., Kushima, A., Shahsavari, R., Vliet, K.J.V, Buehler, M.J., Yip, S., and Ulm, F.J. (2009). "A realistic molecular model of cement hydrates", *PNAS*, 106(38), 16102–16107.

[30] Barbosa, V.F., MacKenzie , K.D., and Thaumaturgo, C. (2000). "Synthesis and characterisation of materials based on inorganic polymers of alumina and silica: sodium polysialate polymers", *International Journal of Inorganic Materials*, 2(4), 309–317.

[31] Yang, K., Hwang, H., and Lee, S. (2010). "Effects of Water-Binder Ratio and Fine Aggregate–Total Aggregate Ratio on the Properties of Hwangtoh-Based Alkali-Activated Concrete", *Journal of Materials in Civil Engineering*, 22(9), 887-897.

[32] Ravikumar, D., Peethamparan, S., and Neithalath, N. (2010). "Structure and strength of NaOH activated concretes containing fly ash or GGBFS as the sole binder", *Cement & Concrete Composites* , 32(6), 399–410.

[33] Oh, J.E., Monteiro, P.J.M., Jun, S.S., Choi, S., and Clark, S.M. (2010). "The evolution of strength and crystalline phases for alkali-activated ground blast furnace slag and fly ash-based geopolymers", *Cement and Concrete Research*, 40(2), 189–196.

[34] Kourti, I., Rani, D.A., Boccaccini, A.R, and Cheeseman, C.R. (2011). "Geopolymers from DC Plasma Treated APC Residues, Metakaolin and GGBFS", *Journal of Materials in Civil Engineering*, 23(6), 735-740.

[35] Wongpa, J., Kiattikomol, K., Jaturapitakku, C., and Chindaprasirt, P. (2010). "Compressive strength, modulus of elasticity, and water permeability of inorganic polymer concrete", *Materials and Design*, 10(December), 4748–4754.

[36] He, J., Jie, Y., Zhang, J., Yu, Y., and Zhang, G. (2013). "Synthesis and characterization of red mud and rice husk ash-based geopolymer composites", *Cement & Concrete Composites*, 37(March), 108–118.

[37] Papakonstantinou, G. C., and Balaguru, P.N. (2007). "Fatigue Behavior of High Temperature Inorganic Matrix Composites", *Journal of Materials in Civil Engineering*, 19(4), 321-328.

[38] Ranjbar, N., Mehdi, M.J., Behnia, A., Alengaram, U.J., and Jumaat, M.Z. (2014). "Compressive strength and microstructural analysis of fly ash/palm oil fuel ash based geopolymer mortar", *Materials and Design*, 59, 532–539.

[39] Brew, D.R.M., and MacKenzie, K.J.D. (2007). "Geopolymer synthesis using silica fume and sodium aluminate", *Journal of Materials Science*, 42,(11), 3990-3993.

[40] Xu, H., and Van Deventer, J. S. J. (2000). "The geopolymerisation of alumino-silicate minerals", *International Journal of Mineral Processing*, 59(3), 247–266 .

[41] Jian-xiong , C., Han-bin, C., Pei, X., and Lan-fang, Z. (2004). "A study on complex alkali-slag environmental concrete", *Proceedins of the International Workshop on Sustainable Development and Concrete Technology*, Beijing.

[42] Duxson, P., Provis, J.L., Lukey, G.C., Mallicoat, S.W., Kriven, W.M. and van Deventer, J.S.J. (2005). "Understanding the relationship between geopolymer composition, microstructure and mechanical properties", *Colloids and Surfaces A: Physicochemical and Engineering Aspects*, 269(1-3), 47–58.

[43] Duxson, P., Provis, J.L., Lukey, G.C., Mallicoat, S.W., Kriven, W.M. and van Deventer, J.S.J. (2007). "The effect of alkali and Si/Al ratio on the development of mechanical properties of metakaolin-based geopolymer", *Colloids and Surfaces A: Physicochemical and Engineering Aspects*, 292(1), 8–24.

[44] Temuujin, J. Williams, R.P. and Van Riessen, A. (2009). "Effect of mechanical activation of fly ash on the properties of geopolymer cured at ambient temperature", *Journal of Materials Processing Technology*, 209(12-13), 5276-5280.

[45] Xu, H., and Van Deventer, J.S.J. (2003). "Effect of Source material on Geopolymerization", *Industrial and Engineering Chemical Research*, 42(8), 1698-1706.

[46] Diaz, E.I., Alloche, E.N., and Eklund, S. (2010). "Factors affecting suitability of fly ash source material for geopolymers", *Fuel*, 89(5), 992-996.

[47] Verdolotti, L., Iannace,S., Lavorgna, M., and Lamanna, R. (2008). "Geopolymerization reaction to consolidate incoherent pozzolanic Soil", *Journal of Material Science*, 43(3), 865–873.

[48] Yunfen, H., Dongmin, W., Wenjuan, Z., Hongho, L.U., and Lin, W. (2009). "Effect of Activator and Curing mode on Fly ash based Geopolymers", *Journal of Wuhan University of Technology-Mater. Sci. Ed*., 24(5), 711-715.

[49] Rahier, H., Wastiels, J., Biesemans, M., Willlem, R., Van Assche, G., and Van Mele, B. (2007). "Reaction mechanism, kinetics and high temperature transformations of geopolymers", *Journal of Material Science*, 42(9), 2982–2996.

[50] Li, Z., and Liu, S. (2007). "Influence of Slag as Additive on Compressive Strength of Fly Ash Based Geopolymer", *Journal of Materials in Civil Engineering*, 19(6), 470-474.

[51] Singh, P.S., Bastow, T., and Trigg, M. (2005). "Structural studies of geopolymers by Si and Al MAS-NMR", *Journal of Materials Science*, 40(15), 3951 – 3961.

[52] Papakonstantinou, C.G., and Balaguru, P.N, (2007). "Fatigue Behavior of High Temperature Inorganic Matrix Composites", *Journal of Materials in Civil Engineering*, 19(4), 321-328

[53] Giancaspro, J., Balaguru, P.N., and Lyon, R.E. (2006). "Use of Inorganic Polymer to Improve the Fire Response of Balsa Sandwich Structures", *Journal of Materials in Civil Engineering*, 18(3), 390-397.

[54] Sindhunata, Provis, J.L., Lukey, G.C., Xu, H., and Van Deventer, J.S.J. (2008). "Structural Evolution of Fly Ash Based Geopolymers in Alkaline Environments", *Industrial and Engineering Chemical Research*, 47(9), 2991-2999.

[55] Bakharev, T. (2005). "Durability of geopolymer materials in sodium and Magnesiumsulfatesolutions", *Cement and Concrete Research*, 35(6), 1233-1246.

[56] Thakur, R.N., and Ghosh, S.(2009). "Effect of Mix Composition on Compressive Strength and Microstructure of Fly Ash Based Geopolymer Composites", *ARPN Journal of Engineering and Applied Sciences*, 4(4), 68-74.

[57] Chindaprasirt, P., Chareerat, T., Hatanaka, S., and Caod, T. (2010). "High strength geopolymer using fine high calcium fly ash", *Journal of Materials in Civil Engineering*, 23(3), 264–270.

[58] García-Lodeiro, I., Palomo, A., and Fernandez-Jimenez, A. (2007). "Alkali-aggregate reaction in activated fly ash systems", *Cement and Concrete Research*, 37(2), 175-183.

[59] Yang, K., and Song, J. (2009). "Workability Loss and Compressive Strength Development of Cementless Mortars Activated by Combination of Sodium

Silicate and Sodium Hydroxide", *Journal of materials in Civil Engineering*, 21(3), 119-127.

[60] Li, Z., Zhang, Y. and Zhou, X. (2005). "Short Fiber Reinforced Geopolymer Composites Manufactured by Extrus", *Journal of Materials in Civil Engineering*, 17(6), 624-631.

[61] Thokchom , S., Ghosh , P., and Ghosh, S.2009). "Effect of Na2O Content on Durability of Geopolymer Mortars in Sulphuric Acid*", International Journal of Natural Sciences and Engineering*, 2(2), 77-82.

[62] Fernando, P. João, C., and Said, j. (2010). "Durability and Environmental Performance of Alkali-Activated Tungsten Mine Waste Mud Mortars", *Journal of Materials in Civil Engineering*, 22(9), 897-904.

[63] Hardjito, D., Wallah, S.E., Sumajouw, D.M.J., and Rangan, B.V. (2004). "On the Development of Fly - Based Geopolymer Concrete", *ACI Materials Journal*, 101(6), 467-472.

[64] Reddy, B.S.K., Varaprasad, J., and Reddy, K.N.K. (2010). "Strength and workability of low lime fly-ash based geopolymerconcrete", *Indian Journal of Science and Technology*, 3(12), 1188-1189.

[65] Fernandez-Jimenez, A.M., Palomo, A., and Lopez-Hombrados, C. (2006). "Engineering Properties of Alkali-Activated Fly Ash Concrete", *ACI Materials Journal*, 103(2), 106-112.

[66] Sarker , P.K. (2010). "Bond strength of reinforcing steel embedded in fly ash-based geopolymer concrete", *Materials and Structures*, 44(5), 1021-1030.

[67] Borges, P.H.R., Lucas F. Fonseca, L.F., Nunes1, V.A., Panzera, T.H., and Martusce, C.C. (2013). "Andreasen particle packing method on the development of geopolymer concrete for civil engineering", *Journal of Materials in Civil Engineering*, 26(4), 692–697.

[68] Vora, P.R., and Dave, U.V. (2013). "Parametric Studies on Compressive Strength of Geopolymer Concrete", *Procedia Engineering*, 51, 210 – 219.

[69] Ravikumar, D., Peethamparan, S., and Neithalat, N. (2010). "Structure and strength of NaOH activated concretes containing fly ash or GGBFS as the sole binder", *Cement and Concrete Composites*, 32(6), 399–410.

[70] Yang, K., Hwang, H., and Lee, S. (2010). "Effects of Water-Binder Ratio and Fine Aggregate–Total Aggregate Ratio on the Properties of Hwangtoh-Based Alkali-Activated Concrete", *Journal of Materials in Civil Engineering*, 22(9), 887-896.

[71] Sumajouw, M.D.J., and Rangan, B.V. (2006). **"**Low-Calcium Fly Ash-based Geopolymer Concrete: Reinforced Beams and Columns", *Research Report GC 3*, Faculty of Engineering, Curtin University of Technology, Australia.

[72] Dattatreya, J.K., Rajamane, N.P., Sabitha, D., Ambily, P.S., and Nataraja, M.C., (2011). "Flexural behaviour of reinforced Geopolymer concrete beams", *International Journal of civil and structural engineering*, 2(1), 138-159.

[73] Jeyasehar, C.A., Saravanan, G., Salahuddin, M., and Thirugnanasambandam, S. (2013). "Development of Fly Ash based geopolymer precast concrete elements".(2013), *Asian Journal of Civil Engineering* ,14(4), 605-615.

[74] Sumajouw, D.M.J., Hardjito, D., Wallah, S.E., and Rangan, B.V. (2007). "Fly ash-based geopolymer concrete: study of slender reinforced columns", *Journal of Material Science*, 42(9), 3124–3130.

[75] Chang, E.H. (2009). "Shear and Bond Behaviour of Reinforced Fly Ash-Based Geopolymer Concrete Beams" *Thesis presented for the Degree of Doctor of Philosophy of Curtin University of Technology*, Australia.

[76] Maranan, G., Manalo, A., Karunasena, K., and Benmokrane, B. (2015). "Bond stress-slip behaviour: The case of GFRP bars in geopolymer concrete", *Journal of Materials in Civil Engineering*, 27(1), 1-8.

[77] Dias, D.P., and Thaumaturgo. C. (2005). "Fracture toughness of geopolymeric concretes reinforced with basalt fibers", *Cement & Concrete Composites*, 27(1), 49-54.

[78] Kupwade-Patil, K., and Allouche, E.N. (2013). "Impact of Alkali Silica Reaction on Fly Ash-Based Geopolymer Concrete", *Journal of materials in Civil Engineering*, 25(1), 131-139.

[79] Lee, W.K.W., and Van Deventer, J.S.J. (2004). "The interface between natural siliceous aggregates and geopolymers", *Cement and Concrete Research*, 34(2), 195-206.

[80] Song , J.X., Marosszeky, M ., Brungs , M ., and Munn , R . (2005). “Durability of fly ash based Geopolymer concrete against sulphuric acid attack”, *In; 10DBMC International Conference On Durability of Building Materials and Components*, Lyon, France.

[80] Bernal, S.A., Mejía de Gutiérrez, R., Pedraza, A.L, Provis, J.L. Rodriguez, E.D., and Delvasto, S. (2011). “Effect of binder content on the performance of alkali-activated slag concretes”, *Cement and Concrete Research*, 41(1), 1-8.

[81] Kupwade-Patil, K., and Allouche, E.N. (2013). “Examination of Chloride-Induced Corrosion in Reinforced Geopolymer Concretes”, *Journal of Materials in Civil Engineering*, 25(10), 1465-1476.

[82] Goretta, K.C., Gutierrez-Mora, F., Singh, D., Routbort, J.L., Lukey, G.C., and Van Deventer, J.S.J. (2007). “Erosion of geopolymers made from industrial waste”, *Journal of Material Sciennce*, 42(9), 3066-3072.

[83] Gourley, J. T., and Johnson, G. B. (2005). "Developments in Geopolymer Precast Concrete" *International Workshop on Geopolymers and Geopolymer Concrete*, 2005, Perth, Australia.

[84] Phan, L.T., and Carino, N.J. (2000). “Fire Performance of High-strength Concrete: Research Needs,” *In; Advanced Technology in Structural Engineering, ASCE/SEI Structures Congress 2000*, Philadelphia, U.S.A.

[85] Bamonte, P., and Gambarova, P.G. (2013). “A study on the mechanical properties of self-compacting concrete at high temperature and after cooling”, *Materials and Structures*, 45(February), 1375–1387.

[86] American Society of Testing and Materials. (2007). “ASTM E119 - 07 Standard Test Methods for Fire Tests of Building Construction and Materials”, *Annual Book of ASTM Standards*, Philadelphia.

[87] International Standard. (2009). “ISO 834-1:2009 “Fire –resistance tests-Elements of building construction-Part 1: General requirements”, *International Organisation of Standards Publication*, Geneva.

[88] Bureau of Indian Standards. (2007). “IS: 3809-1979, Indian standard fire resistance test of structures”, *Bureau of Indian Standards*, New Delhi, India.

[89] Willam, K., Xi, Y., Lee, K., and Kim, B. (2009). "Thermal Response of Reinforced Concrete Structures in Nuclear Power Plants", *A report submitted at College of Engineering and Applied Science*, University of Colorado, Boulder.

[90] Phan, L. (1996). "Fire Performance of High Strength Concrete: A Report of the State -of-The -Art", *Bulding and Fire Research Laboratory*, National Institute of Standards, Maryland.

[91] Lin, W., Lin, T.D., and Powers-Couche, L.J. (1996). "Microstructures of Fire-Damaged Concrete", *ACI Materials journal*, 93(3), 199-205.

[92] Janotka, I., and Bagel, L. (2002). "Pore Structures, Permabilities, and Compressive Strengths of Concrete at Temperatures up to 800 °C", *ACI Materials Journal*, 99(2), 196-200.

[93] Ahmed, A.E., Al-Shaikh, A.H, and Arafat, T.I. (1992). "Residual compressive and bond strength of lime stone aggregate concrete subjected to elevated temperatures", *Magazine of concrete research*, 44(159), 117-125.

[94] Kodur, V.K.R., and Sultan, M.A. (2003). "Effect of Temperature on Thermal Properties of High-Strength Concrete", *Journal of Materials in Civil Engineering*, 15(2), 101-107.

[95] Youssef, M.A., and Moftah, M. (2007). "General stress–strain relationship for concrete at elevated temperatures", *Engineering Structures*, 29(10), 2618–2634.

[96] Li, L., and Purkiss, J. (2005). "Stress–strain constitutive equations of concrete material at elevated temperatures", *Fire Safety Journal*, 40(7), 669–686.

[97] Xiao, J., and Konig, G. (2004,) "Study on concrete at high temperature in China an overview", *Fire Safety Journal*, 39(1), 89–103.

[98] Sukumar, B., Nagamani, K., and Srinivasa, R.R. (2008). "Evaluation of strength at early ages of self-compacting concrete with high volume fly ash", *Construction and Building Materials*, 22(7), 1394–1401.

[99] Chan, N., Yin, S., Peng, G., and Anson, M. (1999). "Fire Behavior of High-Performance Concrete Made with Silica Fume at Various Moisture Contents", *ACI Materials Journal*, 96(3), 405-409.

[100] Pan, Z., Sanjayan, J.G., and Rangan B.V. (2009). "An Investigation of the Mechanisms for Strength Gain or Loss of Geopolymer Mortar after Exposure to Elevated Temperature", *Journal of Materials Science*, 44(7), 873-1880.

[101] Kong, D.L.Y., Sanjayan, J.G., and Sagoe-Crentsil, K. (2007). "Comparative performance of geopolymers made with metakaolin and fly ash after exposure to elevated temperatures", *Cement and Concrete Research*, 37(12), 1583–1589.

[102] Kong, D.L.Y., and Sanjayan, J.G. (2008). "Damage behavior of geopolymer composites exposed to elevated temperatures", *Cement and Concrete Composites*, 30(10), 986-991.

[103] Pan, Z., and Sanjayan, J.G. (2010). "Stress–strain behaviour and abrupt loss of stiffness of geopolymer at elevated temperatures", *Cement & Concrete Composites*, 32(9), 657–664.

[104] Dombrowski, K., Buchwald, A., and Well, M. (2006). "The Influence of Calcium content on the Structure and Thermal Performance of Fly Ash Based Geopolymers", *Journal of Materials Science*, 42(9), 3033-3043.

[105] Pernica, D., Reis, P.N.B., Ferreira, J.A.M., and Louda, P. (2009). "Effect of test conditions on the bending strength of a geopolymer-reinforced composite", *Journal of Materials Science*, 45(3), 744-749.

[106] Kong, D.L.Y., and Sanjayan, J.G. (2010). "Effect of elevated temperatures on geopolymer paste, mortar and concrete", *Cement and Concrete Research*, 40(2), 334–339.

[107] Dimas, D., Giannopoulou, I., and Panias, D. (2009). "Polymerization in sodium silicate solutions: a fundamental process in geopolymerization technology", *Journal of Materials Science*, 44(14), 3719–3730.

[108] Provis, J.L., Yong, C.Z., Duxson, P., and Van Deventer, J.S.J. (2009). "Correlating mechanical and thermal properties of sodium silicate-fly ash geopolymers", *Colloids and Surfaces A: Physicochemical Engineering Aspects*, 336(1-3), 57-63.

[109] Alarcon-Ruiz, L., Platret, G., Massieu, E., and Ehrlacher, A. (2005). "The use of thermal analysis in assessing the effect of temperature on a cement paste", *Cement and Concrete Research*, 35(3), 609–613.

[110] Rahul, P.C., Mundhada, A.R. (2012), "Effect of Fire on Flexural Strength of Reinforced Concrete Beam", *International Journal of Engineering Research & Technology*, 1(3), 1-6.

[111] LI, Q., YUAN, G., and LI, Z., (2008). "Mechanical Properties of RC Beam After Exposed to Fire in Loading State", *Concrete Annual Papers*, 30(3), 289-294.

[112] Shi , X., Tan , T., and Guo , Z. (2004). "Influence of Concrete Cover on Fire Resistance of Reinforced Concrete Flexural Members", *Journal of Structural Engineering*, 130(8), 1225-1232.

[113] Kodur, V.K.R., and Phan, L. (2007). "Critical factors governing the fire performance of high strength concrete systems", *Fire Safety Journal*, 42(6-7), 482-488.

[114] Park,R., and Paulay, T. (1975). "Reinforced Concrete Structures", *John Wiley & Sons*, USA.

[115] Srikanth, M., Kumar, G.R., and Giri, S. (2007). "Moment Curvature of Reinforced Concrete Beams Using Various Confinement Models and Experimental Validat", *Asian Journal of Civil Engineering (Building and Housing)*, 8(3), 247-265.

[116] Youcef, Y.S., and Chemrouk, M. (2012). "Curvature Ductility Factor of Rectangular Sections Reinforced Concrete Beams", *World Academy of Science, Engineering and Technology*, 6(11), 994-999.

[117] Bosco, C., Carpinteri, A., and Debernardi, P.G. (1990). "Minimum Reinforcement in High-Strength Concrete", *Journal of Structural Engineering*, 116(2), 427-437.

[118] Kalkan, I. (2010). "Deflection Prediction for Reinforced Concrete Beams Through Different Effective Moment of Inertia Expressions", *International Journal of Engineering Research & Development*, 5(1,) 72-79.

[119] Bureau of Indian Standard. (2000). " IS 456:2000 Plain and Reinforced Concrete-Code of Practice", *Bureau of Indian Standards*, New Delhi 11000.

[120] British Standard. (1985). "BS 8110-2:1985 Structural use of concrete", *BSI*, 389 Chiswick High Road, London.

[121] European Standard. (2003). “Eurocode 2 “Design of concrete structures - Part 1-1: General rules and rules for building”, *Management Centre: rue de Stassart*, 36 B-1050, Brussels.

[122] Chi, M., and Kirstein, A.F. (1958). “Flexural Cracks in Reinforced Concrete Beams”, *Journal of the American Concrete Institute*, 29(10), 865-678.

[123] Allam, S.M., Shoukry, M.S., Rashad, G.E., and Hassan, A.S. (2012). “Crack width evaluation for flexural RC members”, *Alexandria Engineering Journal*, 51(3), 211–220.

[124] Frosch, R.J. (1999). “Another look at cracking and crack control in reinforced concrete”, *ACI Structural Journal*, 96(3), 437-442.

[125] Gergely, P., Lutz, L.A. (1968). “Maximum Crack Width in RC Flexural Members, Causes, Mechanism and Control of Cracking in Concrete”, *SP-20, American Concrete Institute*, 87–117.

[126] Birkeland, P. W., and Birkeland, H. W. (1966). “Connections in Precast Concrete onstruction”, *ACI Journal Proceedings*, 63(3), 345-368.

[127] Mast, R. F. (1968). ‘‘Auxiliary reinforcement in concrete connections’’, *Journal of ASCE Structural Divsion Procedings*, 94(6), 1485–1504.

[128] Hofbeck, J. A., Ibrahim, I. O., and Mattock, A. H., (1969). “Shear Transfer in Reinforced Concrete”, *ACI Journal Proceedings*, 66(2), 119-128.

[129] American Concrete Institute Committee 318. (1999). “ACI 318-99 and 318R-99 Building Code Requirements for Structural Concrete”, *American Concrete Institute*, Farmington Hills, U.S.A.

[130] Mattock, A. H., Li, W. K., and Wang, T. C. (1976). “Shear Transfer in Lightweight Reinforced Concrete”, *PCI Journal*, 32(1), 20-39.

[131] Mattock, A. H. (2001). “Shear Friction and High-Strength Concrete” *ACI Structural Journal*, 98(1), 50-59.

[132] Lawrence, F. K., and Andrew, D. (2002). “Shear Friction Tests with High-Strength Concrete”, *ACI Structural Journal*, 99 (1), 98-103.

[133] Bureau of Indian Standards. (1987). “IS: 1269-1987 Specification for 53 grade Ordinary Portland Cement”, *Bureau of Indian Standards*, New Delhi, India.

[134] Bureau of Indian Standards. (1970). "IS: 383-1970 Specification for coarse and fine aggregate from natural sources for concrete", *Bureau of Indian Standards*, New Delhi, India.

[135] Bureau of Indian Standards. (1963). "IS: 2386-1963 Methods of test for aggregates for concrete, Part III: Specific gravity, density, voids, absorption and bulking", *Bureau of Indian Standards*, New Delhi, India.

[136] Bondar, D., Lynsdale, C.J., Milestone, N.B., Hassani, N., and Ramezanianpour, A.A. (2011). "Engineering properties of alkali-activated natural pozzolans concrete", *ACI Materials Journal*, 108(1), 64–72.

[137] Bureau of Indian Standards. (1959). "IS: 1199-1959 Indian standard methods of sampling and analysis of concrete, *Bureau of Indian Standards*, New Delhi, India

[138] Bureau of Indian Standards. (1959). "IS: 516-1959, Indian standard methods of test for strength of concrete", *Bureau of Indian Standards*, New Delhi, India.

[139] Weng, L., and Sagoe-Crentsil, K. (2007). "Dissolution Processes, hydrolysis and condensation reactions during geopolymer synthesis: Part II- High Si/Al ratio systems", *Journal of Material Science*, 42(9), 3007-3014.

[140] Peng, G.F., Chan, S.Y.N., and Anson, m. (2001). "Chemical kinetics of C–S–H decomposition in hardened cement paste subjected to elevated temperatures up to 800", *Advances in Cement Research*, 13(2), 47–52.

[141] Peng, G.F., Bian, S.H., Guo, Z.Q., Zhao, J., Peng, X.L., and Jiang, Y.C. (2008). "Effect of thermal shock due to rapid cooling on residual mechanical properties of fiber concrete exposed to high temperatures", *Construction and Building Materials*, 22(5), 948–955.

[142] Lanre, O., and Asce, A. (2007). "The influence of weather on the performance of laterized concrete", *Journal of Engineering and applied science*, 2(1), 129- 135.

[143] Mathew, G. and Paul, M. (2013). "Influence of Fly Ash and GGBFS in Laterised Concrete Exposed to Elevated temperatures", *Journal of materials in Civil Engineering*, 26(3), 411- 419.

[144] Shoukry, S.N., William, G.W., Downie, B., and Raid , M.Y. (2011). "Effect of moisture and temperature on the mechanical properties of concrete", *Construction and Building Material*, 25(2), 688-696.

[145] Brooks, R.M. (2009). "Residual compressive strength of laterized concrete subjected to elevated temperatures", *Fire safety engineering design of structures*, Butterworth Heinemann, Elsevier India Pvt. Ltd..

[146] Ferna´ndez-Jime´nez , A., and Palomo, A. (2005). "Mid-infrared spectroscopic studies of alkali-activated fly ash structure", *International Journal of Inorganic Materials*, 86(1-3), 309–317.

[147] Sugama, T., Warren, J. and Butcher, T. (2011). "Self-degradable Slag/Class F Fly Ash-Blend Cements", *Report prepared for The U.S. Department of Energy*, Energy Efficiency and Renewable Energy, Geothermal Technologies Program, 1000 Independence Avenue SW, Washington, D.C. 20585.

[148] Guo, X., Shi, H., and Dick, W. (2010). "Compressive strength and microstructural characteristics of class C fly ash geopolymer", *Cement & Concrete Composites*, 32(2), 42–147.

[149] Kwak, H., and Kim, S. (2002). "Nonlinear analysis of RC beams based on moment–curvature relation", *Computers and Structures*, 80(7-8), 615–628.

****

LIST OF PUBLICATIONS

Sl.No.	Journal paper	Status	Remark
1	Benny Joseph and George Mathew (2012). "Influence of aggregate content on the behaviour of fly ash based geopolymer concrete", *Scientia Iranica A* ,19,(5), pp 1188-1194	Published	23 Citation
2	Benny Joseph and George Mathew(2013). "Interface Shear Strength of Fly Ash Based Geopolymer Concrete", *Annals Of Faculty Engineering Hunedoara -International Journal of Engineering*, XI,(3), pp 105-110.	Published	1 Citation
3	"Strength Loss Characteristics of Fly Ash Based Geopolymer Concrete Exposed to Elevated Temperatures" *Alexandria Engineering Journal.* Publisher- **Elsevier**	Communicated on 14-8-15	Under Review
4	"Flexural Behaviour of Geopolymer Concrete Beams Exposed to Elevated Temperatures" *Journal of Advanced Structural Engineering.* Publisher- **Springer**	Communicated on 12-2-15	Under Review
5	"Microstructural Analysis of Fly Ash Based Geopolymer Exposed to Elevated Temperatures" *Materials and Design.* *Publisher*- **Elsevier**	Communicated on 17-8-15	With Editor

APPENDIX A

A1- Sieve analysis results

Table A.1. Sieve analysis of fine aggregate

Sieve size (mm)	Mass retained (g)	Cumulative mass retained (g)	Cumulative% mass retained	Cumulative % finer	IS Range for zone II
4.75	0	0	0	100	90 – 100
2.36	11	11	1.1	98.9	75 – 100
1.18	207	218	21.8	78.2	55 – 90
0.60	363	581	58.1	41.9	35 – 59
0.30	284	865	86.5	13.5	8 – 30
0.15	125	990	99.0	1.0	0 – 10

Table A.2. Sieve analysis of coarse aggregate

Passing through IS Sieve (mm)	Mass retained (g)	Cumulative mass retained (g)	% mass retained	Cumulative % mass retained
40	0	0	0	0
20	1242	1242	41.4	41.4
10	1438	2680	47.9	89.3
4.75	252	2932	8.4	97.7
2.36	68	3000	2.3	100
1.18	0	0	0	100
0.60	0	0	0	100
0.30	0	0	0	100
0.15	0	0	0	100

A2-Preparation of NaOH solution

For preparing NaOH solution of a particular molarity, the required mass of NaOH pellet [11] dissolved in required mass of water and the details of the quantity of material used for making I kg of NaOH solution is shown in Table 1.

Table A1.3. Mass of NaOH pellet and water for making 1kg of NaOH solution [11]

Sl.No.	Molarity	Mass of NaOH (g)	Mass of water (g)
1	8.0	262	738
2	10	314	686
3	12	361	639
4	14	404	596
5	16	444	556

A3-Calculation of quantity of different ingredient

For proportioning the different ingredients the absolute volume method was adopted.

Calculation of the quantity of ingredient for a typical proportion is shown below.

Material calculation for $1m^3$ of concrete

$(CA/S_c + FA/S_g + FLA/S_f + AL/S_a + W/S_w) * 1/1000 =$ 0.98 (air void =2%)

$CA/S_c + FA/S_g =$ **0.7** m^3, $FA/(FA+CA) =$ **0.35**, $FLA/S_f + AL/S_a + W/Sw =$ **0.28** m^3

FA/(FA+CA)=0.35 ie FA-0.35FA=0.35CA , FA=0.5385CA

CA/Sc +FA/Sg* 1/1000= $0.7m^3$

CA/2.72+0.5385CA/2.64=700, CA= 1224.63 kg

FA= 0.5385*1224.63= 659.46 kg.

$(FLA/S_f + AL/S_a + W/S_w) * 1/1000 =$ 0.28

Weight of alkali liquid to weight of fly ash ratio = **0.55**

(FLA/1.9) +(0.55FLA/1.54) + 4.23 = 280

0.89 FLA +4.23 = 280

Weight of fly ash =	209.85 kg
Weight of alkali liquid =0.55*209.85 =	170.41kg
Weight ratio of sodium silicate solution to sodium hydroxide solution=	2.5
Weight of sodium hydroxide solution =170.41/(1+2.5) =	0.69 kg
Weight of sodium silicate solution= 170.41-48.69 =	121.72 kg
Molarity of sodium hydroxide solution =	10
Weight of sodium hydroxide pellet@314 gm/Kg of solution=0.314*48.69 =	15.28 kg
Weight of water in sodium hydroxide=48.69-15.28 =	33.41 kg
Weight of water in sodium silicate solution= 121.72*0.49 =	59.64 kg
Weight of Sodium silicate solid=121.72 - 59.64=	62 kg
Weight of water /weight of total geopolymer solid	
= (33.41+59.64+4.23)/(15.28+ 62+309.85)=	0.25

APPENDIX B

Table B.1: Quantity of materials for 1 m^3 of geopolymer concrete- Group M1

Sl.No.	Mix ID	Total aggr. (% volume)	Fine aggre/ total aggregate ratio (by mass)	Coarse aggregate (kg)	Sand (kg)	Fly ash (kg)	Alkali content (kg)	Super Plasticizer (kg)
1	M1A60R20	60	0.20	1273.07	318.27	420.57	231.31	8.41
2	M1A60R25	60	0.25	1195.69	394.58	420.57	231.31	8.41
3	M1A60R30	60	0.30	1112.14	476.66	420.57	231.31	8.41
4	M1A60R35	60	0.35	1031.99	555.73	420.57	231.31	8.41
5	M1A60R40	60	0.40	948.62	632.73	420.57	231.31	8.41
6	M1A65R20	65	0.20	1379.16	344.79	365.16	210.84	7.3
7	M1A65R25	65	0.25	1295.34	427.46	365.16	210.84	7.3
8	M1A65R30	65	0.30	1204.82	516.38	365.16	210.84	7.3
9	M1A65R35	65	0.35	1117.99	602.04	365.16	210.84	7.3
10	M1A65R40	65	0.40	1027.67	685.46	365.16	210.84	7.3
11	M1A70R20	70	0.20	1485.25	371.31	309.85	170.41	6.2
12	M1A70R25	70	0.25	1394.98	460.34	309.85	170.41	6.2
13	M1A70R30	70	0.30	1297.5	556.11	309.85	170.41	6.2
14	M1A70R35	70	0.35	1203.99	648.35	309.85	170.41	6.2
15	M1A70R40	70	0.40	1106.72	738.18	309.85	170.41	6.2
16	M1A75R20	70	0.20	1591.34	397.83	254.54	139.99	5.1
17	M1A75R25	70	0.25	1494.62	493.22	254.54	139.99	5.1
18	M1A75R30	70	0.30	1390.18	595.83	254.54	139.99	5.1
19	M1A75R35	70	0.35	1289.99	694.66	254.54	139.99	5.1
20	M1A75R40	70	0.40	1185.77	790.91	254.54	139.99	5.1

Table B.2: Quantity of materials for 1 m^3 of geopolymer concrete- Group M2

Sl. No	Mix ID	Alkali/fly ash ratio	Sodium silicate/ NaOH (kg)	Coarse aggregate (kg)	Sand (kg)	Fly ash (kg)	Alkali solution (kg)	Super plasticizer (kg)
1	M2AL35S1	0.35	1.5	1203.99	648.35	329.56	115.35	6.59
2	M2AL35S2	0.35	2.0	1203.99	648.35	327.33	114.56	6.55
3	M2AL35S3	0.35	2.5	1203.99	648.35	325.75	114.01	6.51
4	M2AL35S4	0.35	3.0	1203.99	648.35	324.7	113.65	6.49
5	M2AL35S5	0.35	3.5	1203.99	648.35	323.78	113.32	6.47
6	M2AL45S1	0.45	1.5	1203.99	648.35	322.28	145.03	6.45
7	M2AL45S2	0.45	2.0	1203.99	648.35	319.49	143.77	6.39
8	M2AL45S3	0.45	2.5	1203.99	648.35	317.67	142.95	6.35
9	M2AL45S4	0.45	3.0	1203.99	648.35	316.22	142.3	6.32
10	M2AL45S5	0.45	3.5	1203.99	648.35	315.13	141.81	6.30
11	M2AL55S1	0.55	1.5	1203.99	648.35	314.11	172.76	6.28
12	M2AL55S2	0.55	2.0	1203.99	648.35	312.1	171.65	6.24
13	M2AL55S3	0.55	2.5	1203.99	648.35	309.85	170.41	6.19
14	M2AL55S4	0.55	3.0	1203.99	648.35	308.17	169.49	6.16
15	M2AL55S5	0.55	3.5	1203.99	648.35	306.83	168.76	6.14
16	M2AL65S1	0.65	1.5	1203.99	648.35	292.67	190.23	5.85
17	M2AL65S2	0.65	2.0	1203.99	648.35	292.67	190.23	5.85
18	M2AL65S3	0.65	2.5	1203.99	648.35	292.67	190.23	5.85
19	M2AL65S4	0.65	3.0	1203.99	648.35	292.67	190.23	5.85
20	M2AL65S5	0.65	3.5	1203.99	648.35	292.67	190.23	5.85

Table B.3 : Quantity of materials for 1 m^3 of Geopolymer concrete - Group M3

Sl. No	Mix ID	Alkali/fly ash ratio	Water/ geo. solid ratio	Coarse aggregate (kg)	Sand (kg)	Fly ash (kg)	10 molar NaOH solution (kg)	Sodium silicate (kg)	Super plasticizer (kg)
1	M3AL35W1	0.35	0.24	1203.99	648.35	329.56	32.99	82.5	6.60
2	M3AL35W2	0.35	0.26	1203.99	648.35	321.41	32.14	80.35	6.43
3	M3AL35W3	0.35	0.28	1203.99	648.35	313.53	31.28	78.22	6.27
4	M3AL35W4	0.35	0.30	1203.99	648.35	304.32	30.40	76.07	6.09
5	M3AL35W5	0.35	0.32	1203.99	648.35	297.75	29.77	74.44	5.95
6	M3AL45W1	0.45	0.24	1203.99	648.35	322.03	41.40	103.51	6.44
7	M3AL45W2	0.45	0.26	1203.99	648.35	313.56	40.31	100.79	6.27
8	M3AL45W3	0.45	0.28	1203.99	648.35	305.08	39.22	98.07	6.10
9	M3AL45W4	0.45	0.30	1203.99	648.35	296.6	38.13	95.34	5.93
10	M3AL45W5	0.45	0.32	1203.99	648.35	289.95	37.28	93.2	5.80
11	M3AL55W1	0.55	0.24	1203.99	648.35	314.11	49.36	123.4	6.28
12	M3AL55W2	0.55	0.26	1203.99	648.35	305.59	48.02	120.05	6.11
13	M3AL55W3	0.55	0.28	1203.99	648.35	297.62	46.77	116.92	5.95
14	M3AL55W4	0.55	0.30	1203.99	648.35	289.77	45.52	113.84	5.79
15	M3AL55W5	0.55	0.32	1203.99	648.35	282.48	44.39	110.97	5.65
16	M3AL65W1	0.65	0.24	1203.99	648.35	292.67	41.45	135.89	5.85
17	M3AL65W2	0.65	0.26	1203.99	648.35	292.67	49.03	135.89	5.85
18	M3AL65W3	0.65	0.28	1203.99	648.35	290.37	53.93	134.81	5.81
19	M3AL65W4	0.65	0.30	1203.99	648.35	282.48	52.46	131.14	5.65
20	M3AL65W5	0.65	0.32	1203.99	648.35	275.42	51.15	127.87	5.51

Table B.4. 7 days average cube compressive strength of GP concrete with different aggregates content

Sl.No.	Total aggregate content (% of volume of concrete)	Fly ash + Alkali + Water (% volume of concrete)	Fine aggregate /Total aggregate ratio	Compressive strength at 7 days (MPa)	Average compressive strength at 7 days (MPa)	Standard Deviation
1	60	38	0.2	39.56	38	1.27
				36.44		
				38.00		
			0.25	39.00	39	1.36
				40.67		
				37.33		
			0.30	41.73	40	1.41
				38.27		
				40.00		
			0.35	43.40	42	1.14
				42.00		
				40.60		
			0.40	39.00	39	1.29
				40.58		
				37.42		
2	65	33	0.20	40.00	40	1.12
				41.37		
				38.63		
			0.25	42.70	41	1.39
				41.00		
				39.30		
			0.30	42.00	42	1.46
				43.79		
				40.21		
			0.35	44.00	44	1.51
				45.85		
				42.21		
			0.40	43.82	42	1.49
				42.00		
				40.18		

Table B.4. 7 days average cube compressive strength of GP concrete with different aggregates content

Sl.No.	Total aggregate content (% of volume of concrete)	Fly ash + Alkali + Water (% volume of concrete)	Fine aggregate /Total aggregate Ratio	Compressive strength at 7 days (MPa)	Average compressive strength at 7 days (MPa)	Standard Deviation
	70	28	0.20	44.25	43	1.02
				43.00		
				41.75		
			0.25	45.00	45	1.19
				46.46		
				43.94		
			0.30	48.56	47	1.27
				45.44		
				47.00		
			0.35	53.79	52	1.46
				50.21		
				52.00		
			0.40	47.47	46	1.20
				44.53		
				46		
	75	23	0.20	34.32	33	1.08
				31.68		
				33.00		
			0.25	36.35	35	1.10
				33.65		
				35.00		
			0.30	42.48	41	1.21
				39.52		
				41.00		
			0.35	45.00	45	1.25
				46.53		
				43.47		
			0.40	40.00	40	1.19
				41.46		
				38.54		

Table B.5. 28 days average cube compressive strength of G.P and OPC concrete with different total aggregate content

Sl No	Mix ID	Cube compressive strength (MPa)	Average cube compressive strength (MPa)	Standard deviation
1	M1A60R35	46.18	45	0.96
		45.00		
		43.82		
2	M1A65R35	48.20	47	0.98
		45.80		
		47.0 0		
3	M1A70R35	56.00	56	1.09
		57.33		
		54.67		
4	M1A75R35	49.00	49	0.99
		50.21		
		47.79		
5	OPC67R29	59.35	58	1.10
		56.65		
		58.00		

Table B.6. 28 days average tensile strength of G.P and OPC concrete with different total aggregate content

Sl.No.	Mix ID	Splitt strength (MPa)	Average split tensile strength (MPa)	Standard deviation
1	M1A60R35	3.10	3.10	0.21
		2.84		
		3.36		
2	M1A65R35	3.62	3.34	0.23
		3.06		
		3.34		
3	M1A70R35	3.82	3.45	0.30
		3.45		
		3.08		
4	M1A75R35	5.10	4.51	0.48
		3.92		
		4.51		
5	OPC67R29	3.84	4.39	0.45
		4.39		
		4.94		

Table B.7 28 days average flexural strength of G.P and OPC concrete with different total aggregate content

Sl No	Mix ID	Flexural strength (MPa)	Average flexural strength (MPa)	Standard deviation
1	M1A60R35	4.26	3.79	0.38
		3.79		
		3.32		
2	M1A65R35	4.33	3.82	0.42
		3.31		
		3.82		
3	M1A70R35	5.36	4.74	0.51
		4.12		
		4.74		
4	M1A75R35	4.95	4.95	0.59
		5.67		
		4.23		
5	OPC67R39	4.79	4.79	0.53
		5.44		
		4.14		

Table B. 8. 28 days modulus of elasticity of G.P and OPC concrete with different total aggregate content

Sl No	Mix ID	Modulus of elasticity (MPa)	Average Modulus of elasticity (MPa)	Standard deviation
1	M1A60R35	42370.89	42369	1.54
		42369.00		
		42367.11		
2	M1A65R35	45082.00	45082	1.59
		45083.95		
		45080.05		
3	M1A70R35	59070.08	59068	1.70
		59068.00		
		59065.92		
4	M1A75R35	47520.98	47519	1.62
		47517.02		
		47519.00		
5	OPC70R35	51623.00	51623	1.65
		51625.02		
		51620.98		

Table B.9. 28 days poisson's ratio of G.P and OPC concrete with different total aggregate content

Sl No	Mix ID	Poisson's Ratio	Average Poisson's ratio	Standard deviation
1	M1A60R35	0.192	0.192	0.09
		0.192		
		0192		
2	M1A65R35	0.361	0.202	0.13
		0.202		
		0.043		
3	M1A70R35	0.450	0.242	0.17
		0.242		
		0.034		
4	M1A75R35	0.330	0.195	0.11
		0.060		
		0.195		
5	OPC70R35	0.190	0.203	0.15
		0.203		
		0.387		

Table B.10. Average cube compressive strength at different alkaline liquid/Fly ash and sodium silicate /NaOH solution ratio

Sl.No.	Alkaline liquid/fly ash	Sodium silicate/NaOH	Compressive strength (MPa)	Average compressive strength (MPa)	Standard deviation
1	0.35	1.5	32.04	31	0.85
			31.00		
			29.96		
		2.0	34.93	34	0.76
			34.00		
			33.07		
		2.5	40.21	39	0.99
			39.00		
			37.79		
		3.0	36.00	36	0.59
			36.72		
			35.28		
		3.5	35.24	34	1.01
			32.76		
			34.00		
2	0.45	1.5	35.31	34	1.07
			34.00		
			32.69		
		2.0	42.00	40	1.63
			40.00		
			38.00		
		2.5	48.75	47	1.43
			47.00		
			45.25		
		3.0	44.52	43	1.24
			43.00		
			41.48		
		3.5	39.16	38	0.95
			36.84		
			38.00		

Table B.10. Average cube compressive strength at different alkaline liquid/Fly ash and sodium silicate /NaOH solution ratio

Sl.No.	Alkaline liquid/fly ash	Sodium silicate/NaOH	Compressive strength (MPa)	Average compreesive strength (MPa)	Standard deviation
3	0.55	1.5	47.00	47	1.13
			48.38		
			45.62		
		2.0	55.29	54	1.05
			52.71		
			54.00		
		2.5	60.18	58	1.78
			58.00		
			55.82		
		3.0	52.00	52	1.59
			53.95		
			50.05		
		3.5	44.98	43	1.62
			41.02		
			43.00		
4	0.65	1.5	42.82	41	0.67
			40.18		
			41.00		
		2.0	43.91	43	0.74
			43.00		
			42.09		
		2.5	44.00	44	0.81
			44.99		
			43.01		
		3.0	42.55	42	0.48
			42.00		
			41.41		
		3.5	41.00	41	0.65
			41.80		
			40.20		

Table B.11. Average cube compressive strength with different molarities of NaOH s Solution

Molarity of NaOH solution (M)	Compressive strength (MPa)	Average compressive strength at 7 days (MPa)	Standard deviation
8	45	45	1.20
	46.47		
	43.53		
10	55.04	54	0.85
	52.96		
	54		
12	47	47	0.75
	47.92		
	46.08		
14	43	43	1.65
	45.02		
	40.98		
16	42.53	41	1.25
	41		
	39.47		

Table B. 12. 7 days average cube compressive strength with different curing temperature

Sl.No.	Alkaline liquid/ fly ash	Curing temperature (°C)	Compressive strength (MPa)	Average Compressive Strength (MPa)	Standard deviation
1	0.35	Room temp	15.82	14	1.49
			14		
			12.18		
		60	25.27	28	1.04
			26.73		
			28		
		70	31.09	30	0.89
			28.51		
			30		
		80	33.07	32	0.87
			30.93		
			32		
		90	36	36	0.58
			36.71		
			35.29		
		100	39	39	1.65
			41.02		
			36.98		
		110	34.28	32	1.86
			32		
			29.72		
		120	31.20	30	0.98
			28.80		
			30		

Table B. 12. 7 days average cube compressive strength with different curing temperature

Sl.No.	Alkaline liquid/ fly ash	Curing temperature (°C)	Compressive strength (MPa)	Average compressive strength (MPa)	Standard deviation
2	0.45	Room temp	14	14	1.21
			15.48		
			12.52		
		60	33.25	32	1.02
			32		
			30.75		
		70	34	34	1.00
			35.22		
			32.78		
		80	36.08	35	0.88
			35		
			33.85		
		90	39.79	38	1.42
			38		
			36.26		
		100	43.19	44	0.66
			44.81		
			44		
		110	40.45	39	1.22
			39		
			37.51		
		120	35.97	35	0.79
			35		
			34.03		

Table B. 12. 7 days average cube compressive strength with different curing temperature

Sl.No.	Alkaline liquid/ fly ash	Curing temperature (°C)	Compressive strength (MPa)	Average compressive strength (MPa)	Standard deviation
3	0.55	Room temp	17.35	16	1.10
			14.65		
			16		
		60	37	37	0.99
			38.21		
			35.79		
		70	41	41	0.39
			41.48		
			40.52		
		80	44.67	44	0.55
			44		
			43.33		
		90	50.51	49	1.23
			47.49		
			49		
		100	56.32	55	1.08
			53.68		
			55		
		110	48	48	1.37
			49.68		
			46.32		
		120	45.15	44	0.94
			44		
			42.85		

Table B. 12. 7 days average cube compressive strength with different curing temperature

Sl.No.	Alkaline liquid/ fly ash	Curing temperature (°C)	Compressive strength (MPa)	Average compressive strength (MPa)	Standard deviation
4	0.65	Room temp	15	15	0.89
			16.09		
			13.91		
		60	35.58	34	1.29
			34		
			32.42		
		70	38.72	38	0.59
			37.28		
			38		
		80	41.97	40	1.61
			40		
			38.03		
		90	44.16	42	1.76
			39.84		
			42		
		100	45	45	1.26
			46.54		
			43.46		
		110	41.30	40	1.06
			38.70		
			40		
		120	36.96	36	0.78
			35.04		
			36		

Table B.13. 7 days average cube compressive strength of GP concrete with different temperature curing

Curing period (hours)	Compressive strength (MPa)	Average compressive Strength at 7 days (MPa)	Standard deviation
6	25	25	1.03
	26.26		
	23.74		
12	36	36	0.87
	37.07		
	34.93		
24	54	54	1.48
	55.81		
	52.19		
48	57.64	56	1.34
	54.36		
	56		
57	59.08	57	1.70
	57		
	54.92		

Table B.14. 7 days cube compressive strength of GP concrete with different water to geopolymer ratio

Sl.No.	Alkaline liquid/ fly ash	Water/geopolymer solid	compressive strength at 7 days (MPa)	Average compressive strength at 7 days (MPa)	Standard deviation
1	0.35	0.24	41.46	40	1.19
			38.54		
			40		
		0.26	39.43	38	1.17
			38		
			36.57		
		0.28	36.41	35	1.15
			33.59		
			35		
		0.30	31	31	1.10
			32.35		
			29.65		
		0.32	31.33	30	1.09
			28.67		
			30		
2	0.45	0.24	50.48	49	1.21
			49		
			47.52		
		0.26	46.41	45	1.15
			43.59		
			45		
		0.28	42	42	1.11
			43.36		
			40.64		
		0.30	39	39	1.08
			40.32		
			37.68		
		0.32	36.29	35	1.05
			35		
			33.71		

Table B.14. 7 days cube compressive strength of GP concrete with different water to geopolymer ratio

Sl.No.	Alkaline liquid/ fly ash	Water/geopolymer solid	compressive strength at 7 days (MPa)	Average compressive strength at 7 days (MPa)	Standard deviation
3	0.55	0.24	61.94	60	1.58
			60		
			58.06		
		0.26	57.89	56	1.54
			56		
			54.11		
		0.28	53.84	52	1.50
			50.16		
			52		
		0.30	50.79	49	1.46
			47.21		
			49		
		0.32	47.76	46	1.44
			46		
			44.24		
4	0.65	0.24	48.82	47	1.49
			47		
			45.18		
		0.26	44	44	1.45
			45.78		
			42.22		
		0.28	41.71	40	1.40
			38.29		
			40		
		0.30	35.57	37	1.36
			37		
			38.67		
		0.32	32	32	1.31
			33.60		
			30.40		

APPENDIX C

Table C.1. Cube compressive strength of GP and OPC concrete specimens after exposure to elevated temperatures

Exposure Temp. (˚C)	GP concrete						OPC concrete					
	Air cooled			Water cooled			Air cooled			Water cooled		
	Comp. Strength (MPa)	Avg Comp. Strength (MPa)	SD*	Comp. Strength (MPa)	Avg Comp. Strength (MPa)	SD*	Comp .Strength (MPa)	Avg Comp Strength (MPa)	SD*	Comp. Strength (MPa)	Avrg. Comp. Strength (MPa)	SD*
Ambient (28)	58.122	57.3	0.45	-	-	-	60.86	59.85	0.68	-	-	-
	57.3						59.85					
	56.478						58.84					
200	43.53	42.52	0.68	40.41	39.40	0.68	60.925	59.60	1.17	55.519	54.37	0.88
	42.52			39.40			59.60			54.37		
	41.51			38.39			58.275			53.221		
400	38.152	37.33	0.45	36.662	35.85	0.44	43.472	42.66	0.44	39.85	39.85	1.14
	37.33			35.85			42.66			41.158		
	36.508			35.038			41.848			38.542		
600	31.822	30.82	0.67	29.187	28.00	0.94	33.562	32.44	0.84	32.38	31.48	0.54
	30.82			28.00			32.44			30.58		
	29.818			26.813			31.318			31.48		
800	33.635	32.88	0.38	31.982	31.30	0.31	21.682	21.00	0.31	19.55	19.55	0.62
	32.88			31.30			21.00			20.514		
	32.125			30.618			20.318			18.586		
SD*-Standard deviation												

Table C.2. Tensile strength of GP and OPC concrete specimens after exposure to elevated temperatures

Exposure Temp. (˚C)	GP Concrete						OPC Concrete					
	Air Cooled			Water Cooled			Air Cooled			Water Cooled		
	Split Tensile Strength (MPa)	Avg Split Tensile Strength (MPa)	SD*	Split tensile strength Strengt h (MPa)	Avg Split Tensile Strength (MPa)	SD*	Split Tensile Strength (MPa)	Avg Split Tensile Strengt h (MPa)	SD*	Spit Tensil Srtrengh (MPa)	Spit Tensil Srtrengh (MPa)	SD*
Ambient (28)	6.50	5.44	0.76	-	-	-	6.300	5.47	0.46	-	-	-
	5.44						5.47					
	4.37						4.639					
200	4.92	4.17	0.38	4.747	3.89	0.49	5.422	4.45	0.63	5.475	4.30	0.92
	4.17			3.89			4.45			4.30		
	3.41			3.033			3.478			3.125		
400	3.76	2.61	0.89	3.487	2.47	0.69	4.182	3.04	0.87	3.693	2.89	0.43
	2.61			2.47			3.04			2.890		
	1.45			1.453			1.898			2.087		
600	2.89	1.76	0.86	2.278	1.37	0.55	2.459	1.48	0.64	2.532	1.45	0.78
	1.76			1.37			1.48			1.45		
	0.62			0.462			0.500			0.368		
800	3.00	1.94	0.75	2.597	1.58	0.69	1.985	1.06	0.57	1.2	0.95	1.10
	1.94			1.58			1.06			0.95		
	0.87			0.563			0.135			0.73		
SD*-Standard deviation												

Table C.3. Flexural strength of GP and OPC concrete specimens after exposure to elevated temperatures

Exposure Temp. (˚C)	GP concrete						OPC concrete					
	Air cooled			Water cooled			Air cooled			Water cooled		
	Flexural Strength (MPa)	Avg Flexural Strength (MPa)	SD*	Flexural Strength (MPa)	Avg Flexural Strength (MPa)	SD*	Flexural Strength (MPa)	Avg Flexural Strength (MPa)	SD*	Flexural Strength (MPa)	Avg Flexural Strength (MPa)	SD*
Ambient 28	6.31	5..30	0.68	-	-	-	6.262	5.440	0.45	-	-	-
	5.30						5.440					
	4.29						4.618					
200	5.12	4.23	0.53	5.11	4.10	0.68	5.533	4.53	0.67	5.155	4.40	0.38
	4.23			4.10			4.53			4.40		
	3.33			3.09			3.528			3.645		
400	4.23	2.89	1.21	3.746	2.61	0.86	4.435	3.36	0.77	4.299	3.19	0.82
	2.89			2.61			3.36			3.19		
	1.54			1.474			2.285			2.080		
600	3.00	1.86	0.87	2.453	1.52	0.58	2.836	1.72	0.83	2.645	1.49	0.89
	1.86			1.52			1.72			1.49		
	1.21			1.213			1.104			0.998		
800	2.73	1.90	0.47	2.739	1.65	0.96	1.715	0.72	0.66	1.242	0.61	0.87
	1.90			1.65			0.72			0.61		
	1.06			1.060			0.341			0.127		
SD*-Standard deviatio												

Table C.4. Modulus of Elasticity of GP and OPC concrete specimens after exposure to elevated temperatures

Exposure Temp. (°C)	GP concrete						OPC concrete					
	Air cooled			Water cooled			Air cooled			Water cooled		
	Modulus of elasticity (GPa)	Avg. Modulus of Elasticity (GPa)	SD*	Modulus of elasticity (GPa)	Avg. Modulus of Elasticity (GPa)	SD*	Modulus of elasticity (GPa)	Avg. Modulus of elasticity (GPa)	SD*	Modulus of elasticity (GPa)	Avg. Modulus of Elasticity (GPa)	SD*
Ambient (28)	56.72	57.10	0.72.	-	-	-	40.43	40.20	0.35	-	-	1.55
	56.90						40.24			-		
	57.60						39.93			-		
200	39.60	39.51	0.39	35.51	35.57	0.33	40.68	41.80	1.05	39.82	39.00	1.07
	39.20			35.83			40.58			38.70		
	39.73			35.37			39.34			38.31		
400	22.42	22.34	0.16	20.88	20.84	0.13	17.78	18.00	0.38	17.04	16.90	
	22.21			20.73			17.92			16.46		
	22.39			20.91			18.30			17.20		
600	13.02	13.25	0.28	12.34	12.10	0.68	3.72	3.70	0.66	3.68	3.60	0.22
	13.38			12.42			4.16			3.70		
	13.35			12.1			3.22			3.42		
800	14.07	13.98	0.12	11.96	12.3	0.43	1.28	1.20	0.33	1.21	1.10	0.14
	13.9			12.40			1.31			1.08		
	13.97			12.54			1.01			1.01		
SD* Standard deviation												

APPENDIX D

D.1 PROPERTIES OF GP CONCRETE AND STEEL AFTER EPOSED TO ELEVATED TEMPERATYRES

Table D.1. Mechanical properties of GP concrete after exposure temperatures

Temperatue (°C)	Modulus of elasticity (MPa)	Cube comp.strength (MPa)	Flexural strength
Ambient	57100	57.8	5.3
200	37510	42	4.23
400	22340	37	2.89
600	13250	31.1	1.86
800	13250	32.92	1.9

Table D.1. Mechanical properties of Reinforcing steel after exposure to temperatures

Temperature	Yield strength of steel (MPa)	Modulus of elasticity of steel (MPa)
Ambient (°C)	460	205240
200°	460	205090
400°	440	202620
600°	400	188490
800°	360	172250

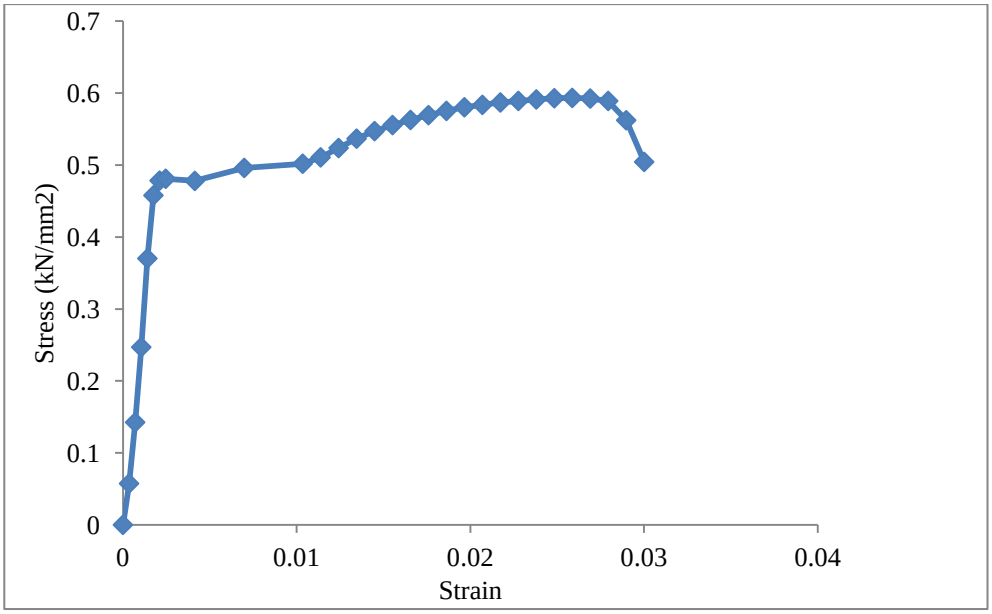

Fig. D.1.Stress strain curve of reinforcing steel at ambient temperature

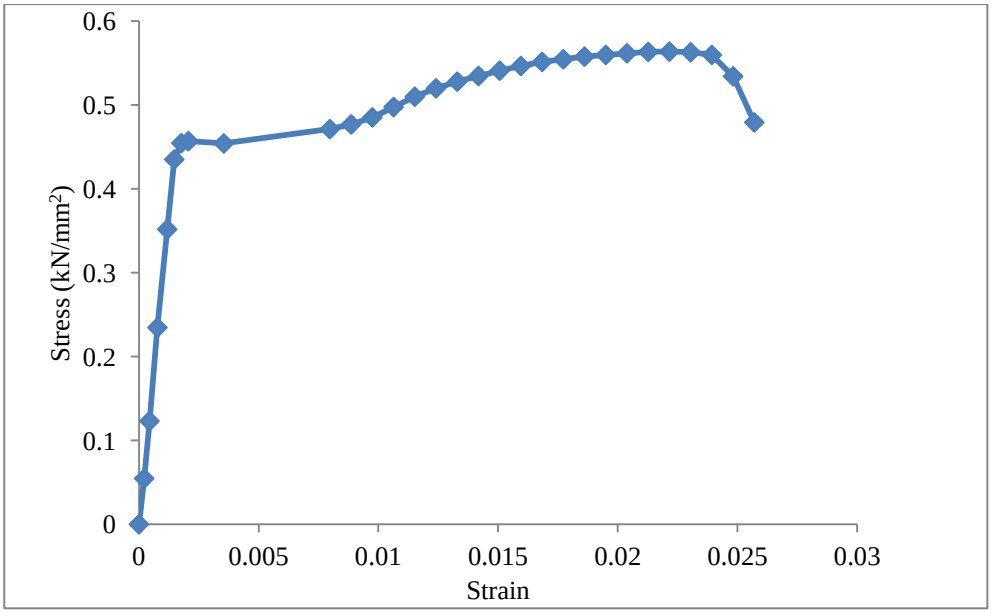

Fig. D.2. Stress strain curve of reinforcing steel at 200 °C temperature

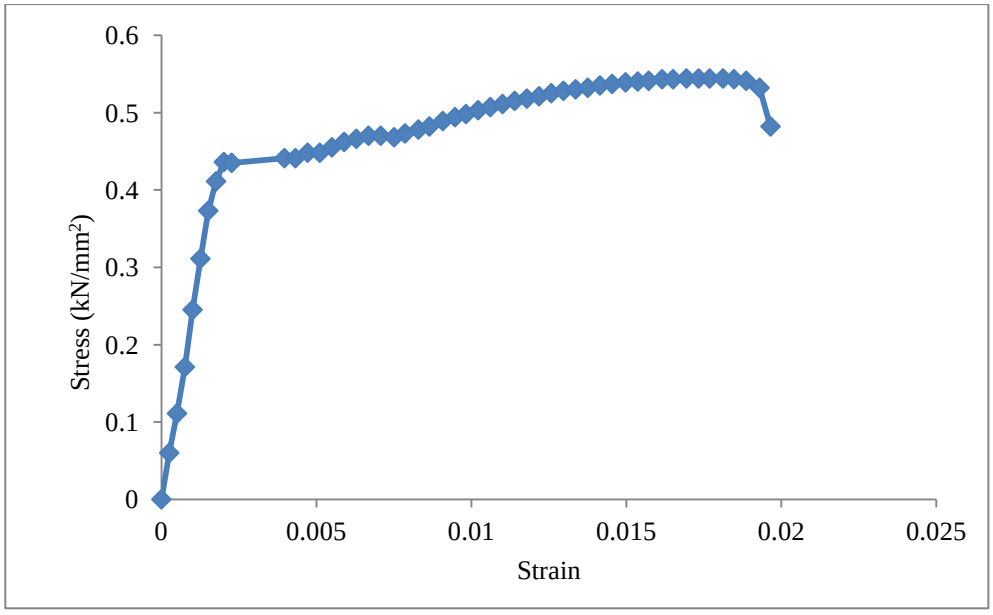

Fig. D.3.Stress strain curve of reinforcing steel at 400 °C temperature

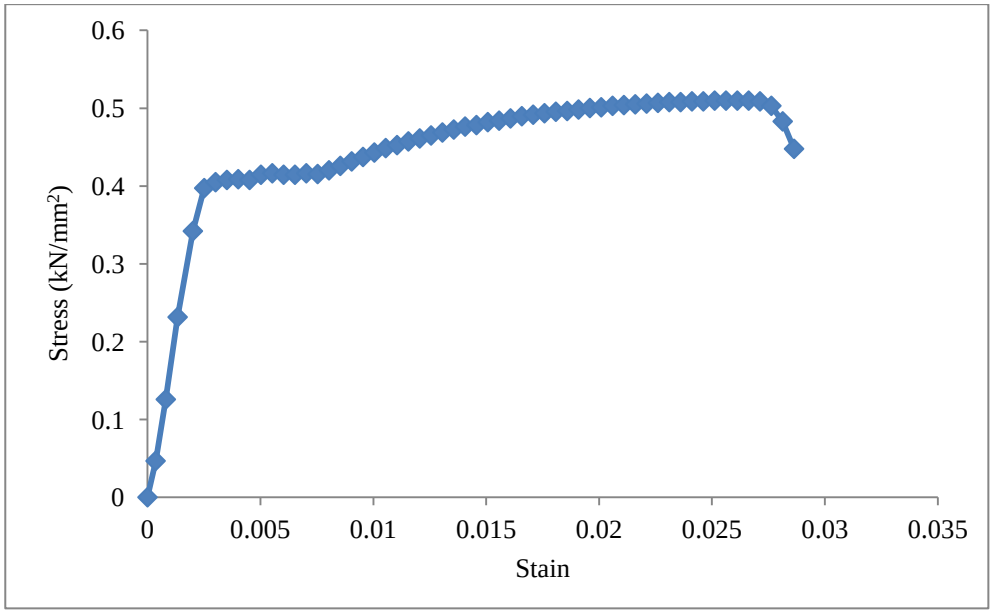

Fig. D.4. Stress strain curve of reinforcing steel at 600 °C temperature

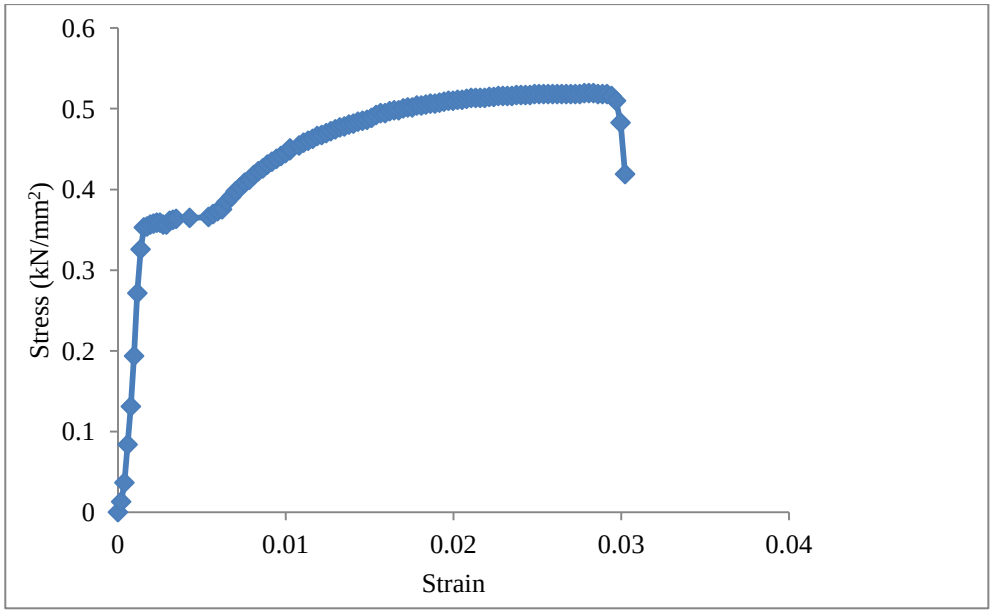

Fig. D.5.Stress strain curve of reinforcing steel at 800 °C temperature

D. 2 LOAD DIFFLECTION CURVE OF GP CONCRETE BEAMS AFTER EXPOSED TO ELEVATED TEMPERATURES

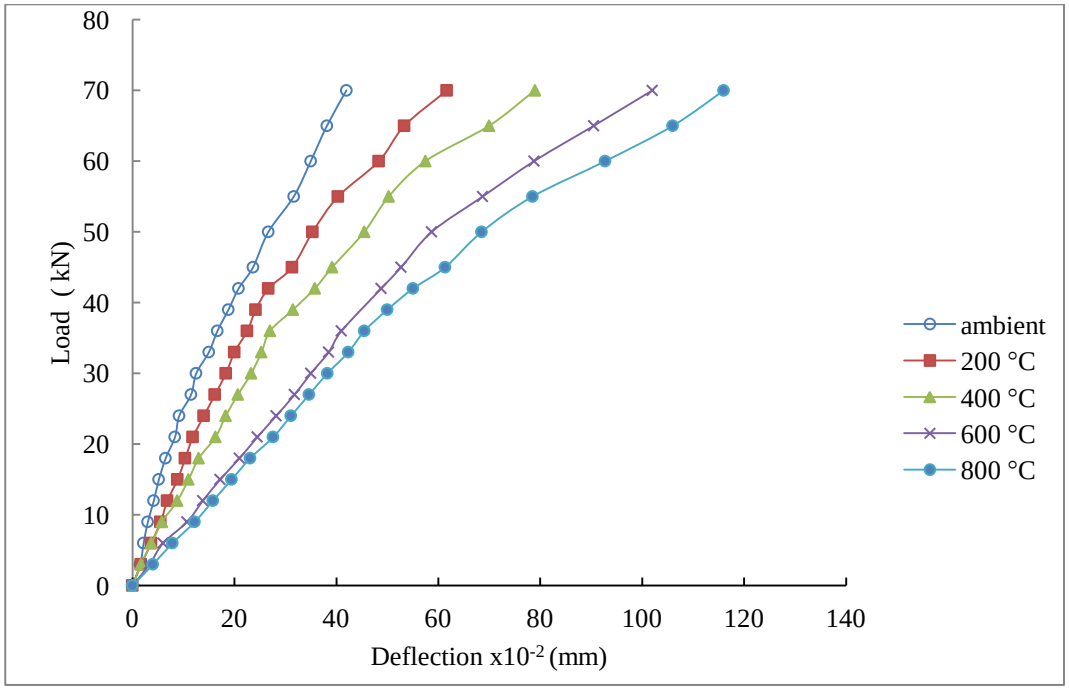

Fig. D.6. Load deflection curve of geopolymer concrete beam with 20 mm cover after exposure to elevated temperature

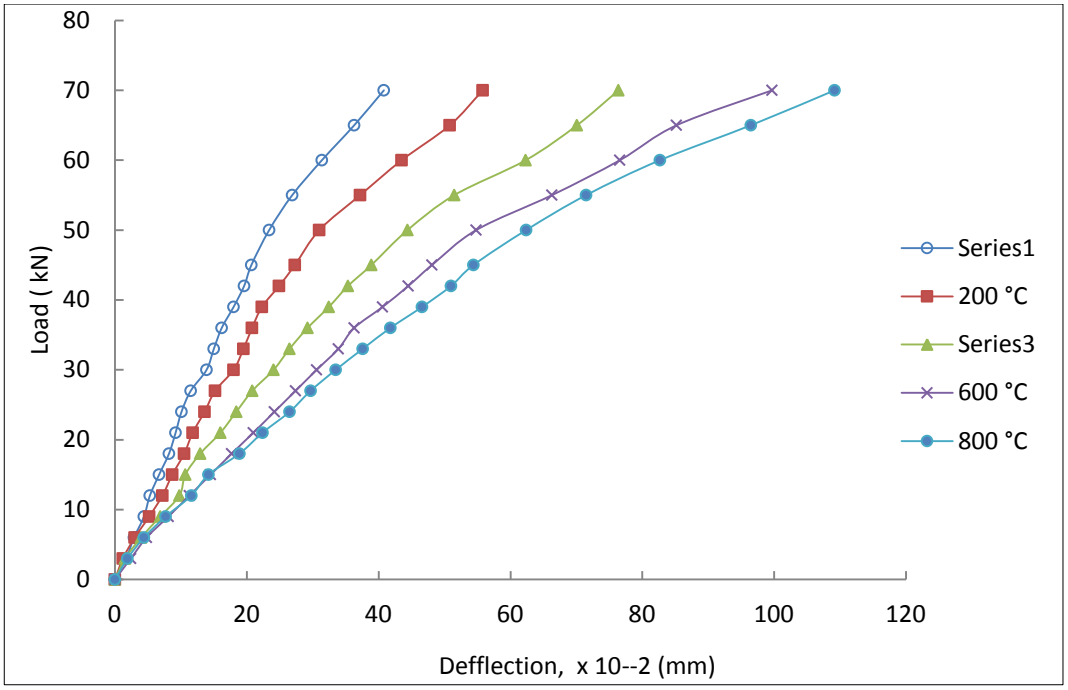

Fig. D.7. Load deflection curve of geopolymer concrete beam with 30 mm cover after exposure to elevated temperature

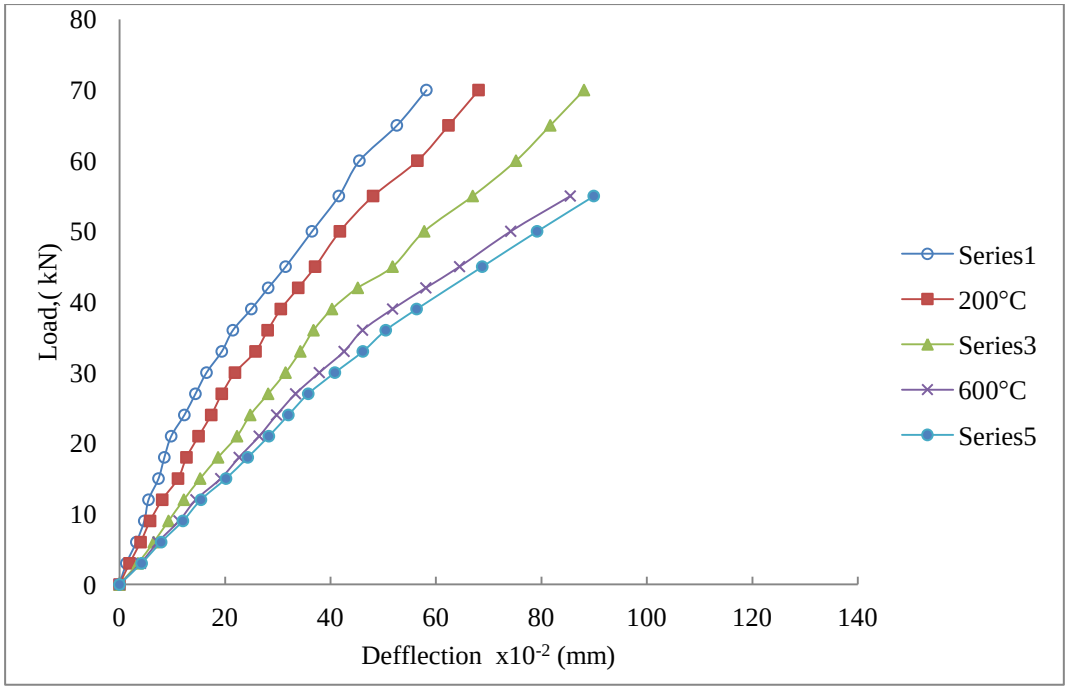

Fig. D. 8. Typical load deflection curve of geopolymer concrete beam with 40 mm cover after exposure to elevated temperature

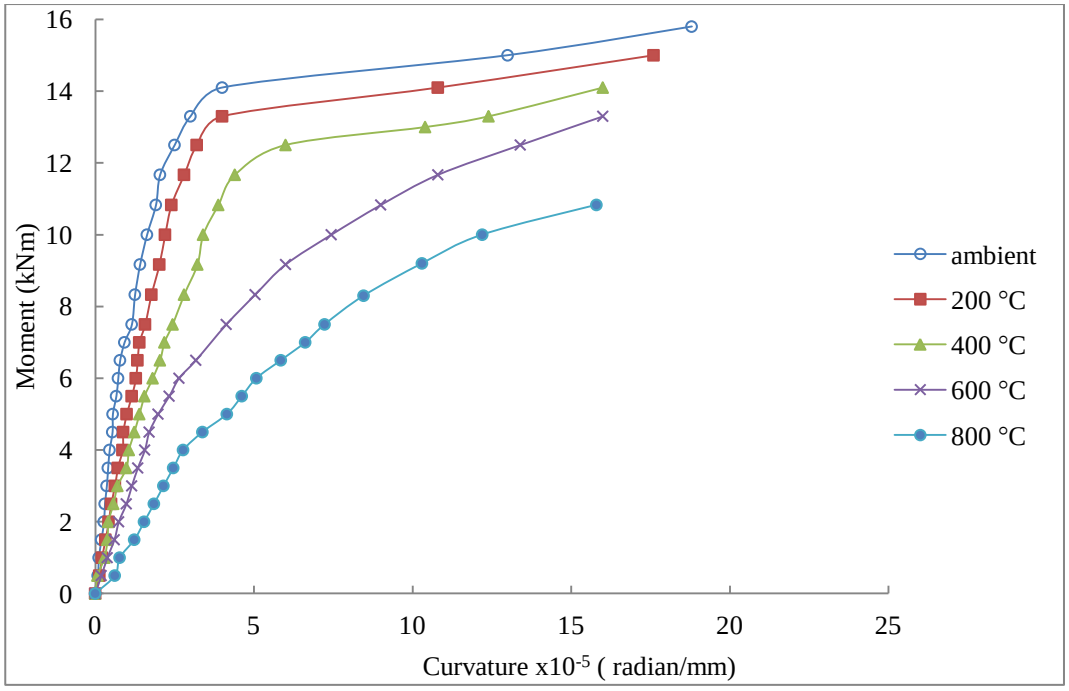

Fig. D.9. Moment curvature curve of GP concrete beam with 20 mm cover after exposure to elevated temperatures

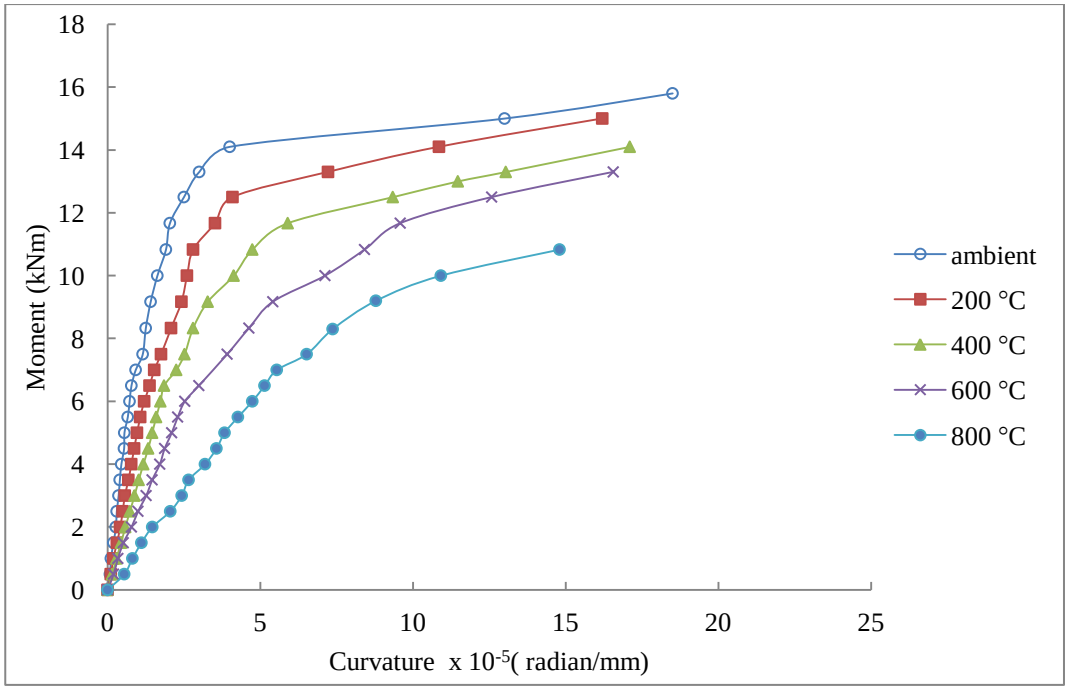

Fig. D.10. Moment curvature curve of GP concrete beam with 30 mm cover after exposure to elevated temperatures

D.3 SAMPLE CALCULATION FOR THEORETICAL m – φ RELATIONSHIP

Case 1: Compressive strain in concrete $\varepsilon_{cc} \leq 0.0002$

Total compress force $C = C_c + C_s$

Cc = Compressive strength of parabolic stress block

$= 0.67\ f_{ck}\ b\ (500 \times \varepsilon_{cc} - 83333.3333 \times \varepsilon_{cc}^{2})$

$C_s\ A_{sc}\ E_s\ \varepsilon_{cc}(x-d^1)/x$

$T = A_{st}\ Es\ \varepsilon_{cc}\ (d-x)/x$

Where A_{sc}, $A_{st,}$, E_s , x, d and d^1 respectively are area of compression steel, area of tension steel, modulus of elasticity of steel at particular temperature, depth of neutral axis, effective depth, effective cover at compression zone.

Assume a value for ε_{cc} and make the condition C = T by adjusting the trial value of 'x'

Theoretical moment of resistance $M = C_c\ (Y+ d –x) + C_s(d-d^1)$

$Y = 0.67\ f_{ck}[(333.3333\ x^2\ \varepsilon_{cc}^{2}) – (62500\ x^2\ \varepsilon_{cc}\ )]\ b/C_c$

Radius of curvature $\varphi = \varepsilon_{cc}/x$

Case 2: Compressive strain in concrete $\varepsilon_{cc} > 0.0002$

Total compress force $C = C_1 + C_2 + C_3$

C_1 = Compressive strength of rectangular part of stress block

$= 0.67\ f_{ck}\ (x-y)\ b$, where 'x' is the depth of neutral axis and 'y' is the depth of parabolic part of stress block.

$y = (0.002\ x)/\ \varepsilon_{cc}$

C_2 = Parabolic part of stress block $= [(2/3)0.67 f_{ck} yb]$

$C_3 = A_{sc}\ Es\ \varepsilon_{cc}\ (x-d^1)/x$, where E_s is modulus of elasticity of steel at particular temperature exposure and d^1 is the depth of effective cover at compression zone.

Tensile force $T = A_{st}\ f_y$, Where A_{st} and f_y respectively are area of tension steel and yield strength of steel at particular temperature.

Assume a value for ε_{cc} and make the condition C = T by adjusting the trial value of 'x'

Theoretical moment of resistance $M = C_1\ [(d – (x-y)/2] + C_2\ [d – ((5/9)y)] + C_3\ (d – d^1)$

Radius of curvature $\varphi = \varepsilon_{cc}/x$

Calculated m-φ values for beam having cover 20 mm and at ambient temperature is shown in the table D.3

Table D.3. m-φ for beam having cover 20 mm and at ambient temperature

Depth of neutral axis x (mm)	Radius of curvature ϕ (Radian/mm)	Compressive strain in concrete ε_{cc}	M (kNm)
37.94	1.3200E-06	0.00005	0.94
38.00	2.6200E-06	0.0001	1.87
38.30	5.2200E-06	0.0002	3.7
38.60	7.7700E-06	0.0003	5.5
38.85	1.0000-05	0.0004	7.26
39.15	1.2800E-05	0.0005	8.98
39.45	1.5200E-05	0.0006	10.70
39.80	1.7588E-05	0.0007	12.30
21.56	1.0000E-04	0.0022	13.50
21.33	1.6000E-04	0.0035	14.80

D.4 MOMENT CURVATURE CURVE OF GP CONCRETE BEAMS AFTER EXPOSURE TO ELEVATED TEMPERATURES

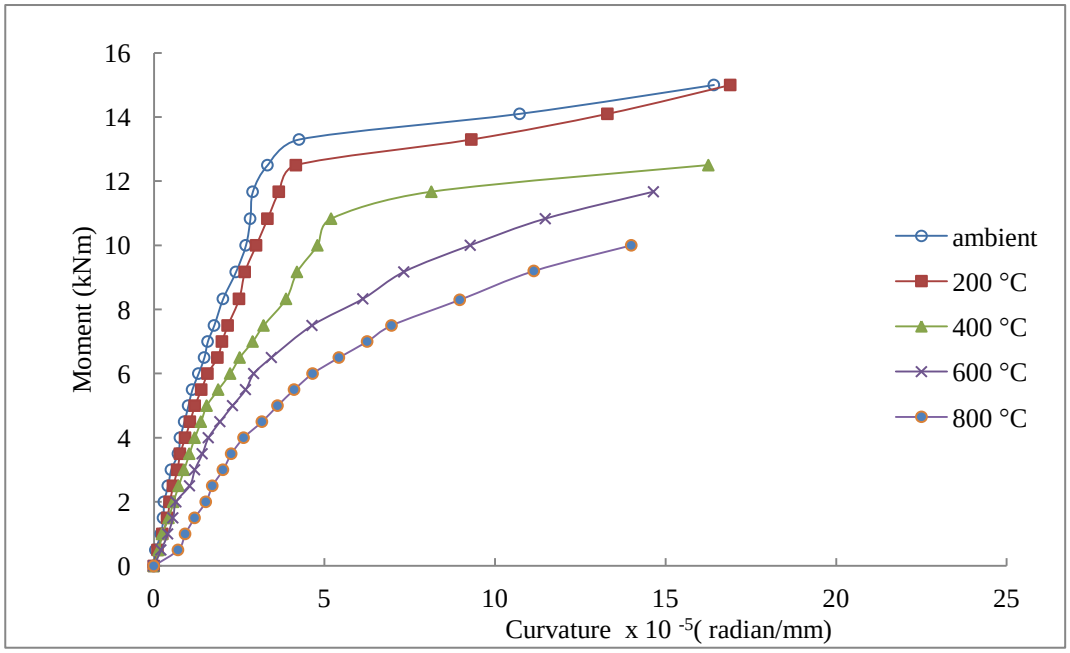

Fig. D.11. Moment curvature curve of GP concrete beam with 40mm cover after exposure to elevated temperatures

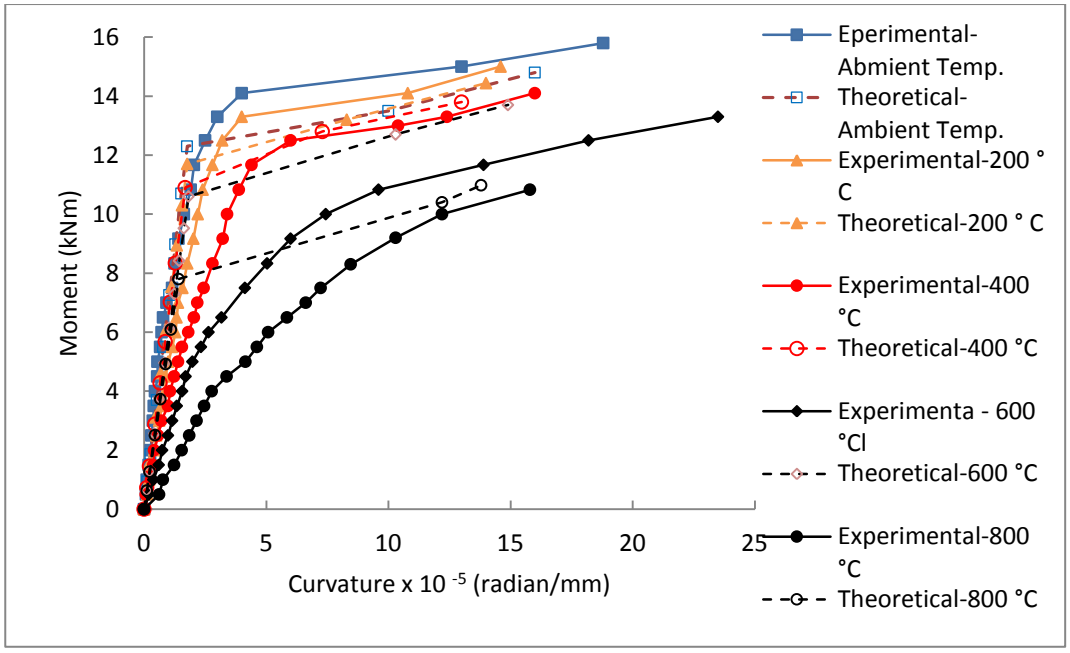

Fig. D.12. Experimental and theoretical moment curvature curve of GP concrete beam after exposure different temperatures